DOKTORI (PhD) ÉRTEKEZÉS

BÁRKÁNYI ÁGNES

DOI: 10.18136/PE.2014.530

Pannon Egyetem
2014

Pannon Egyetem
Vegyészmérnöki és Folyamatmérnöki Intézet

Hidrodinamikai viszonyok hatásának vizsgálata polimerizációs reaktorok termékminőségére

DOKTORI (PhD) ÉRTEKEZÉS

Bárkányi Ágnes

Konzulensek
Dr. Lakatos Béla, egyetemi docens
Dr. Németh Sándor, egyetemi docens

Vegyészmérnöki- és Anyagtudományok Doktori Iskola
Pannon Egyetem
2014

Hidrodinamikai viszonyok hatásának vizsgálata polimerizációs reaktorok termékminőségére

Értekezés doktori (PhD) fokozat elnyerése érdekében
a **Pannon Egyetem Vegyészmérnöki- és Anyagtudományok Doktori Iskola**
Doktori Iskolájához tartozóan*.

Írta:

Bárkányi Ágnes

Konzulensek: Dr. Lakatos Béla

Elfogadásra javaslom igen / nem …….
(aláírás)

Dr. Németh Sándor

Elfogadásra javaslom igen / nem …….
(aláírás)

A jelölt a doktori szigorlaton .....%-ot ért el,

Az értekezést bírálóként elfogadásra javaslom:

Bíráló neve: …..... igen /nem
…….
(aláírás)

Bíráló neve: …..... igen /nem
…….
(aláírás)

A jelölt az értekezés nyilvános vitáján ….....%-ot ért el.

Veszprém, …….
a Bíráló Bizottság elnöke

A doktori (PhD) oklevél minősítése….....

……
Az EDHT elnöke

University of Pannonia
Department of Process Engineering

Analysis of hydrodynamic effects on product quality in polymerization reactors

PhD Thesis

Ágnes Bárkányi

Supervisors
Béla Lakatos, CSc
Sándor Németh, PhD

Doctoral School in Chemical Engineering and Material Science
University of Pannonia
2014

Kivonat

Hidrodinamikai viszonyok hatásának vizsgálata polimerizációs reaktorok termékminőségére

A dolgozat diszperz rendszerekben lejátszódó folyamatok matematikai modellezésével és vizsgálatával foglalkozik. Az olyan rendszerek, amelyekben a diszperz elemekben kémiai reakció játszódik le nagyon érzékenyek a mikro-szintű folyamatokra. Ilyen folyamat a diszperz elemek ütközése, amelynek során komponens és hőátadás megy végbe az elemek között, az elemek szétesése, vagy törése, és az elemek koaleszcenciája.

A kutatási munka első feladata egy olyan részletességű matematikai modell kidolgozása volt, amely alkalmas az összetett és sok elemből álló rendszerekben a mikro- és makro-szintű folyamatok leírására. Az ilyen típusú rendszerek vizsgálatára jól alkalmazható a populáció mérleg modell. Az elsődleges cél vinil-klorid szuszpenziós polimerizációjának vizsgálata volt szakaszos, kevert reaktorban. Ebben a rendszerben a diszperz elemek a monomer cseppek, amelyekben bonyolult polimerizációs reakciók mennek végbe. Mivel ezek a reakciók erősen exotermek, ezért a reakcióban a cseppeknek nem csak a térfogata és a bennük lévő egyes komponensek koncentrációja, de a hőmérséklete is jelentősen változik. Ezt a modellezési feladatot egy több-dimenziós populáció mérleg egyenlet felírásával oldhatjuk meg. A modell tartalmazza az időben folytonos események (pl. a kémiai reakció), valamint a diszperz elemeknek az időben diszkrét, véletlenszerű változásaiból (pl. ütközésekből) adódó tulajdonságváltozásait. A dolgozat második részében egy megoldási módszert mutatok be, amely alkalmas a kidolgozott több-dimenziós populáció mérlegegyenlet megoldására. Kidolgoztam egy esemény vezérelt Monte Carlo módszert, amivel meghatározható a diszperz elemekben a folytonos idejű reakciókban történő megváltozásokat és ezzel párhuzamosan a diszkrét események miatt bekövetkező megváltozásokat.

Mivel az iparban a reaktorokat nagyrészt folyamatos üzemmódban üzemeltetik, ezért fontos, hogy a kifejlesztett szimulációs technika erre a típusra is alkalmas legyen. A dolgozat harmadik része a mikrokeveredés hatásának vizsgálatát mutatja be folyamatos üzemű, egyfázisú reaktor példáján keresztül. Szimulációs vizsgálatokkal szemléltethető, hogy milyen hatása van a reagens koncentráció térbeli eloszlásának, ha a komponensek elkeveredése nem tökéletes az egyes fluidum elemek között.

Abstract

Analysis of hydrodynamic effects on product quality in polymerization reactors

The main subject of this thesis is the modelling and simulation of suspension polymerization of vinyl chloride. A multi-dimensional population balance equation was developed for modelling the disperse system and the micro- and meso-scale processes. Two parallel processes are taking place inside the reactor: polymerization reactions inside the dispersed phase, continuous in time, and the meso-scale interactions of dispersed elements, discrete in time. A coupled continuous time – Monte Carlo method was developed for solution of the multi-dimensional population balance equation. The effects of inhomogeneities of initiator distribution, the initial size distribution of monomer droplets and the effects of temperature rise in droplets on polymer properties and monomer conversion were analysed by simulation studies.

Since in industry most of the reactors are operated in a continuous manner, therefore in the thesis there is a case study for the analysis of the effects of micromixing in a continuous reactor. The developed coupled continuous time – Monte Carlo method was improved for solution of the continuous case.

Auszug

Die Untersuchung der hydrodynamischen Effekte auf die Produkt Qualität in den Polymerisation Reaktoren

Das Hauptziel der Dissertation ist die Modellierung und das Simulation der Suspension Polymerisation des Vinylchlorids. Eine multi-dimensionale Population Bilanz Gleichung wurde für die Modellierung des dispersen Systems und der Micro- und Meso-Skala Prozesse ausgebildet. Zwei parallele Prozesse verlaufen im Reaktor: die Polymerisation Reaktionen in der dispersen Phase, die sind kontinuierlich in der Zeit, und die Meso-Level Wechselwirkungen der dispersen Elemente, die sind diskret in der Zeit. Eine gekuppelte kontinuierliche Zeit – Monte Carlo Methode wurde für die Lösung der multi-dimensionalen Population Bilanz Gleichung ausgebildet. Der Effekt der Inhomogenität der Initiator Verteilung, der einleitenden Monomer Tropfen Verteilung und der Temperaturerhöhung in den Tropfen auf die Polymer Qualität und der Monomer Konversion wurden durch Simulationen analysiert.

In der Industrie funktionieren die meisten Reaktoren kontinuierlich, deshalb gibt es ein Beispiel für die Analyse des Effekts des Micro-Mischens in einem kontinuierlich funktionierenden Reaktor. Die ausgebildete gekuppelte kontinuierliche Zeit – Monte Carlo Methode wurde für die Lösung der kontinuierlichen Fälle verändert.

Contents

Notations

A	heat transfer surface area of the reactor [m^2] (in Section 1 and 3.); pre-exponential factor (in Section 4.)
a	parameter in Eq.(1.25,26); heat transfer surface area [m^2]
B	birth density function (in Section 2.)
$B(a,b)$	beta function with parameters a and b
b	parameter
C	parameter
$C_{I,II,IV}$	constants
c	parameter
$\boldsymbol{c}$	vector of concentrations
c_I	concentration of initiator in a droplet [mol/ m^3]
c_M	concentration of monomer in a droplet [mol/ m^3]
c_p	heat capacity [J/gK]
D	impeller diameter [m] (in Section 1.); death density function (in Section 2.)
d	diameter [m]
E_a	activation energy
E_f	the next reaction
f	chemical or intrinsic initiator efficiency
h	heat transfer coefficient [W/m^2K]
$h(d,d')$	collision intensity of drops of volume v and v' [m^3/s]
I	initiator
I^*	active initiator radical
$\boldsymbol{I}_{(0,1)}(x)$	indicator function of beta distribution
K	number of components
k	thermal conductivity [W/mK] (in Section 1 and 3); rate constant of a chemical reaction (in Section 4.)
k_d	initiator decomposition rate coefficient [1/s]
k_I	initiation rate coefficient of initiator [$m^3/(mol \cdot s)$]
k_p	propagation rate coefficient [$m^3/(mol \cdot s)$]

k_t	rate coefficient of termination [m^3/(mol·s)]
k_{tc}	rate coefficient of termination by combination [m^3/(mol·s)]
k_{td}	rate coefficient of termination by disproportion [m^3/(mol·s)]
k_{tM}	chain transfer to monomer rate coefficient [m^3/(mol·s)]
N	impeller speed [rpm] (in Section 1.); Poisson process counting events (in Section 2.); number of droplets [#] (in Section 3.)
$N(\xi_1)$	total number of droplets present in some finite subregion of disperse phase space ξ_1
Nu	Nusselt number
$n(\xi,t)$	number density function over a region ξ
n_{M0}	initial value of monomer [mol]
M	monomer
$\boldsymbol{M_a}$	operation of the aggregation event
$\boldsymbol{M_b}$	operation of the breakage event
$\boldsymbol{M}_{c/r}^{dd}$	operation of coalescence/redispersion event
$\boldsymbol{M}_{\boldsymbol{i}}^{K}[n(\boldsymbol{c},T,t)]$	generalized coalescence/redispersion model of micromixing
M_w	molecular weight of monomer [g/mol]
MN	number average molecular weight [g/mol]
MW	weight average molecular weight [g/mol]
m	mass [g]
P_i	the closed polymer chain with chain length i
PDI	polydispersity index
Pr	Prandtl number
Q	liquid volumetric flowrate [m^3/s]
$\dot{Q}_{reaction}$	nascent heat due to polymerization reactions [J/s]
$\dot{Q}_{trans\_d}$	heat transfer from dispersed phase to the continuous phase [J/s]
$\dot{Q}_{trans\_j}$	heat transfer to the cooling jacket from continuous phase [J/s]
q	flow rate [m^3/s]
R	universal gas constant [J/molK]
$R(E_s)$	the probability that reaction E_s occurs
R_i	the growing polymer chain with chain length i

Re	Reynolds number
$r_{1,2}$	random numbers
S_a	frequency of binary collisions with coalescence [m^3/s]
S_b	breakage rate of droplets of state $(\upsilon,\boldsymbol{c},T)$ [1/s]
S_{col}^{dd}	frequency of binary collisions without coalescence [m^3/s]
T	temperature [K]
t	time [s]
U	overall heat transfer coefficient [W/m^2K]
$\bar{u}$	average velocity of droplet [m/s]
V_c	volume of continuous phase [m^3]
$\boldsymbol{v}$	velocity of droplet in region R
$\boldsymbol{v_e}$	external droplet velocity
$\boldsymbol{v_i}$	internal droplet velocity
X	monomer conversion [-]
X_c	critical conversion [-]
$\boldsymbol{x}$	vector coordinates of region R

Greek symbols

α	constant
β_a	resulting volume of such an event aggregation
$\beta_b(d,d')$	probability density function for droplets from the breakup of droplets of state (d) at time that have state (d')
$\beta_{\upsilon\upsilon''}$	diffusive component transfer coefficient
ΔH_r	heat of polymerization [J/mol]
Δt_k	denote the next event time [s]
δ	Dirac delta function
ρ	density [g/cm^3]
ρ_d	density of dispersed phase [g/cm^3]
ε	energy dissipation rate [m^2/s^3] (in Section 1); volume fraction of the continuous phase (in Section 2)
Θ	contact time [s]
$\lambda(d,d')$	coalescence efficiency

λ_k	intensity, mean frequency of *k* event
μ_c	viscosity of continuous phase [poise]
μ_j	*j*th moment of dead polymer chains
ν_j	*j*th moment of live polymer chains
$\nu(\upsilon', \mathbf{c}', T', t)$	average number of droplets formed from the breakup of a single droplet of state $(\upsilon', \mathbf{c}', T')$ at time *t*
σ	interfacial tension [dyn/cm]
τ_{micro}	the next event time [s]
υ	volume of droplet [m^3]
ϕ	disperse phase volume fraction [-]
ω	random number

Subscripts

1	monomer rich phase
2	polymer rich phase
c	continuous phase
d	dispersed phase
j	cooling jacket of the reactor
m	monomer
p	polymer
v	vessel
w	wall of the reactor

Introduction

The macromolecular architecture (e.g. molar mass, molecular weight distribution (MWD), copolymer composition distribution (CCD), chain sequence length distribution (CSLD), branching distribution (BD), stereoregularity, etc.) depends not only on the chemical nature of the monomers, the type of polymerization mechanism and the physical state of the reacting system (e.g. polymerization process) but also on the type of reactor configuration. It should be emphasized that product quality is a much more complex issue in polymerization processes than in conventional short chain reactions since the molecular and morphological properties of a polymer product strongly influence its physical, chemical, thermal, rheological, mechanical properties as well as the polymer's end-use applications. Therefore, the development of comprehensive mathematical models to predict the polymer quality in terms of process operating conditions in a polymer reactor is the key to the efficient production of high quality, tailored polymer products and the improvement of plant operability and economics.

To discover, recognize the relationship between the properties of the product and the reaction conditions, rigorous mathematical models are needed, which can describe the properties of various phases in reactor, the relationship between the phases, together with the hydrodynamic effects.

The aim of this work is to develop such a mathematical model, which can describe the phenomena in liquid-liquid dispersions together with complex reactions inside the dispersed phase. The solution of such complex multi-dimensional mathematical model equations seems to be a crucial problem. Therefore, the other aim of this work is to develop a robust; easy to implement method which is appropriate to simulate the phenomena in liquid-liquid dispersions, such as suspension polymerization of vinyl chloride.

Since in industry the most of reactors are operated continuously, therefore, in the thesis there is an example for the analysis of the effect of micromixing in a continuous reactor.

1. Literature survey

In this section, the most important classification of polymers and polymerization processes is introduced. The process of suspension polymerization and the suspension polymerization of vinyl chloride is described in detail. After that, the scales of the modelling of polymerization reactors and the most important methods of solution of the model equations are introduced.

1.1. Polymerization

Polymers are macromolecules built up by the linking together of large numbers (e.g. hundreds, thousands even tens of thousands) of much smaller molecules, called monomers. The reactions by which monomers combine are termed polymerizations. Polymer materials can be classified according to one or more of the following criteria:

- Chemical nature of monomers.
- Molecular structure of polymers.
- Polymer chain growth mechanism.
- Type of polymerization process.

Notice that the above criteria are not unique and several other alternative classifications have been proposed in the literature (Ram, 1997).

Classification by the molecular structure of polymers

a) According to the number of different structural units present in a polymer chain, polymers can be classified into:
   - Homopolymers which are built by the linking together of a large number of a single repeating unit.
   - Copolymers formed from more than one type of monomers. They are called bipolymers, terpolymers, multipolymers according to the number of different structural units in a polymer chain.

b) Another common classification of polymers is according to the polymer chain structure. Thus, polymers can be
   - linear,

- branched,
- comb-like,
- star-like,
- cyclic,
- dendrimer polymers.

c) Polymer molecules can be further classified according to their degree of stereoisomerism (e.g. the relative arrangements of configuration units in a chain). Stereoisomerism in polymers can be:

- Optical isomerism arises from different configurations of substituents on a saturated carbon atom.
- Geometrical isomerism arises from different configurations of substituents on a carbon-carbon double bond or on a cyclic structure.

Classification by the kinetic mechanism

- Step-growth polymerization refers to a type of polymerization mechanism in which bi-functional or multifunctional monomers react to form first dimers, then trimers, longer oligomers and eventually long chain polymers.
- Free-radical polymerization is a method of polymerization by which a polymer forms by the successive addition of free radical building blocks. All free-radical polymerizations have at least three basic reaction types occurring simultaneously during polymerization. These include initiation reactions which continuously generate radicals during the polymerization, propagation reactions which are responsible for the growth of polymer chains by monomer addition to a radical centre and bimolecular termination reactions between two radical centres which give a net consumption of radicals.
- Anionic polymerization can be initiated by bases or Lewis bases such as alkali metals, alkoxides, amines, phosphines, Grignard compounds and sodium naphthaline. Polymerization is carried out at low temperatures in solvents of low polarity giving tightly bound ion pairs rather than mainly separate ions.

- Cationic polymerization is a type of chain growth polymerization in which a cationic initiator transfers charge to a monomer which becomes reactive. This reactive monomer goes on to react similarly with other monomers to form a polymer.
- Group transfer polymerization is a relatively new type of mechanism relies on a silicon-based initiator, most commonly a silyl ketene acetal. The initiator is un-reactive with respect to monomer except in the presence of a catalyst which may be either a nucleophile or Lewis acid.
- Coordination anionic polymerization is a form of addition polymerization in which monomer adds to a growing macromolecule through an organometallic active centre. The polymers tend to be linear and not branched and have much higher molar mass than polymer prepared by free radical polymerization.

Classification of polymerization processes

- Bulk polymerization is carried out by adding a soluble initiator to pure, liquid state monomer. The initiator should dissolve in the monomer. The reaction is initiated by heating or exposing to radiation. As the reaction proceeds, the mixture becomes more viscous. The reaction is exothermic and a wide range of molecular masses are produced.
- In solution polymerization a monomer is dissolved in a non-reactive solvent that contains a catalyst. The reaction results in a polymer which is also soluble in the chosen solvent. Heat released by the reaction is absorbed by the solvent, and so the reaction rate is reduced. Moreover the viscosity of the reaction mixture is reduced, not allowing auto acceleration at high monomer concentrations. Once the maximum or desired conversion is reached, excess solvent has to be removed in order to obtain the pure polymer.
- Precipitation polymerization is a heterogeneous polymerization process that begins initially as a homogeneous system in the continuous phase, where the monomer and initiator are completely soluble, but upon initiation the formed polymer is insoluble and thus precipitates.

- Suspension polymerization is a heterogeneous radical polymerization process that uses mechanical agitation to mix a monomer or mixture of monomers in a liquid phase, such as water, while the monomers polymerize, forming spheres of polymer. The polymerization reaction takes place in monomer droplets.
- Emulsion polymerization is a type of radical polymerization that usually starts with an emulsion incorporating water, monomer, and surfactant. The most common type of emulsion polymerization is an oil-in-water emulsion, in which droplets of monomer (the oil) are emulsified (with surfactants) in a continuous phase of water. The excess of surfactant form micelles (ca. 5-10 μm in diameter) which are clusters of surfactant molecules.
- Solid catalysed polymerization. Although some catalysts are used in liquid form, most are heterogeneous, solid catalysts which can be supported or unsupported. The monomer in contact with the catalyst could be gaseous (gas phase process), a pure liquid (liquid solution process) or dissolved in a diluent (slurry process). In all cases, the porous catalyst fractures and fragments of the catalyst are dispersed in the polymer and become the locus of polymerization.
- Interfacial polymerization is an alternative to bulk polymerization of condensation polymers which would require high temperatures. Two immiscible solvents are used, with monomer in one solvent reacting with monomer in the other solvent. Reactions often occur on a time scale that so fast that for our purposes they might as well be called instantaneous. Higher molecular weights are obtained because monomer is more likely to encounter a growing chain than the opposing monomer.
- Solid-state polymerization in the solid state can produce macroscopic polymer single crystals and, in some cases, crystals of high optical quality. The propagation reaction is controlled by the crystal structure and symmetry of the monomer. Thus, in certain cases the propagation reaction may lead to a crystal-to-crystal transformation.

1.1.1. Suspension polymerization

Suspension polymerization is used for the commercial manufacturing of many important polymers including poly(vinyl chloride), poly(methyl methacrylate), expandable polystyrene, styrene-acrylonitrile copolymers and a variety of ion exchange resins. Suspension polymerization was first developed by Hoffman and Delbruch in 1909. The first suspension polymerization based on acrylic monomers leading to the formation of beads was performed by Bauer and Lauth in 1931 (Dowding and Vincent, 2000).

In suspension polymerization, one or more water-insoluble monomers containing oil-soluble initiator(s) are dispersed in a continuous liquid phase by a combination of strong stirring and the use of small amounts of suspending agents (stabilizers). The stabilizers hinder the coalescence of the monomer droplets first, and later stabilize the polymer beads whose tendency to agglomerate may become critical when the polymerization has advanced to the point where the polymer beads become sticky (Yuan et al., 1991).

Monomer solubility in the continuous phase is often low and polymer is produced inside the drops. Although the drop viscosity increases with monomer conversion, the effective viscosity of the suspension remains low and efficient agitation is possible. The ratio of surface area to volume for small drops is relatively high and local heat transfer is good. If the continuous phase is aqueous and well mixed, heat transfer from the reactor is also good. That permits effective control of temperature and of those variables, which depend on temperature, and which include reaction rates and polymer molecular weight (Meyer and Keurentjes, 2005).

There are three different types of suspension polymerization processes.

a. *Bead (or Pearl) Suspension Polymerization*. The monomer dissolves its polymer. The monomer droplets pass through a viscous syrupy state and finally are transformed to solid clear little spheres. Examples of this process are poly(methyl methacrylate) and polystyrene.

b. *Powder Suspension Polymerization*. The polymer is not dissolved in its monomer. A bulk precipitation polymerization occurs in each droplet, and

opaque, irregular grains or powders are finally formed. An example of this type is PVC.

c. *Mass Suspension Polymerization*. This is a two stage process. In the first stage a rubber is dissolved in the grafting liquid monomer mixture. The mixture is polymerized initially in a bulk process. When the conversion reaches 25-30%, the highly viscous reaction mass is transferred to a suspension reactor filled with water containing stabilizer. The reaction proceeds until the desired monomer conversion is reached. An example of this process is the production of high impact polystyrene and acrylonitrile-butadiene-styrene resin (Yuan et al, 1991).

The most important issue in the practical operation of suspension polymerization is the control of the final particle size distribution. Suspension polymer particle diameters range is usually between 50 and 200 μm, the exact size depending on the monomer type, the concentration of stabilizers, and the agitation conditions in the reactor (Yuan et al, 1991).

The physical conditions in a suspension polymerization reactor affect the drop size distribution significantly. Drop size depends on the physical properties of the two phases, the phase ratio, the nature of the suspension flow, and the condition of the phase interface. Drop breakage in agitated suspensions can be caused either by frictional forces (through viscous shear) or by inertial forces (through turbulence) (Brooks, 2010). In industrial suspension polymerization, the volume fraction of the dispersed phase is usually high and drop breakup is accompanied by drop coalescence. Thus, both the average drop size and the drop size distribution are influenced by drop breakage and drop coalescence.

Interfacial tension and drop stability depend largely on the nature of the drop stabilizer. If no stabilizer were used to protect the drops, the suspension would be unstable and the final polymer particles would reach an undesirable size. The adsorption of stabilizer molecules at the interface between monomer and the continuous phase reduces the interfacial tension and hence reduces the energy required to form drops. Drop stability against coalescence depends largely on the ability of the stabilizer to form a thin protective film at the interface. That gives the drops better elastic properties (Rosen, 2004). The effect of the elastic

properties is enhanced by increasing the concentration of the suspending agent, until a certain surface coverage of the drops is reached. At that point, a ‘‘critical surface coverage’’ is established and a further increase in the suspending agent concentration will have a very little effect on the drop stability (Borwankar and Wasan, 1986).

1.1.1.1 Suspension polymerization of vinyl chloride

PVC is one of the most important mass products of the polymer industry, it is the third most widely produced plastic after polyethylene and polypropylene. PVC is widely used in construction because it is durable, cheap, and easily worked. Approximately 75% of the world’s PVC is produced by the suspension polymerization process (Kiparissides et al, 1997). Advantages of suspension polymerization are not restricted to temperature control. In this technique, the dispersion viscosity is low, the levels of impurities in the polymer product is low, therefore the separation cost is low and the final product is in particle form. PVC is immiscible with vinyl chloride. Subsequent polymer coagulation makes bulk processes difficult to control. In suspension polymerization, however, that problem is avoided. There, coagulation is largely confined to the drop interiors and aggregation of polymerizing drops is restricted. That is why suspension polymerization is used for the large-scale production of PVC. In that case, the initial drop diameters, and the final particle sizes, range between 10 and 100 mm.

Although PVC is produced in high volume it is produced in batch reactors the present tendency being of working in reactor so large volume (160-200 m^3).

In suspension polymerization of VCM, the droplets of liquid vinyl chloride monomer (VCM) containing oil-soluble initiator(s) are dispersed in the continuous aqueous phase by a combination of strong stirring and the use of suspending agents (stabilizers) (Kiparissides et al, 1997). The most commonly used suspending agents for vinyl chloride suspension polymerization are water-soluble polymers such as hydroxylpropyl methylcellulose (HPMC) and partially hydrolysed polyvinyl acetate, commonly called PVA (Saeki and Emura, 2002). When partially hydrolyzed polyvinyl acetate (PVA) is used as a stabilizer, its behaviour depends on the extent to which the acetate groups are hydrolyzed (Atanase and Riess, 2010). Good drop stabilization can be achieved in aqueous

media when the degree of hydrolysis (DH) is between 70 and 80 %; then, drops can retain their integrity even when agitation levels are reduced (Zerfa and Brooks, 1996a,b). PVAs with a DH less than 60 % are poor drop stabilizers in aqueous media but they can affect polymer morphology inside the (nonaqueous) drops. That is important in the suspension polymerization of vinyl chloride (VC). In that case, small particles of poly(vinyl chloride) (PVC) precipitate inside the monomer drops. Therefore, a mixture of two stabilizers is often used: a primary stabilizer which protects the drops from coalescence and a secondary stabilizer which affects the behaviour of the PVC particles inside the drops and increases polymer porosity. The addition of a secondary stabilizer can also affect the particle size distribution of the polymer particles (Brooks, 2010). PVC porosity can also be increased by using non-ionic surfactants as secondary stabilizers. PVA can become grafted onto the polymer formed inside the drops, so that a skin forms on the final particle surface. Formation of that skin, which is difficult to remove, can affect the final polymer properties (Zerfa and Brooks, 1996a; Zerfa and Brooks, 1996b; Zerfa and Brooks, 1998).

In suspension polymerization of VCM, each monomer droplet contains a large number of live radicals (10^8) and behaves like a small batch reactor with bulk polymerization kinetics (Zhang and Ray, 1997). There are many works which describe the kinetic mechanism of free radical polymerization of vinyl chloride (Sidiropoulou and Kiparissides, 1990; Kalfas and Ray, 1993; Xie et al, 1991b; De Roo et al, 2005):

Initiation: $I \xrightarrow{k_d} 2I^*$

Chain initiation: $I^* + M \xrightarrow{k_I} R_1$

Propagation: $R_1 + M \xrightarrow{k_p} R_2 \;\ldots\; R_i + M \xrightarrow{k_p} R_{i+1}$

Chain transfer to monomer: $R_1 + M \xrightarrow{k_{tM}} R_1 + P_1 \;\ldots\; R_i + M \xrightarrow{k_{tM}} R_1 + P_i$

Termination reactions:

Spontaneous: $R_i \xrightarrow{k_t} P_i$

Combination: $R_i + R_j \xrightarrow{k_{tc}} P_{i+j}$

Disproportionation: $R_i + R_j \xrightarrow{k_{td}} P_i + P_j$

Transfer to monomer and polymer reactions are very important in VC polymerization since their frequency relative to the chain propagation reaction controls the molecular weight. Transfer to monomer causes a shift of the molecular weight distribution (MWD) to lower values. On the other hand, transfer to polymer can lead to the formation of branched polymers which causes a shift of the MWD to higher values. Transfer to monomer and intra-molecular reactions are considered to be responsible for the formation of the short side chains observed in PVC. Note that transfer reactions do not change the total number of live polymer chains and, therefore, the rate of polymerization and the number-average molecular weight will not be affected (Sidiropoulou and Kiparissides, 1990).

VCM is usually polymerized in a batch tank reactor by dispersing the liquid monomer under pressure in water in a well stirred jacketed reactor. The reactor's contents are heated to the required temperature where the initiator(s) start(s) to decompose and polymerization begins. The polymerization temperature is usually over the range 50 °C – 75 °C (Smallwood, 1986). The heat of polymerization is transferred from the monomer droplets to the aqueous phase and then to the reactor wall, which is cooled by chilled water flowing through the reactor's jacket. When all the free liquid monomer has been used up, the pressure in the reactor starts to fall as a result of the monomer mass transfer from the vapour phase to the polymer phase due to the sub-saturation conditions. In industrial PVC production, the reaction is usually stopped when a certain pressure drop has been recorded.

Since PVC is effectively insoluble in its own monomer once the polymer chains are first generated they precipitate immediately to form two separate phases in the polymerizing droplet. From a kinetic point of view the polymerization of VCM is considered to take place in three stages (Kiparissides et al, 1997).

During the first stage, primary radicals formed by the thermal fragmentation of initiator rapidly react with monomer molecules to produce PVC macromolecules which are insoluble in the monomer phase. The reaction mixture consists mainly of pure monomer since the polymer concentration is less than its solubility limit (conversion <0.1%).

The second stage extends from the time of appearance of the separate polymer phase to a critical conversion X_c at which the separate monomer phase disappears. The reaction mixture consists of four phases, namely the monomer-rich phase, the polymer rich phase, the aqueous phase, and the vapour phase. The reaction takes place in the monomer and polymer phases at different rates and is accompanied by transfer of monomer from the monomer phase to the polymer phase so that the latter is kept saturated with monomer. The disappearance of the monomer phase is associated with a pressure drop in the reactor.

Finally, at higher conversions ($X_c<X<1.0$) only the polymer-rich phase swollen with monomer exists. The monomer mass fraction in the polymer phase decreases as the total monomer conversion approaches a final limiting value.

From the point of view of the morphology of PVC grains the following five-stage kinetic-physical mechanism have been postulated to describe the nucleation, stabilization, growth and aggregation of PVC primary particles (Xie et al, 1991a,b; Kiparissides et al, 1997; Yuan et al, 1991).

During the first polymerization stage (VCM conversion range: $0<X<0.01\%$), primary radicals, formed via thermal decomposition of initiator molecules, rapidly react with monomer to produce polymer chains that almost instantaneously become insoluble in the monomer phase. In fact, the polymer chains precipitate out of the continuous VCM phase when they reach a specific chain length (i.e., of about 10–30 monomer units). It has been postulated that approximately 10–50 polymer chains are subsequently combined together to form nano-domains also called basic particles. The nano-domains are swollen with monomer and have an initial diameter of about 10–20 nm.

In stage two (VCM conversion range: $0.01<X<1\%$), the formation of PVC domains, also called primary particle nuclei, takes place. Because of the limited stability of the domains they rapidly undergo coagulation leading to the nucleation of the primary particle nuclei. The initial size of these primary particle nuclei has been found to be in the range of 80–100 nm. Typically, a primary particle nucleus may consist of about 1000 nano-domains. Contrary to nano-domains, the primary particle nuclei carry sufficient negative electrostatic charges to form stable colloidal dispersions in the monomer phase. During this stage, the primary

particles grow in size mostly by coagulation with smaller nano-domains rather than by polymerization of the absorbed monomer.

In stage three (VCM conversion range: $1<X<20\%$), growth and aggregation of the primary particles occur. Primary particle nuclei are continuously produced up to a monomer conversion of about 5–10%. During this stage, the primary particles grow in size by the capture of unstable nano-domains and the polymerization of the absorbed monomer. The latter growth process is progressively becoming the dominant mechanism as the volume of the polymer phase increases. The size and the number of the primary particles depend on the growth rate and the electrostatic-steric stability of the primary particles. At monomer conversions of about 7–20%, massive aggregation of the primary particles results in the formation of a continuous three-dimensional primary particle network within the VCM droplet. The three-dimensional primary particle network structure, its initial porosity, and its mechanical strength will depend on the size and the number of primary particles, the electrostatic and steric forces between the primary particles, the polymerization temperature and the polymer viscoelastic properties.

In stage four (VCM conversion range: $20<X<70–75\%$), the growth and fusion of the primary particles continues. That is, the primary particles increase in size due to polymerization and also undergo substantial fusion. Both processes result in a continuous decrease in particle porosity. At low monomer conversions (i.e., in the so-called “sticky” stage, $X<30\%$), the polymerizing droplets can undergo limited coalescence leading to the formation of multi-cellular grains. At higher monomer conversions, the droplets/particles become less “sticky” and the coalescence rate decreases significantly. On the other hand, inside the polymerizing monomer droplets, the primary particles continue to grow until the disappearance of the separate monomer phase (i.e., at about 70–75% monomer conversion).

Finally, in stage five (VCM conversion range: $70–75<X<90–95\%$), polymerization continues only in the monomer swollen polymer phase, however, at a lower rate, until the monomer has been depleted. During this stage, the vapour pressure in the reactor continuously decreases due to the transfer of VCM from the overhead gas phase to the monomer starved polymer phase. Note that the

polymerization is usually terminated at a monomer conversion of about 95–98%. At the final VC conversion, the size of the individual primary particles is in the range of 1–1.5 μm while the size of the primary particle aggregates is about 3–10 μm. It is important to point out that the two key parameters that determine the porosity of PVC grains are: the critical monomer conversion, X_c, at which a three-dimensional primary particle network is formed and the extent of particle network contraction due to the fusion of the primary particles. The structure and strength of the primary particle network will be affected by the size, the total number and the interaction forces between the primary particles that are, in turn, influenced by the polymerization conditions (i.e. polymerization temperature, agitation rate, type and concentration of stabilizers).

1.2. Modelling of batch suspension polymerization reactors

Mathematical modelling is a powerful methodology to improve the understanding and operation of polymer processes. A good process model can be used to predict the influence of operating conditions on reaction rate and polymer properties, to guide the selection and optimization of standard operating conditions for existing and new polymer grades (Meyer and Keurentjes, 2005).

A major objective of polymerization reaction engineering is to understand how the reaction mechanism, the physical transport phenomena (e.g. mass and heat transfer, mixing), reactor type and reactor operating conditions affect the properties of the final product. These properties include all the molecular structure properties and the macroscopic morphological properties of the polymer product. The various chemical and physical phenomena occurring in a polymer reactor can be classified into the following three levels of modelling:

- Micro-scale modelling
- Meso-scale modelling
- Macro-scale modelling

The relationships of scales are described in the next figure:

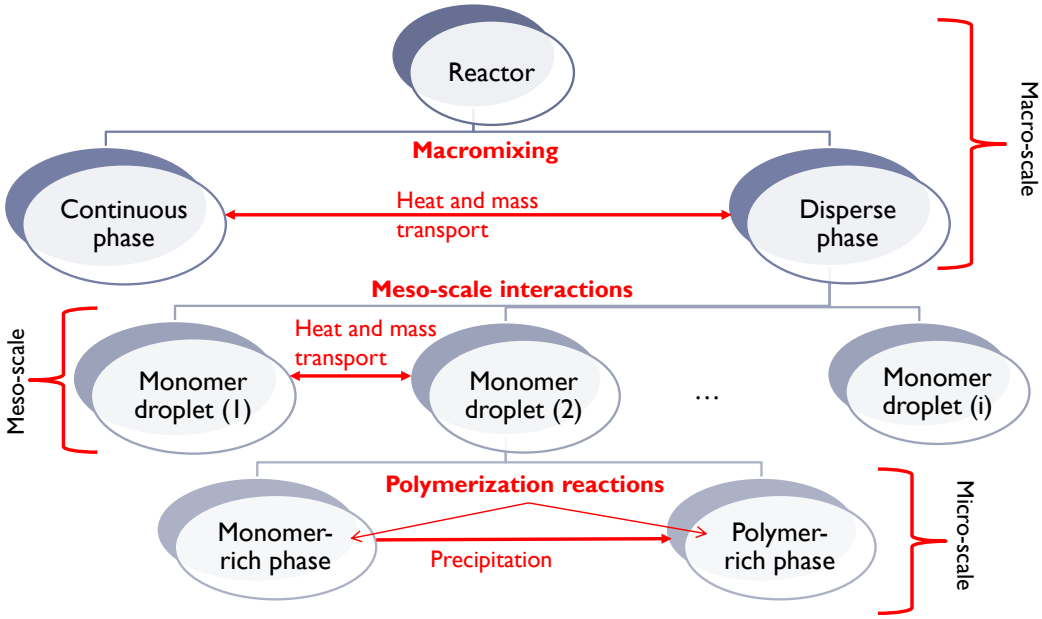

Figure 1.1. Scales in suspension polymerization reactors and the relationships of scales

1.2.1. Micro-scale modelling

Polymer reactions related with the kinetic mechanism and micromixing occur at the micro-scale. If the elementary reaction steps of a polymerization mechanism are known several mathematical techniques are available for calculating the molecular property distributions, in terms of the kinetic rate constants and the concentration of the reactants. The various mathematical methods can be classified into two main categories:

1. Statistical, and
2. Detailed species conservation methods.

Statistical methods rely on representing the growing polymer chain by a process of selecting monomers from the reaction mixture according to some statistical distribution. The success of this approach depends on a correct, and frequently intuitively based, correspondence of the polymerization process with a postulated stochastic process. It is, therefore, less easily adaptable to different reactor configurations since the appropriate correspondence may be difficult to find or, in fact, may not exist. On the other hand, when statistical methods do work, they usually lead to results in a comparatively simple way and can

sometimes reveal features of a polymerization system that a mass balance approach does not (Kiparissides, 1996)

The most powerful approach for modelling polymerization kinetics is the detailed species balance method. Based on the classical physical law of conservation of mass, one can derive an infinite set of differential or algebraic difference equations, depending on the reactor type, for the different molecular species (e.g. monomer(s), growing polymer chains, dead polymer chains) present in the reaction mixture. The resulting system of species balance equations must be solved to obtain information on the desired molecular property distributions (Kiparissides, 1996).

In Section 2.1, the kinetic description of free-radical polymerization of vinyl chloride was given. From that, we can see that the number of species is really large. One of the challenges in modelling polymerization systems is how to reduce a very large number of individual species (living and dead chains with lengths from 1 to $>10^5$, often with other distributed attributes such as the number of branch points) to a tractable size. The classic approach to this problem is to reduce the system of equations through definition of the principal moments of the various distributions. Construction of moment balances allows tracking the average polymer properties: for molecular weight this would be number-average and weight-average (Meyer and Keurentjes, 2005).

The moments for the distributions of growing (ν_j) and dead (μ_j) polymer are defined as:

$$\nu_j = \sum_{n=1}^{\infty} n^j [R_n] \tag{1.1}$$

$$\mu_j = \sum_{n=1}^{\infty} n^j [P_n] \tag{1.2}$$

After that the mass balances for the different components in a perfectly mixed batch reactor are as follows:

Mass balance for initiator:

$$\frac{d(\upsilon c_I)}{dt} = -\upsilon k_d c_I \tag{1.3}$$

Mass balance for monomer:

$$\frac{d(\upsilon c_M)}{dt} = -\upsilon\left(2 f k_d c_I c_M + k_p c_M \nu_0 + k_{tM} c_M \nu_0\right) \tag{1.4}$$

Moment balances for live polymer radicals:

$$\frac{d(\upsilon \nu_0)}{dt} = \upsilon\left(2 f k_d c_I - k_t \nu_0{}^2\right) \tag{1.5}$$

$$\frac{d(\upsilon \nu_1)}{dt} = \upsilon\left(2 f k_d c_I - k_t \nu_0 \nu_1 + k_{tM} c_M \left(\nu_0 - \nu_1\right) + k_p c_M \nu_0\right) \tag{1.6}$$

$$\frac{d(\upsilon \nu_2)}{dt} = \upsilon\left(2 f k_d c_I - k_t \nu_0 \nu_2 + k_{tM} c_M \left(\nu_0 - \nu_2\right) + k_p c_M \left(\nu_0 + 2\nu_1\right)\right) \tag{1.7}$$

Applying the Quasi-Steady-State Assumption (QSSA) for to the growing polymer chains:

$$\nu_0 = \sqrt{\frac{2 f k_d c_I}{k_t}} \tag{1.8}$$

$$\nu_1 = \frac{2 f k_d c_I + \left(k_p + k_{tM}\right) c_M \nu_0}{k_{tM} c_M + k_t \nu_0} \tag{1.9}$$

$$\nu_2 = \frac{2 f k_d c_I + k_p c_M \left(\nu_0 + 2\nu_1\right) + k_{tM} c_M \nu_0}{k_{tM} c_M + k_t \nu_0} \tag{1.10}$$

Moment balances for dead polymer chains are:

$$\frac{d(\upsilon \mu_0)}{dt} = \upsilon\left(k_{tM} c_M + k_t \nu_0\right)\nu_0 \tag{1.11}$$

$$\frac{d(\upsilon \mu_1)}{dt} = \upsilon\left(k_{tM} c_M + k_t \nu_0\right)\nu_1 \tag{1.12}$$

$$\frac{d(\upsilon \mu_2)}{dt} = \upsilon\left(\left(k_{tM} c_M + k_t \nu_0\right)\nu_2 + k_t\left(\nu_0 \nu_2 + \nu_1^2\right)\right) \tag{1.13}$$

The most commonly used model development for modelling the suspension polymerization of vinyl chloride is the two-phase model. The key feature in all these models is that PVC is practically insoluble in its monomer, and polymerization proceeds simultaneously in the two phases almost from the start of the reaction (Xie et al, 1991b, Sidiropoulou and Kiparissides, 1990). Talamini (1966) and Crosato-Arnaldi et al. (1968) first proposed a two phase polymerization scheme and modelling approach. Talamini's model assumes that

no transfer of radicals takes place between the two phases. The following important factors were neglected in the model: unequal initiator partition between the two phases; consumption of initiator; volume shrinkage due to the density difference between VCM and PVC. Later Abdel-Alim and Hamielec (1972) modified this model by taking into account the change in the volumes of the two phases as well as the change in the initiator concentration with reaction time. Moreover, first extended the model to conversions above X_f accounted for the diffusion control of the propagation and termination reactions at high conversions. However, unequal initiator partition and radical migration were neglected in the model. To modify Talamini's model, Ugelstad et al. (1971, 1973) proposed radical exchange between the two phases. Kuchanov and Bort (1973) considered that the desorption of radicals from the polymer phase can be ignored because only a small fraction of the radicals with short chain lengths can desorb from the polymer phase. They further assumed that the ratio of mole fraction of initiator in both phases remains constant.

Olaj (1977) further assumed that all of the radicals formed in the monomer phase transfer to the polymer phase, i.e. there is no termination reaction in the monomer phase. Hence, in Olaj's model, the reaction order with respect to initiator concentration is 1.0, which is higher than that observed experimentally.

More recently, Suresh and Chanda (1982) proposed a concept of 'kinetic solubility' which assumes that rapidly growing polymer chains have considerably greater solubility than the thermodynamic solubility of preformed polymer molecules of the same size and so can remain in solution even under thermodynamically unfavourable conditions. In the model development, radical precipitation and transfer to monomer were considered but radical termination in the monomer phase was neglected. Hence, the rate equation has features which are similar to Olaj's model.

Kelsall and Maitland (1983) considered the unequal partition of initiator between the two phases and derived model equations. During their simulation of VCM polymerization, radical migration between phases was treated as a mass transfer process. The validity of their model has not been examined experimentally.

Sidiropoulou and Kiparissides (1990) developed a fairly comprehensive but realistic model for describing the suspension polymerization of vinyl chloride in addition to the prediction of polymerization rate and molecular weight averages.

In suspension polymerization, the polymerization reactions take place in the monomer droplets. All droplets work as a micro reactor, but these micro reactors are connected with each other. These phenomena can be describing with micromixing, which contain the heat and mass transfer between the monomer droplets.

1.2.2. Meso-scale modelling

At meso-scale, the analysis of a particulate system is aimed at the synthesis of the behaviour of population of particles and its environment from the behaviour of single particles in their local environments. The population is described by the density function of a suitable extensive variable, usually the number of particles, or preferably by other variables such as the mass or volume of particles. The usual transport equations expressing conservation laws for material systems apply to the behaviour of single particles (Ramkrishna, 2000).

The population balance approach provides fundamental framework for mathematical description of processes of disperse systems. Within this framework it appears that Hulburt and Katz (1964) and Valentas and Amundson (1966) were among the first who introduced the population balance equation (PBE) into the modelling of chemical engineering processes involving dispersed phase operations. Population balance modelling is an active field of research due to its application to several engineering and scientific problems. They are of interest to physicists (astrophysicists, high-energy physicists, geophysicists, meteorologists) and chemists (colloidal chemists, statistical physicists). Biophysicists concerned with populations of cells of various kinds, food scientists dealing with preparations of emulsions or sterilization of food all have an indispensable need for population balances (Ramkrishna, 2000).

Population balance concepts are of importance to aeronautical, chemical, civil (environmental), mechanical, and materials engineers. Chemical engineers have put population balances to the most diverse use. Applications have covered a wide

range of dispersed phase systems, such as solid-liquid dispersions (although with incidental emphasis on crystallization systems (Motz et al, 2002; Puel et al, 2003; Mesbah et al, 2009; Majumder et al, 2012)), and gas-liquid (Buffo et al, 2012), gas-solid, and liquid-liquid dispersions. Analyses of separation equipment such as for liquid-liquid extraction (Modes et al, 1999; Weinstein et al, 1998; Attarakih et al, 2006), or solid-liquid leaching (Diez et al, 2006; Dixon, 1996; Crundwell, 1995); and reactor equipment, such as bioreactors (microbial processes) (Mantzaris and Daoutidis, 2004; Dhanasekharan et al, 2005; Zhu et al, 2000), fluidized bed reactors (catalytic reactions) (Ahmadzadeh et al, 2008; Moguel et al, 2010; Tan et al, 2005), and dispersed phase reactors (transfer across interface and reaction) (Bannari et al, 2008; Kotoulas and Kiparissides, 2006; Alexopoulos and Kiparissides, 2007; Jahanzad et al, 2005; Hosseini et al, 2012) all involve population balances.

In dispersed phase reactors assuming complete mixing, droplet population balance based modelling is now being used to describe the complex hydrodynamic behaviour of the dispersed phase. In such equipment the dynamically changing behaviour of the dispersed particles, or strictly speaking droplets (or bubbles), makes it necessary to consider a detailed mathematical rather than lumped modelling approach. These details are necessary to describe the discontinuous events such as breakage and coalescence occurring due to the interaction of the constituents (droplets) and of the turbulent continuous.

The term breakage considers the interaction of a single droplet with the turbulent continuous phase where the droplet undergoes breakage if the turbulent kinetic energy transmitted to the droplet exceeds its surface energy (Coulaloglou and Tavlarides, 1977). On the other hand, droplet coalescence is expected to occur due to the interaction between two droplets and the turbulent continuous phase. The coalescence between two droplets is considered to occur if the intervening liquid film has sufficient contact time to be drained out.

Thus systems, which are described by population balance models are consisting of particles or droplets dispersed in a continuous phase. The particles may interact between themselves as well as with the continuous phase. Such behaviour may vary from particle to particle depending upon a number of properties that

may be associated with the particle. The variables representing such properties may be either discrete or continuous. The discreteness or continuity of the property pertains to its variation from particle to particle or droplet to droplet (Ramkrishna, 2000).

1.2.2.1 Drop breakage

There are a few examples in the literature of calculation of the breakage frequency of liquid drops in the turbulent flow (such as that prevailing in a stirred vessel) of a second immiscible, liquid phase. Coulaloglou and Tavlarides (1977) and Narsimhan and Gupta (1979) have presented models based on somewhat different physical arguments for drop breakage. The former consider breakage to be binary and instantaneous, but to be reinforced by successful separation of the two droplet fragments before drainage of the intervening film. The probability calculated is that of the contact time between the drops being less than the required drainage time.

Narsimhan and Gupta, on the other hand, consider breakup by bombardment of the drop by eddies (smaller than the drop), with at least, as much energy required to create the minimum amount of new interface. The breakage frequency is calculated as the ratio of the probability that an eddy of the appropriate amount of energy is incident upon the drop surface, to the average arrival time of the eddies. Thus, in this model the temporal element lies in the waiting period for the appropriate eddy to arrive but upon its arrival breakup occurs instantly.

Deformation and breakage of a drop in a turbulent flow, as considered by Coulaloglou and Tavlarides (1977), depends on drop size, density, interfacial surface tension, viscosity of the both phases, holdup fraction, local flow and local energy dissipation. For the breakage frequency they gave the following equation:

$$S_b(d) = \frac{C_I d^{-2/3} \varepsilon^{1/3}}{1+\phi} \exp\left[-\frac{C_{II} \sigma (1+\phi)^2}{\rho_d d^{5/3} \varepsilon^{2/3}} \right] \tag{1.14}$$

To describe binary breakage events, Coulaloglou and Tavlarides (1977) utilized a purely statistical distribution to express the daughter size distribution, $\beta_b(d,d')$, by assuming that the function is normally distributed as reported by Valentas and Amundson (1966) and written as

$$\beta_b(d,d') = \frac{4.6}{d'^3}\exp\left[-4.5\frac{(2d^3 - d'^3)^2}{\left(d'^3\right)^2}\right] \tag{1.15}$$

However, the use of a more sophisticated beta distribution function to describe the daughter density function has been proposed by Hsia and Tavlarides (1980). This beta distribution has the advantage over the normal distribution proposed by Coulaloglou and Tavlarides (1977) in that it produces a zero probability for the infinitely small daughter drops and the daughter drops equal to the size of the mother drop (Azizi and Taweel, 2011). This beta function is expressed as

$$\beta_b(d,d') = 90\frac{d^2}{d'^3}\left(\frac{d^3}{d'^3}\right)^2\left(1-\frac{d^3}{d'^3}\right)^2 \tag{1.16}$$

Liao and Lucas (2009) gave a review about drop and bubble breakup in turbulent dispersion. The breakup of fluid particles in turbulent dispersions is influenced by the continuous phase hydrodynamics and interfacial interactions. Generally, the breakup mechanism can be expressed as a balance between external stresses from the continuous phase, which attempt to destroy the fluid particle, and the surface stress of the particle plus the viscous stress of the fluid inside it, which restores its form. This balance leads to the prediction of a maximum stable particle diameter. Therefore, the breakup of a fluid particle is determined by the hydro- dynamic conditions in the surrounding liquid and the properties of the particle. Breakup mechanisms can be classified into four main categories as: turbulent fluctuation and collision; viscous shear stress; shearing-off process; interfacial instability.

In the turbulent case, the breakup of fluid particles is caused mainly by turbulent pressure fluctuations along the surface, or by particle-eddy collisions. The particle can be assumed to modify its spherical form with the fluctuation of the surrounding fluid or due to collisions with eddies. When the amplitude of the oscillation is close to that required to make the particle surface unstable, it starts to deform and stretch in one direction leading to a neck that contracts further and fragments finally into two or more daughter particles.

Viscous shear forces in the continuous phase will cause a velocity gradient around the interface and deform the fluid particle, leading to breakup. Shear

stresses also appear due to the wake effect. If a trailing bubble or drop has its larger part outside a wake region, the shear stress across the wake boundary may split it as a result of elongation, bubble surface indentation and necking. The particle is firstly elongated into two lumps separated by a thread and breaks into two almost equal size daughters corresponding to the lumps and a series of smaller particles called satellites corresponding to the thread.

As the size of the fluid particle increases, the breakup mechanisms become further complicated by additional phenomena such as shearing-off and interfacial instability, both of which result from a velocity difference across the interface. The shearing-off process is characterized by a number of small particles sheared-off from a large one, which is also called erosive breakage. In highly viscous flows, the shearing-off is determined by the balance between the viscous shear force and the surface tension at skirts of the cap/slug bubble. When the relative velocity is high enough, bubble skirt becomes unsteady and sheds from large bubbles with the generation of a large number of small bubbles at the rim.

All the above breakup mechanisms depend on the flow dynamic characteristics in the continuous phase. However, in practice even in the absence of a net flow in the continuous phase, such as bubbles rising in a liquid and drops falling in a continuous gas or immiscible liquid, the breakup can be caused by interfacial instabilities. This includes the Rayleigh–Taylor instability, which occurs when a light liquid is accelerated into a heavy fluid, that is, where there is a density difference. When the density ratio is approximately of unity, the breakup process will be dominated by the Kelvin–Helmholtz instability.

In the past few decades, the drop rate functions given by Coulaglou and Tavlarides (1977) seem to have been the most widely used (Azizi et al., 2011; Bordás et al., 2012; Orciuch et al., 2012).

1.2.2.2 Drop coalescence

Liao and Lucas (2010) gave a review on mechanisms and models for the coalescence process of fluid particles. Together with breakup and mass transfer, coalescence is responsible for the evolution of drop and bubble sizes in multi-phase flows. Compared to breakup, coalescence is considered more complex, since it involves not only interactions of bubbles with the surrounding liquid, but

also between bubbles themselves once they are brought together by the external flow or by body forces. Generally, three theories or criteria have been proposed for the coalescence process. The most popular theory is the film drainage model. After collision, two bubbles may cohere together and be prevented from coalescing by a thin film of liquid trapped between them. Attractive forces between them drive the film to drain out until it collapses, and coalescence follows. For simplicity, the coalescence is usually divided into three manageable sub-processes: (1) two bubbles collide, trapping a small amount of liquid between them; (2) bubbles keep in contact till the liquid film drains out to a critical thickness; (3) the film ruptures resulting in coalescence. In reality, the duration of collisions is limited due to the prevailing fluctuations and coalescence will occur only if the interaction time is sufficient for the intervening film to drain out down to the critical rupture thickness. On the other hand, the attraction force between two colliding interfaces, usually of molecular nature, is too weak in comparison with the turbulent force to control the coalescence probability. Whether coalescence will occur or not depends on the impact of colliding bubbles. During ‘‘energetic collisions’’, when the approach velocity of two colliding bubbles exceeds a critical value, immediate coalescence will be the dominant mechanism without liquid film capturing and thinning.

In a more recent work, Lehr and Mewes (2001) introduced the critical approach velocity model, which is an empirical theory based on experimental observation that small approach velocities lead to high coalescence efficiency.

There are empirical and physical models for coalescence frequency. Physical models calculate the coalescence frequency from the collision frequency and the coalescence efficiency. To define the mechanisms of each collision, models have been derived based on physical quantities:

$$S_a(d,d') = h(d,d')\lambda(d,d') \tag{1.17}$$

Coulaloglou and Tavlarides (1977) derived a turbulent collision frequency model (assuming binary collisions) for drops with immobile interfaces by postulating that the mechanism of collision is analogous to collisions between molecules as described in the kinetic theory of gases. Coulaloglou and Tavlarides (1977) also presented an expression for the coalescence efficiency term. The

formula is based on the film drainage between colliding dispersed phase entities, and it is applicable to the case of deforming entities with immobile interfaces. It assumes that turbulence causes the two entities to collide and holds them together for a definite time while the intervening film thins under a constant force applied by turbulence. Coalescence will therefore only occur when the contact time of the bubbles is longer than the time required for draining the film entrapped in between them until it reaches its critical thickness.

Kamp et al. (2012) published a comparative study about modelling of coalescence in turbulent liquid/liquid dispersions. They compared the model of Coulaloglou and Tavlarides (1977) and model of Tobin and Ramkrishna (1999). They concluded that the model of Coulaloglou and Tavlarides (1977) is able to predict the experimental data better than the model of Tobin and Ramkrishna (1999).

The binary droplet collision rate is given by Tsouris and Tavlarides (1994), with only one adjustable parameter. The collision frequency (m^3/s) is defined as

$$h(d,d') = \frac{\pi\alpha^{1/2}}{\sqrt[3]{2}}\varepsilon^{1/3}(d+d')^2\left(d^{2/3}+d'^{2/3}\right)^{1/2} \tag{1.18}$$

Alopaeus et al. (1999) found that equation (1.18) gives a collision frequency several orders of magnitude greater than those of Coulaglou and Tavlarides (1977).

Nowadays these equations are the most widely used in the literature (Azizi and Taweel, 2011; Bordás et al., 2012; Orciuch et al., 2012).

The coalescence efficiency by Coulaloglou and Tavlarides (1977) is:

$$\lambda(d,d') = \exp\left[-\frac{C_{IV}\mu_c\rho_c\varepsilon}{\sigma^2(1+\phi)^3}\left(\frac{dd'}{d+d'}\right)^4\right] \tag{1.19}$$

The collision frequency without coalescence (m^3/s) is:

$$S_{col}^{dd}(d,d') = h(d,d') - S_a(d,d') \tag{1.20}$$

1.2.3 Macro-scale modelling

From meso-scale, by averaging and summarizing the properties, we can go to macro-scale. At this scale the overall mass and energy balances, the heat and mass transfer from the reactor as well as the reactor dynamics and control can be described. In the most of the suspension polymerization processes the mass transport between the continuous and dispersed phase is negligible, but the heat transport is really important from the point of view of cooling. The macro-scale model can be applied for design of the control system of the polymerization reactor (Kiparissides, 1996).

PVC is produced in batch reactors and the end-use polymer properties are influenced by operational parameters of the reactor: for example the polymerization temperature, stirring conditions, reactor size, type of suspending agents, concentration, in addition to the type and number of initiators. The temperature of polymerization is one of the most important parameters. Only 1 or 2 °C differences in temperature can induce significant changes in the properties of polymer products. The product is characterized by Fikentscher K-value, this is a number related to the average molecular weight, molecular weight distribution, particle diameter, particle size distribution and porosity. Because all of these parameters are influenced by temperature, one of the most important operational parameter is the temperature. Tight control of the temperature is required for the reactor to produce high quality product, which is in the form of PVC powder (Nagy and Agachi, 1997).

The suspension polymerization of VCM is a discontinuous process. The physico-chemical properties are changing during the batch, important changes of the heat and mass transfer are taking place, and thus the control of the temperature becomes difficult. The disturbances occurring during the batch, especially polymerization, present many challenging control problems including nonlinear dynamic behaviour. At the moment of maximum rate of reaction, the removal of heat is very difficult due to the increased viscosity of the reaction mixture and the polymer deposit on the inner walls of the reactor. In this situation, the system may become unstable, especially if there are additional disturbances (e.g. variable temperature of the cooling medium). The polymerization is a batch process, there

is no steady state operating point. For this reason, the step response of the system depends on the moment at which the identification of the uncontrolled process is initiated. The constraint imposed is a variation of temperature of maximum ± 0.5 °C around the set point in order to ensure the proper quality of the product (Nagy and Agachi, 1997).

The first step of the realization of a good temperature control system is to develop a suitable macro-scale mathematical model of the reactor. Since PVC is produced in stirred tanks, we can take the following simplification:

- The temperature distribution of the continuous phase is homogeneous, i.e. that the temperature of continuous phase is the same everywhere inside the reactor.

Generally, the temperature of the continuous phase can be described by the following equation, since the reactions take place in the dispersed phase, and they are exothermic:

$$V_c \rho_c c_{p_c} \frac{dT_c}{dt} = \dot{Q}_{trans\_d} - \dot{Q}_{trans\_j} \tag{1.21}$$

where Q_{trans_d} is the heat transfer from dispersed phase and Q_{trans_j} is the heat transfer to the cooling jacket.

$$\dot{Q}_{trans\_d} = h_{dc} \cdot a_{dc} \cdot (T_d - T_c) \tag{1.22}$$

where h_{dc} is the heat transfer coefficient between the dispersed and continuous phase, a is the heat transfer surface area, T_d and T_c are the temperature of the dispersed and continuous phase, respectively. The heat transfer coefficient is influenced by a number of physical properties of the phases like the viscosity and the density, the stirring speed and type of agitator.

$$\dot{Q}_{trans\_j} = U \cdot A \cdot (T_c - T_j) \tag{1.23}$$

where U is the overall heat transfer coefficient, A is the heat transfer area, T_j is the temperature of cooling jacket. The overall heat transfer coefficient is employed in calculating the rate of heat transfer from one fluid at an average bulk temperature T_1 through a solid surface to a second fluid at an average bulk temperature T_2 (where $T_1 > T_2$). In case of heat transfer across a plane wall of uniform thickness, U is related to the individual film heat transfer coefficients, h_v and h_j, of the two fluids by the equation:

$$U = \frac{1}{\frac{1}{h_v} + \frac{d_w}{k_w} + \frac{1}{h_j}} \tag{1.24}$$

where d_w is the thickness of the wall and k_w is the thermal conductivity of the wall (Sinnott, 2005).

For calculation of the overall heat transfer coefficient, first the heat transfer coefficient to the vessel wall has to be calculated. For agitated vessels, the correlation used to estimate the coefficient of heat transfer to the vessel wall is (Sinnott, 2005):

$$Nu = C \cdot \mathrm{Re}^a \cdot \mathrm{Pr}^b \cdot \left(\frac{\mu}{\mu_w}\right)^c \tag{1.25}$$

In detail:

$$\frac{h_v \cdot D}{k_f} = C \cdot \left(\frac{N \cdot D^2 \cdot \rho}{\mu}\right)^a \cdot \left(\frac{c_p \cdot \mu}{k_f}\right)^b \cdot \left(\frac{\mu}{\mu_w}\right)^c \tag{1.26}$$

where h_v is the heat transfer coefficient to vessel wall or coil, D is the agitator diameter, N is the agitator speed, ρ is the liquid density, k_f is the liquid thermal conductivity, c_p is the liquid specific heat capacity and μ is the liquid viscosity. The values of C (a constant) and the indices a, b and c depend on the type of agitator, the use of baffles, and whether the transfer is to the vessel wall or to coils (Sinnott, 2005). The heat transfer coefficient to the jacket can be calculated by a similar method. Using Eq.1.24, and the overall heat transfer coefficient for the reactor can be calculated.

The molecular properties of the polymer (e.g. MWD, CCD, DBD) produced in continuous polymerization reactors will strongly depend on both the macroscopic mixing of different volume elements (e.g. residence time distribution) and microscopic molecular scale mixing (e.g. the state of fluid aggregation). When the polymerization kinetics is known, these effects can, in principle, be calculated.

1.3. Modelling of micromixing in turbulent, non-isothermal continuous stirred reactors

Beside batch reactors, continuous stirred reactors are widely used in chemical and metallurgical industries, since they can provide excellent mixing performance for gas dispersion, solid suspension and chemical reaction. The interaction of rotating impellers with stationary baffles produces complex and highly 3 dimensional turbulent flow with quasi-periodicity. Modelling of reactive flows is an arduous task due to its high inter-disciplinary nature. For example, a good understandings of turbulence (more often in multiphase systems), mixing, chemistry, and in particular, the interactions among them are necessary.

Mixing is an important elementary process in chemical engineering, and its effects are especially important when scaling up equipment involved with chemical reactions. For many reactions in a bench-scale vessel, strong stirring is easily available to guarantee good mixing, however, for commercial scale units, mixing problems are most likely encountered and sometimes can be severe. This is because the local hydrodynamics in industrial vessels may be very different from that in smaller ones, and the mixing time is typically much larger, making the same reactions more difficult to carry out, and to reach the technical-economical specifications obtained in bench-scale devices. Hence, the key factor is mixing, in particular the mixing on micro-scales. Intensive studies on mixing, especially on micro-mixing, in stirred tanks are of great significance to the design, optimization and scale-up (or scale-down) of this type of reactors (Cheng et al., 2012).

Mixing at molecular scale (micromixing) can intensively influence the selectivity, yield and quality of final products in many chemical processes, such as polymerization, crystallization, and organic synthesis (Baldyga and Bourne, 1990; Judat et al., 2004; Fourcadea et al., 2001). For better control of the chemical reactions, a significant amount of work has been carried out on micromixing processes, from stirred tanks (Martín et al., 2008; Nouri et al., 2008) to static mixers (Fang and Lee, 2001).

To evaluate the micromixing performance, many methods have been developed over the past decades. Among them the chemical reaction methods (Fournier at al., 1996; Baldyga and Bourne, 1990) are commonly used.

In reactive flow systems, the importance of mixing can be best represented by comparing its characteristic time scales with those of chemical reactions (Cheng et al., 2012). As illustrated in Fig.1.2, the largest flow time scale is the recirculation time t_{cir}, which lies generally between the average residence time t_{res} and the turbulence integral time scale t_u, and the smallest one is the Kolmogorov time scale t_η. The time scale of macro-mixing t_{macro} is generally equivalent to t_{cir} (if dead zones exist, t_{macro} may be one magnitude larger than t_{cir}). Time scale of micro-mixing, t_{micro} is generally on the same magnitude as t_u. Thus, mixing is closely related to the flow. Based on the relationship between the time scales of reactions and flows, reactive flow systems can be roughly classified into three zones, i.e., the kinetic-controlling zone, the overlapping zone and the mixing-controlling zone, as shown in Fig. 1.2.

The methods using mixing sensitive chemical reactions as molecular probes can be classified into three schemes: single reaction (A+B→R), consecutive competing reactions (A + B→R; R+B→S), and parallel competing reactions (A + B→R; C+B→S). Recently, “Villermaux/Dushman” method (also known as the iodide–iodate method) (Guichardon and Falk, 2000; Guichardon et al., 2000) has been mostly used for micromixing characterization (Kunowa et al., 2007; Baccara et al., 2009; Yang et al., 2006). Kölbl et al. (2008) applied this method to characterize multi lamination-type mixers. Mixing sensitive results were obtained at various operating conditions.

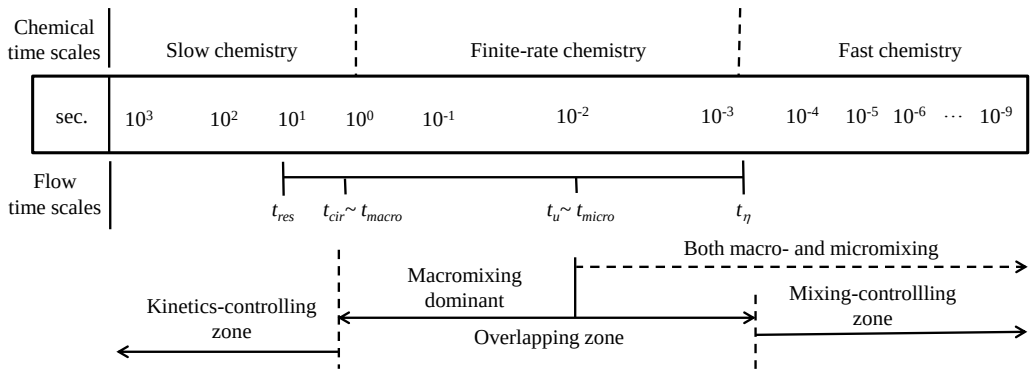

Figure 1.2. Characteristic time scales of chemical reactions and typical turbulent flows (Cheng et al., 2012)

Let's assume that species A and B are fed into a tank separately to react to form R, i.e., A + B→R. All the possible states of mixing (before reaction occurs) are summarized in Fig.1.3, whether or not they are realistic. The most desired case is the well macro-mixed and well micro-mixed (Fig.1.3.a), which may exist for very slow reacting systems. For the poorly macro-mixed and totally segregated case (Fig.1.3.e), reactions cannot take place at all. The well macro-mixed and partially segregated state (Fig.1.3.c) is physically unrealistic as the macro-mixing time is generally larger than that of micro-mixing, however it is commonly used to derive micro-mixing models in a Lagrangian framework. The poorly macro-mixed and well micro-mixed case (Fig.1.3.b) cannot exist since good micro-mixedness certainly assumes well macro-mixedness. However, it was commonly used in the RTD (residence time distribution) theory. For many fast or quasi-instantaneous reactions, the most likely state is the poorly macro-mixed and partially segregated (Fig.1.3.d), for which the spatial distribution of species average concentrations and the degree of segregation must be described properly.

For modelling the mixing at molecular scale the coalescence/redispersion (CR) model may be used. This model has been proposed by Harada et al. (1962) and Curl (1963), and formulated also in Monte Carlo form by Spielman and Levenspiel (1965), has been a successful tool of characterising micromixing processes. This model represents the fluid as a population of large number of fluid elements which interact with each other by random pair-wise coalescence, instantaneous concentration homogenization and subsequent redispersion into identical pairs. Evangelista et al. (1969)extended this model for several chemical species. A non-isothermal CR model was applied by Sheikh and Vigil (1998), while Lakatos et al. (1999), Lakatos and Ulbert (2001) and Ulbert and Lakatos (2005) applied the CR model to describe micromixing in solution crystallization developing a two population model.

In deterministic case, total concentration equalization occurs in each CR event so that this model involves only a single parameter, i.e. the frequency coefficient of interactions between the fluid elements.

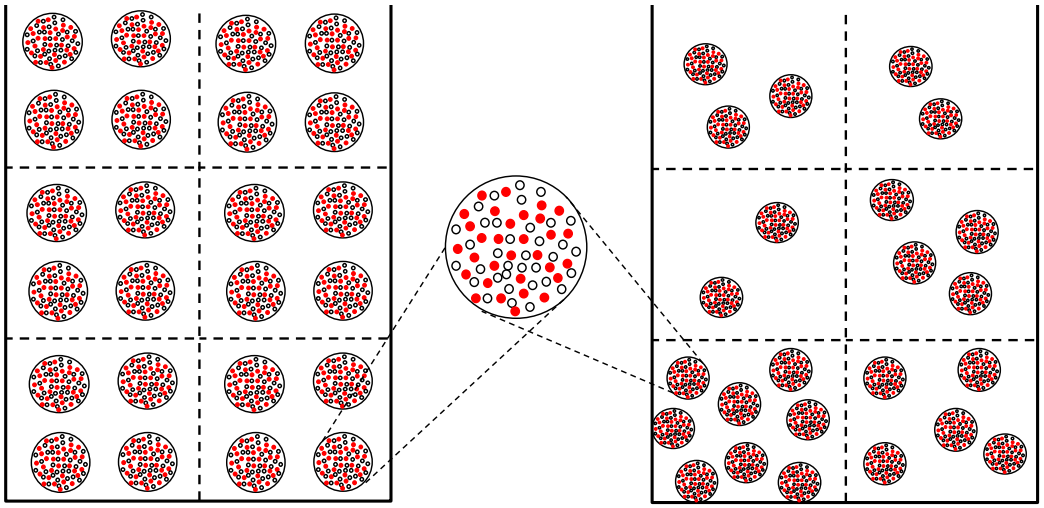

a, Well macro-mixed and well micro-mixed

b, Poorly macro-mixed and well micro-mixed

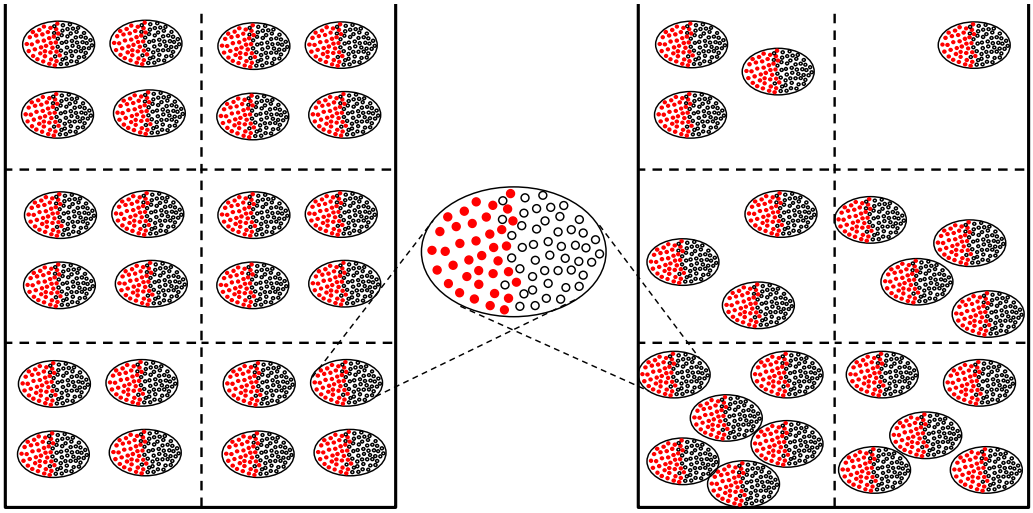

c, Well macro-mixed and partially segregated

d, Poorly macro-mixed and partially segregated

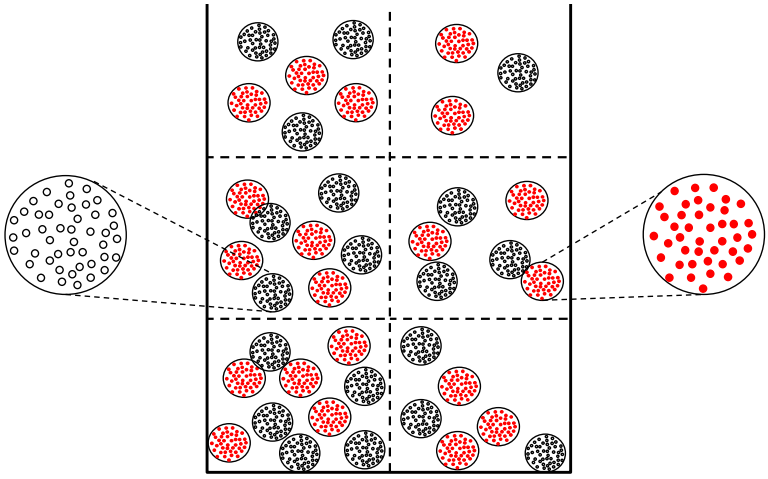

e, Poorly macro-mixed and totally segregated

A molecule; B molecule; A-rich fluid element; B-rich fluid element

Figure 1.3. Different state of mixing (Cheng et al., 2012)

In versions involving random events, proposed by Janicka et al. (1979) and Dopazo (1979), and generalized by Pope (1982) for closing the mixing terms in the transported PDF models, the mass exchange process is modulated with a random variable evenly distributed in the interval [0,1]. In these models, therefore, all chemical species have the same micromixing rate. An extension of the CR model, making possible different micromixing rates for different chemical species, was proposed by Lakatos (2008) deriving the generalized coalescence/ redispersion model using the concept of transition measures of interactive populations of disperse systems Lakatos et al. (2006) and formulated in the framework of population balance approach.

A detailed study of a continuous stirred tank reactor (CSTR) combined with the generalized coalescence/redispersion model of micromixing was presented by Lakatos et al. (2011). Applying the population balance approach, fluid elements are identified as Kolmogorov microscale eddies under the given turbulence conditions, assumed to be generated in the eddy space by the energy cascade process. An infinite order multivariate moment equation model is derived for the joint moments of chemical species from which a second order moment equation reduction is obtained using the cumulant-neglect closure. The properties of the reactor model and the effects of micromixing on chemical reactions the time evolution of which can be described by tracking two chemical species are studied by simulation, comparising completely micromixed and totally segregated reactors in limiting cases of mixing.

1.4. Solution of the multi variable population balance equation

In many cases polymerization reactors are assumed to be perfectly mixed on macro-, meso-, and microscale. But in suspension polymerizations, where a highly active initiator is fed into the monomer droplets, the polymerization rate can be entirely determined by micromixing. If we would like to analyse the effects of interactions between droplets, we need to solve the mesoscale population balance equation.

Population balance equations (PBE) contain external time and location coordinates as well as internal entity property coordinates, the source term of

which usually involves single or multi-integrals. As the form of PBE is very complex and analytical solutions are available only for the simplest cases, numerical techniques are required in most practical applications (Su et al, 2007). A comparative study between the different techniques is given in Alexopoulos et al. (2004), Alexopoulos and Kiparissides (2005), and Roussos et al. (2005). Using any of these methods to solve multidimensional problems quickly becomes a challenging task.

The multiphase flow models fall into two categories according to the simulation methodology of the discrete phases. In an Eulerian or in a Lagrangian reference frame, these are the two-fluids models (Eulerian–Eulerian models) or the fluid-trajectory models (Eulerian–Lagrangian models). Similarly, the numerical methods of PBM can be divided into deterministic and stochastic ones (Zhao and Zheng, 2013).

In deterministic methods, the differential equations of the population balance equations (PBEs), are directly solved through numerical integration using appropriate techniques, e.g., a discretization scheme towards particle size distribution (as in (discrete)-sectional methods) and a presumed monodisperse or log-normal PSD (as in moments methods). In contrast to deterministic integration, stochastic methods utilize the Monte Carlo (MC) method to simulate the evolution of a finite sample of the particle population.

The deterministic methods for PBM are based on the Eulerian reference frame and the PBE can be solved by ODE (ordinary differential equation) solvers together with the conservation equations of multiphase flows. Consequently, these methods are capable of coupling hydrodynamics with the Eulerian–Eulerian models.

The most popular solution methods for single variable population balance equation are the methods of classes (Kumar and Ramkrishna 1996a,b; Vanni, 2000), the method of moments (McGraw, 1997; Rong et al., 2004), the quadrature method of moments (McGraw and Wright, 2003; Marchisio et al., 2003a,b), the direct quadrature method of moments (Marchisio and Fox, 2005) and the standard method of moments using the cumulant-neglect closure (Lakatos et al., 2011; Lakatos, 2011, Ulbert and Lakatos, 2007). Among the discretization techniques,

the fixed and moving pivot technique of Kumar and Ramkrishna (1996a,b) is quite useful for the solution of 1-d PBEs due to its simplicity and robustness (Vanni, 2000; Attarakih et al., 2004; Roussos et al., 2006).

In the class method (CM), the continuous range of the internal size coordinate is partitioned into a finite series of contiguous subintervals or bins. High accuracy can be achieved if a large number of size groups are used, but at the expense of high CPU cost due to increased number of variables to be solved for. The number of classes is a potential problem in computational fluid dynamics (CFD) applications, especially when a multi-fluid flow model needs to be used; hence the CM method is not a feasible approach in practice. In method of moments (MOM), instead of the particle size distribution (PSD) its moments are integrated over the internal coordinates. This approach has many advantages such as low CPU time and relatively high accuracy. The standard method of moment (SMM) needs to be closed which limits its practical application. McGraw (1997) introduced the Gaussian quadrature approximation for PSD which closes the SMM, and proposed the quadrature method of moments (QMOM). QMOM has been widely used for PBE (Marchisio et al., 2003a,b; Wang et al., 2005a,b), and has been extended to bivariate PBE applications (Wright et al., 2001, Yoon and McGraw, 2004a,b). However, with this approach it is difficult to handle systems where there is a strong dependence of the dispersed-phase velocity on internal coordinates (e.g. fluidized bed or bubble column), and the approach can become quite complex in the case of bivariate PBE (Marchisio and Fox, 2005). The direct quadrature method of moments (DQMOM) was proposed by Rong et al. (2004) which can be extended to multi-variable application in a straightforward manner (Rong et al., 2004) and has considered different characteristic lengths with different velocities. Because DQMOM uses different phases to distinguish characteristic lengths, it is more time-consuming than QMOM when coupled with CFD. The accuracy and time consumption of MOM depend largely on the relative magnitude of the moments. The matrix becomes extremely difficult to solve if the moments vary over a large range. In such cases, solution of differential equations and product-difference (PD) algorithms in QMOM or matrix inversion in DQMOM would require excessive computational resources. When the source

term of PBE is too large, negative weights or abscissas may appear in the simulations, which do not have physical meaning and will cause the computation to abort. In FPT, the continuous particle population is discretized into bins, and represented through representative volumes called pivots, one for each bin. The non-pivot particles formed through breakup and/or aggregation of particles located on pivots are represented through pivots adjoining non-pivot particles.

Furthermore, the deterministic PBM method cannot gain information about history, trajectory crossing and internal structure of particles. The deterministic PBM method is also less sensitive to the innate fluctuations for dynamic processes which are also stochastic in nature. Besides, the deterministic PBM methods are generally formulated by complicated mathematical equations, and have at the disadvantage of modelling more than two particle properties (such as size, chemical composition, surface area, and charge level).

For numerical solution of the multi-variable population balance equation there are more techniques in the literature, such as finite difference methods, spectral methods, finite element methods (Mantzaris et al., 2001a,b,c), discretisation techniques (Nandanwar and Kumar, 2008; Pinto et al., 2008), the hierarchical two-tier technique (Immanuel and Doyle, 2005). But all these techniques are useful for the 2-dimensional population balance model. The finite difference method, spectral method and finite element method are members of class methods. The hierarchical two-tier technique is based on a finite-element discretization of the particle population and tracks the total particles within each of the bins. The equation representing the total particles within each bin can be derived from the population balance equation in a straight-forward manner (partial analytical solution).

On the other hand, the stochastic methods for PBM (such as Monte Carlo techniques) are able to simulate any number of particle properties and are easily programmed. Monte Carlo methods (MCM) (Smith and Matsoukas, 1998; Tandon and Rosner, 1999) are based on the solution of PBE in terms of its stochastic equivalent. A population of particles undergoes the “real” physical processes, and events occur according to the appropriate probabilities. In order to reduce the statistical error, a very large number of particles must be used. Due to limitations

on the computational resources, the full incorporation of MCM into CFD codes is still intractable (Rong et al., 2004). Although the population balance-Monte Carlo (PBMC) methods exhibit relatively higher computational expense due to the large number of simulation particles that need to be tracked in order to provide a statistically reasonable representation of the physics, the high-speed development of computer hardware (CPU and memory) and parallel computing motivates their practical applications. As the PBMC methods are methodically closer to the Lagrangian approach, they are more suitable for coupling into the Eulerian–Lagrangian models to obtain the spatiotemporal evolution of particle population. There are many efficient Monte Carlo algorithms which can deal with multiple state variables in a natural way (Tandon and Rosner, 1999; Efendiev and Zachariah, 2002), and can be used for solution of population balance equations (Gillespie, 1977; Garcia et al., 1987; Liffman, 1992; Maisels et al., 2004; Smith and Matsoukas, 1998; Ramkrishna, 2000; Meimaroglou and Kiparissides, 2007; Oullion et al., 2009; Marshall et al., 2013). These methods utilize an artificial realization of the population dynamics of a finite system (finite number of particles in a very small volume) to estimate the properties of the whole system. The estimate becomes exact as the number of particles approaches infinity.

Based on the method employed for the determination of the sampling time step, MC simulations can be grouped into time-driven (Liffman, 1992; Debry et al., 2003) and event-driven ones (Garcia et al., 1987; Smith and Matsoukas, 1998; Tandon and Rosner, 1999; Kruis et al., 2000; Efendiev and Zachariah, 2002).

In time-driven simulation a time step is specified, and then the simulation implements all possible events within that step. In event-driven, first an event is implemented, and then the time is advanced by an appropriate amount.

With regard to the total number of simulated particles, MC methods can be further classified into constant number and constant volume MC methods. In the classical approach, the simulation tracks a constant reaction volume in which the number of particles varies depending on the mechanisms that transform the particle distribution. A practical difficulty with this implementation is that prolonged simulation causes a number of particles to exceed the bounds of the simulation box, e.g. when coagulation reduces the number of particles to one, or

when fragmentation produces more particles than the size of the simulation box. This problem can be avoided by “regulating” the number of particles, periodically or continuously, to maintain the number of simulated particles within bounds.

A more detailed description of the characteristics of the various MC formulations can be found in a number of publications (Maisels et al., 2004; Meimaroglou et al., 2006; Zhao et al., 2007).

MC methods are widely used for solution of PBE of liquid-liquid dispersions. There are many applications for describing the particle size distribution in dispersed system (Das, 1996; Mishra, 2000; Smith and Matsoukas, 1998; Lin et al, 2002; Maisels et al, 2004; Meimaroglou et al, 2006; Zhao and Zheng, 2009; Zhao et al., 2010). Furthermore, MC method is applied for modelling polymerization (Platkowski and Reichert, 1999) and crystallization reactions (Haseltine et al., 2005). However, there are cases when reactions take place in a dispersed phase. For example during suspension polymerization, the polymerization reactions take place in the monomer droplets which can collide with each other or break up. In this case, both continuous processes (polymerization reactions) and discrete event processes (aggregation, breakage and coalescence/ redispersion) occur in parallel, thus the solution of the system of equations requires a special technique: combination of a continuous time and discrete event treatment. This phenomenon was studied by Salikas et al. (2008) but they have not described the problem explicitly. They investigated the free radical suspension polymerization of methyl methacrylate. In their algorithm, the initial droplet-diameter distribution was assumed to follow a normal distribution. A typical sample population usually contains about 10^3-10^5 droplets. The MC algorithm has been initiated and the effects of droplet coalescence and breakage have been simulated. At the beginning of every time step, two consecutive decisions were made, using a random number generator. First, the type of event that will take place; in the next infinitesimal time interval, a specific droplet or pair of droplets that will undergo breakage or coalescence, are chosen from the sample population. In their Monte Carlo method the calculation of polymerization reactions were not introduced.

Irizzary (2008a,b) studied a case when there are chemical reactions in the dispersed phase. In their work, a parallel-competitive reaction takes place in droplets. At the beginning all droplets contain A or B reactants. When the droplets coalesce, the resulting droplets serve as micro-reactors. To simplify the model formulation, it is assumed that:

- Mixing is perfect when coalescence occurs.
- Both reactions are very fast, that is, conversion is instantaneous after coalescence.
- The first reaction is much faster than the second reaction, and both reactions are much faster than the coalescence rate.

He applied the point ensemble Monte Carlo method for solution of population balance equation. He defined a simulation volume and the standard simulation box is partitioned in sub-ensembles of particles with characteristic volume. For the calculation of the next event time the probabilities of all events are calculated. From these probabilities the next event is chosen by generating a random number. Three events are taken into consideration, namely coalescence, nucleation and binary breakage.

2. The detailed population balance model for suspension polymerization

In liquid-liquid dispersions there are two immiscible liquid, for example in suspension or emulsion polymerization. The physical conditions in a suspension polymerization reactor affect the drop size distribution significantly. Drop size depends on the physical properties of the two phases, the phase ratio, the nature of the suspension flow, and the condition of the phase interface. Drop breakage in agitated suspensions can be caused either by frictional forces (through viscous shear) or by inertial forces (through turbulence) (Brooks, 2010). In industrial suspension polymerization, the volume fraction of the dispersed phase is usually high and drop breakup is accompanied by drop coalescence. Thus, the average drop size and the drop size distribution are both influenced by drop breakage and drop coalescence. Thus, the framework of population balances is ideally suited to the description of the complex dynamics of particulate polymerization processes (Kiparissides, 2006).

2.1. The general population balance equation

Population balance models for modelling suspension and emulsion polymerization were applied by Kotoulas and Kiparissides (2006), Alexopoulos and Kiparissides (2007), Kiparissides (2006), Alvarez et al. (1994), Hosseini et al (2012) or Vale and McKenna (2005). All these models have taken into account simply the drop size distributions and its variation. However, in suspension polymerization, because of changes of droplet volume, the concentrations of species and even the temperature of droplets are important thus the population balance equation becomes, in principle, multi-variable.

In this work, the following assumptions were made during the model development:

1. The continuous phase, usually water, is turbulent and homogeneous. This means that on macro scale the reactor is perfectly mixed. In the continuous phase the heat transport is limitless. Monomer solubility in the continuous phase is often very low, therefore there is no component transport between the continuous and dispersed phase.

2. The distribution of dispersed phase is uniform in the continuous phase and the droplets have an initial size distribution.

The following meso-scale interactions were taken into consideration.

1. Droplets: During suspension polymerization, the polymerization reactions take place in the dispersed phase, which means that all monomer droplets work as a micro stirred tank reactor. During polymerization, there are phase changes (monomer to polymer) in the droplets, and volume, concentration and temperature changes occur due to the polymerization reactions. These reactions are highly exothermic, dominantly the propagation reactions.
2. Droplets and continuous phase: There occurs distribution of stabilizers and initiator in droplets. There is heat transport from droplets to the continuous phase. The breakage of droplets takes place due to eddies of continuous phase.
3. Droplets and droplets: There is mass and heat transport due to collisions, as well as coalescence with each other, if the balance of forces allows.

Therefore, analysis of the size distribution of droplets needs to be considered together with the concentration, temperature and other properties of droplets during the process. Nevertheless, the droplets break-up and coalesce continuously in the turbulent flow field. Thus, these processes of droplets proceeds parallel with polymerization inside the droplets.

In line with the basic principles of the population balance approach (Hulburt and Katz, 1964, Ramkrishna, 2000) a destination between the external and internal properties of fluid elements has been made, namely: a fluid element property that remains unchanged even when the fluid element disappears is called external. Properties associated with the existence of fluid elements are called internal.

Most of the suspension polymerization processes take place with free-radical mechanism. When analysing the properties of the polymer product in addition to tracking the changes of concentrations of the initiator and monomer it is reasonable to compute the first three leading moments of the live and dead polymer chains. This formulation requires eight variables and eight differential equations and provides a sufficiently detailed description of polymerization reactions. In addition to the eight-element concentration vector there is the volume

coordinate of droplets and the temperature of droplets. Altogether, it makes 10 internal coordinates and 3 external coordinates. Therefore we have a 10+3 dimensional droplets distribution function $n(\xi,t)$ to be defined over a region ξ. The number of droplets existing at any time t in a small incremental region of disperse phase space $d\xi$ can be represented by

$$dN = nd\xi \tag{2.1}$$

while the total number of droplets present in some finite subregion of disperse phase space ξ_1 is

$$N(\xi_1) = \int_{\xi_1} nd\xi \tag{2.2}$$

The population balance for an ensemble of droplets in ξ_1 can be written from Langrangian perspective as (Tavare, 1995)

Accumulation = Input – Output + Net generation

$$\frac{d}{dt}\int_{\xi_1} nd\xi = \int_{\xi_1} \frac{Q_{in}n_{in}}{V} d\xi - \int_{\xi_1} \frac{Q_{out}n_{out}}{V} d\xi + \int_{\xi_1} (B-D)d\xi \tag{2.3}$$

where B and D represent empirical birth and death density functions at a point in the phase space and $(B-D)d\xi$ is the net appearance rate of droplets. V is a suitable constant solvent capacity of external phase space having input and output of flow rates, Q_{in} and Q_{out} and population densities, n_{in} and n_{out}.

Applying Leibnitz's rule on the left-hand side of Eq.(2.3) we get the following expression:

$$\frac{d}{dt}\int_{\xi_1} nd\xi = \int_{\xi_1} \frac{\partial n}{\partial t} d\xi + \left(n\frac{d\boldsymbol{x}}{dt} \right)\Bigg|_{\xi_1} = \int_{\xi_1} \left[\frac{\partial n}{\partial t} + \nabla \bullet \left(\frac{d\boldsymbol{x}}{dt} n \right) \right] d\xi \tag{2.4}$$

where $\boldsymbol{x}$ is the set of internal properties and external spatial coordinates comprising the disperse phase space ξ. Using the definition of disperse phase space velocity as

$$\frac{d\boldsymbol{x}}{dt} = \boldsymbol{v} = \boldsymbol{v}_e + \boldsymbol{v}_i \tag{2.5}$$

the population balance from the Lagrangian viewpoint over ξ_1 is:

$$\int_{\xi_1} \left[\frac{\partial n}{\partial t} + \nabla \bullet (\boldsymbol{v}_e n) + \nabla \bullet (\boldsymbol{v}_i n) + D - B \right] d\xi = 0 \tag{2.6}$$

Since ξ_1 is arbitrary, the integrand must vanish everywhere. Thus, the population balance is given as

$$\frac{\partial n}{\partial t} + \nabla \bullet (\boldsymbol{v}n) + D - B = 0 \tag{2.7}$$

Eq.(2.7) is the universal population balance model for a droplet population (Tavare, 1995). Substituting the 10+3 coordinates of suspension polymerization of vinyl chloride

$$\frac{\partial n}{\partial t} + \frac{\partial (v_x n)}{\partial x} + \frac{\partial (v_y n)}{\partial y} + \frac{\partial (v_z n)}{\partial z} + \frac{\partial (\upsilon n)}{\partial \upsilon} + \frac{\partial (Tn)}{\partial T} + \frac{\partial (\boldsymbol{c}n)}{\partial \boldsymbol{c}} + D - B = 0 \tag{2.8}$$

Where $\boldsymbol{c}=(c_1,c_2,c_3,c_4,c_5,c_6,c_7,c_8)$ is the concentration vector of components.

In many engineering problems the liquid-liquid suspensions are generally well mixed. In such cases, the main concern is not the spatial variation but the description of the system in terms of droplet size distribution in the internal phase space. For a suitable constant solvent capacity (V) of external phase space having optional number of inputs and outputs of flow rates, Q_k and population density, n_k, the population balance can be integrated over this region. The resulting space-averaged population balance equation can be written as

$$\frac{\partial n}{\partial t} + \frac{\partial (\upsilon n)}{\partial \upsilon} + \frac{\partial (Tn)}{\partial T} + \frac{\partial (\boldsymbol{c}n)}{\partial \boldsymbol{c}} = B - D - \sum_k \frac{Q_k n_k}{V} \tag{2.9}$$

The macroscopic population balance, as simplified in Eq.(2.9), is averaged in the external phase space and distributed in the internal phase space.

In this work a batch suspension polymerization reactor is studied where there are no inlet and outlet streams; therefore the last term on right hand side of Eq.(2.9) is zero. Terms on the left hand side of the population density function are the rates of change due to the deterministic continuous processes, while the ones on the right hand side are due to the stochastic discrete event processes. D and B represent the changing of internal coordinates in the discrete events. These events are the breakage of droplets, the collision of droplets with coalescence and the collision of droplets without coalescence (coalescence/redispersion).

2.2. Birth and Death functions

Birth and death events of the latter type are generally consequence of droplet breakage and/or aggregation processes. Thus at first, the nature of the birth and death rates of droplets will be considered.

2.2.1. Breakage processes

Although the term "breakage" would seem to connote mechanical fracture of droplets it will be applied not only to systems in which droplets undergo random breakage, but also to those in which new droplets arise from existing droplets by other mechanisms. Thus, cell division by asexual means constitutes an example of such a process. The underlying assumption is that the breakage of droplets is independent from each other. Consequently, it would seem that breakage of a droplet resulting from collision with other droplets would not qualify for discussion here. However, commination operations in which droplets are in intimate contact with each other have been traditionally modelled using the methodology to be outlined here. The justification for this treatment may come from viewing the environment of each droplet as an average medium of droplets transmitting forces and leading to droplet breakup.

Let $\boldsymbol{M_b}$ denote the operator of the breakage event. We assume that $\boldsymbol{M_b}$ may be expressed as the difference between a “source” term $\boldsymbol{M_b^+}\left[n(\upsilon,\boldsymbol{c},T,t)\right]$ and a “sink” term $\boldsymbol{M_b^-}\left[n(\upsilon,\boldsymbol{c},T,t)\right]$, both due to breakage processes. Let us assume that during breakage processes the concentration and temperature of droplets do not change only their volume does. The breakage processes are described as

$$\boldsymbol{M_b}\left[n(\upsilon,\boldsymbol{c},T,t)\right]=\boldsymbol{M_b^+}\left[n(\upsilon,\boldsymbol{c},T,t)\right]-\boldsymbol{M_b^-}\left[n(\upsilon,\boldsymbol{c},T,t)\right] \tag{2.10}$$

It is assumed that breakup of particles occurs independently of each other. Let S_b be the specific breakage rate of droplets of state $(\upsilon,\boldsymbol{c},T)$ at time t. It represents the fraction of particles breaking per unit time. Then we have

$$\boldsymbol{M_b^-}\left[n(\upsilon,\boldsymbol{c},T,t)\right]=S_b(\upsilon,\boldsymbol{c},T,t)n(\upsilon,\boldsymbol{c},T,t) \tag{2.11}$$

Eq.(2.11) gives the average number of droplets in state $(\upsilon,\boldsymbol{c},T)$ disappearing by breakage per unit time. In order to characterize the source term, the following quantities are taken into account:

$\beta_b(\upsilon,\boldsymbol{c},T|\upsilon',\boldsymbol{c}',T',t)$ denotes the probability density function with respect to state $(\upsilon,\boldsymbol{c},T)$ for droplets from the breakup of droplets in state $(\upsilon',\boldsymbol{c}',T')$ and time t. This is a continuously distributed fraction over droplet state space.

$\nu(\upsilon',\boldsymbol{c}',T',t)$ denotes the average number of droplets formed from the breakup of a single droplet in state $(\upsilon',\boldsymbol{c}',T')$ at time t.

Collectively, the functions $S_b(\upsilon,\boldsymbol{c},T,t)$, $\beta_b(\upsilon,\boldsymbol{c},T|\upsilon',\boldsymbol{c}',T',t)$ and $\nu(\upsilon',\boldsymbol{c}',T',t)$ may be referred to as the breakage functions. The function $S_b(\upsilon,\boldsymbol{c},T,t)$ has the dimensions of reciprocal time and often is called breakage frequency. Sometimes it is referred to as the transition probability function for breakage. In the definition of this function is the implicit assumption that breakage, when it occurs, is an instantaneous process. By "instantaneous" we imply a time scale small enough compared with that in which the particle state changes or (in the cases where particle state does not vary with time) with the time scale used for observing the population (Ramkrishna, 2000).

The average number of droplets formed by breakage of a droplet in state $(\upsilon',\boldsymbol{c}',T')$ at time t is frequently known. It has a minimum value of 2 but, being an average number, is not restricted to integer values. In contrast, for microbial populations binary division by cells causes the property values of υ restricted to 2. The source term for droplets in state $(\upsilon,\boldsymbol{c},T)$ originating from breakup is

$$\boldsymbol{M}_b^+[n(\upsilon,\boldsymbol{c},T,t)] = \\ = \int_{T_{\min}}^{T_{\max}} \int_0^{\boldsymbol{c}_m} \int_0^{\upsilon} S_b(\upsilon,\boldsymbol{c},T,t) n(\upsilon,\boldsymbol{c},T,t) \nu(\upsilon',\boldsymbol{c}',T',t) \beta_b(\upsilon,\boldsymbol{c}',T'|\upsilon',\boldsymbol{c}',T',t) d\upsilon\, d\boldsymbol{c}\, dT \tag{2.12}$$

Consequently, the breakage processes of droplets in state $(\upsilon,\boldsymbol{c},T)$ can be described as:

$$\boldsymbol{M}_b[n(\upsilon,\boldsymbol{c},T,t)] = \\ = \int_{T_{\min}}^{T_{\max}} \int_0^{\boldsymbol{c}_m} \int_0^{\upsilon} S_b(\upsilon,\boldsymbol{c},T,t) n(\upsilon,\boldsymbol{c},T,t) \nu(\upsilon',\boldsymbol{c}',T',t) \beta_b(\upsilon,\boldsymbol{c}',T'|\upsilon',\boldsymbol{c}',T',t) d\upsilon\, d\boldsymbol{c}\, dT - \\ - S_b(\upsilon,\boldsymbol{c},T,t) n(\upsilon,\boldsymbol{c},T,t) \tag{2.13}$$

2.2.2. Aggregation processes

Aggregation processes are the events in which two or more droplets may be involved. Aggregation processes occur commonly in nature and in engineering processes. Coalescence occurs between bubbles or droplets in a diverse variety of dispersed phase systems arising in industrial processes. Coalescence may occur if drops adhere for a sufficient time to allow them to deform, and to permit drainage of the continuous phase that is trapped between them. Aggregation must occur at least between two particles, although in very crowded systems, it is conceivable that several adjacent droplets could simultaneously aggregate. In sufficiently dilute systems only binary aggregation is significant. Additionally, aggregation includes a variety of processes ranging from coalescence, in which two droplets completely merge along with their interiors, to coagulation, which features a "floe" of droplets loosely held by surface forces without involving physical contact. In intermediate situations, droplets may be in physical contact with each other without merging their interiors. The above details are not expected to have a great influence on the process studied in this work.

The main phenomenological instrument of the population balance model of an aggregation process is the aggregation frequency. It represents the probability per unit time of a pair of aggregating droplets of specified states. Alternatively, it represents the fraction of aggregating droplet pairs of specified states per unit time. This interpretation must, however, be modified for the aggregation frequency commonly used in population balance models in which the population is regarded as well-mixed and external coordinates do not appear explicitly in the population density.

The probability that a droplet in state $(\upsilon,\mathbf{c},T)$ and another droplet of state $(\upsilon',\mathbf{c}',T')$, both present at time t in a continuous phase will aggregate in the time interval t to $t+dt$ is defined as $S_a(\upsilon,\mathbf{c},T;\upsilon',\mathbf{c}',T',t)dt$.

Let $\boldsymbol{M_a}$ denote the operator of the aggregation event. We assume that $\boldsymbol{M_a}$ may be expressed as the difference between a “source” term $\boldsymbol{M_a^+}[n(\upsilon,\boldsymbol{c},T,t)]$ and a “sink” term $\boldsymbol{M_a^-}[n(\upsilon,\boldsymbol{c},T,t)]$, both due to aggregation processes. During aggregation processes not only the volume of droplet will change but the concentration of

species and the temperature of droplets will equalize. The aggregation processes can be described as:

$$\boldsymbol{M_a}\left[n(\upsilon,\boldsymbol{c},T,t)\right]=\boldsymbol{M_a^+}\left[n(\upsilon,\boldsymbol{c},T,t)\right]-\boldsymbol{M_a^-}\left[n(\upsilon,\boldsymbol{c},T,t)\right] \tag{2.14}$$

The sink term $\boldsymbol{M_a^-}\left[n(\upsilon,\boldsymbol{c},T,t)\right]$ gives the decrease in the number of droplets in state *(υ,**c**,T)* due to aggregation with droplets of state *(υ',**c'**,T')*:

$$\begin{aligned}&\boldsymbol{M_a^-}\left[n(\upsilon,\boldsymbol{c},T,t)\right]=\\&=\int_{T_{\min}}^{T_{\max}}\int_{T_{\min}}^{T_{\max}}\int_{\mathbf{0}}^{\boldsymbol{c_m}}\int_{\mathbf{0}}^{\boldsymbol{c_m}}\int_{0}^{\upsilon_m}\frac{S_a(\upsilon,\upsilon')\beta_a(\upsilon,\upsilon')}{p_\upsilon}\delta_{T'}\left[\left(\frac{(T'-T)}{p_\upsilon}+T\right)-T''\right]\\&\delta_{\boldsymbol{c}'}\left[\left(\frac{(\boldsymbol{c}'-\boldsymbol{c})}{p_\upsilon}+\boldsymbol{c}\right)-\boldsymbol{c}''\right]n(\upsilon,\boldsymbol{c},T,t)n(\upsilon',\boldsymbol{c}',T',t)d\upsilon'd\boldsymbol{c}'d\boldsymbol{c}\,dT'dT\end{aligned} \tag{2.15}$$

where $p_\upsilon=p_\upsilon^T p_\upsilon^c$:

$$p_\upsilon^c=\frac{m_{\upsilon'}}{m_\upsilon+m_{\upsilon'}} \tag{2.16}$$

$$p_\upsilon^T=\frac{m_{\upsilon'}C_{\upsilon'}}{m_\upsilon C_\upsilon+m_{\upsilon'}C_{\upsilon'}} \tag{2.17}$$

where *m* is the mass and *C* is the concentration.

The source term $\boldsymbol{M_a^+}\left[n(\upsilon,\boldsymbol{c},T,t)\right]$ describes the increase in the number of droplets in state *(υ,**c**,T)* due to aggregation between droplets in state *(υ',**c'**,T')* and droplets of state *(υ'',**c''**,T'')*. These aggregations result droplets in state *(υ,**c**,T)*:

$$\begin{aligned}&\boldsymbol{M_a^+}\left[n(\upsilon,\boldsymbol{c},T,t)\right]=\\&\int_{T_{\min}}^{T_{\max}}\int_{T_{\min}}^{T_{\max}}\int_{\mathbf{0}}^{\boldsymbol{c_m}}\int_{\mathbf{0}}^{\boldsymbol{c_m}}\int_{0}^{\upsilon}\frac{S_a(\upsilon'',\upsilon-\upsilon'')\beta_a(\upsilon'',\upsilon-\upsilon'')}{p_\upsilon}\delta_T\left[\left(\frac{(T-T')}{p_\upsilon}+T'\right)-T''\right]\\&\delta_{\boldsymbol{c}}\left[\left(\frac{(\boldsymbol{c}-\boldsymbol{c}')}{p_\upsilon}+\boldsymbol{c}'\right)-\boldsymbol{c}''\right]n(\upsilon'',\boldsymbol{c}'',T'',t)n(\upsilon-\upsilon'',\boldsymbol{c}',T',t)d\upsilon''d\boldsymbol{c}'d\boldsymbol{c}''dT'dT''\end{aligned} \tag{2.18}$$

From Eq.(2.17) and (2.18) aggregation is expressed as:

$$\begin{aligned}
&\boldsymbol{M_a}\left[n(\upsilon,\boldsymbol{c},T,t)\right]= \\
&-\int_{T_{\min}}^{T_{\max}}\int_{T_{\min}}^{T_{\max}}\int_{\mathbf{0}}^{\boldsymbol{c_m}}\int_{\mathbf{0}}^{\boldsymbol{c_m}}\int_{0}^{\upsilon_m}\frac{S_a(\upsilon,\upsilon')\beta_a(\upsilon,\upsilon')}{p_\upsilon}\delta_{T'}\left[\left(\frac{(T'-T)}{p_\upsilon}+T\right)-T''\right] \\
&\delta_{\boldsymbol{c}'}\left[\left(\frac{(\boldsymbol{c}'-\boldsymbol{c})}{p_\upsilon}+\boldsymbol{c}\right)-\boldsymbol{c}''\right]n(\upsilon,\boldsymbol{c},T,t)n(\upsilon',\boldsymbol{c}',T',t)d\upsilon'd\boldsymbol{c}'d\boldsymbol{c}\,dT'dT \\
&+\int_{T_{\min}}^{T_{\max}}\int_{T_{\min}}^{T_{\max}}\int_{\mathbf{0}}^{\boldsymbol{c_m}}\int_{\mathbf{0}}^{\boldsymbol{c_m}}\int_{0}^{\upsilon}\frac{S_a(\upsilon'',\upsilon-\upsilon'')\beta_a(\upsilon'',\upsilon-\upsilon'')}{p_\upsilon}\delta_{T}\left[\left(\frac{(T-T')}{p_\upsilon}+T'\right)-T''\right] \\
&\delta_{\boldsymbol{c}}\left[\left(\frac{(\boldsymbol{c}-\boldsymbol{c}')}{p_\upsilon}+\boldsymbol{c}'\right)-\boldsymbol{c}''\right]n(\upsilon'',\boldsymbol{c}'',T'',t)n(\upsilon-\upsilon'',\boldsymbol{c}',T',t)d\upsilon''d\boldsymbol{c}'d\boldsymbol{c}''dT'dT''
\end{aligned} \tag{2.19}$$

where function S_a provides the frequency of binary collisions with coalescence of droplets of volumes υ and υ' resulting in aggregation, while β_a denotes the resulting volume of the event. Concentrations have been assumed to equalize completely (ω=1).

2.2.3. Coalescence/redispersion processes

Coalescence/redispersion processes are the events in which two droplets collide with each other but the drops do not adhere for a sufficient time to allow them to deform, and to permit drainage of the continuous phase that is trapped between them. Hence, they do not aggregate, but mass and heat transfer takes place between them. Consider two droplets that collide and exchange some masses of chemical species (k) and heat between themselves, before separating again as it is shown in Fig.2.1.

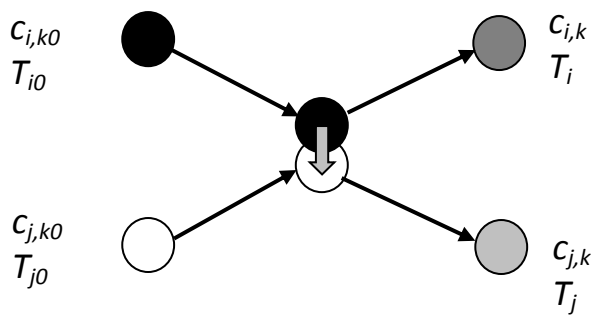

Figure 2.1. Mass and heat exchange interaction of two fluid elements in a coalescence/dispersion event

Droplets are assumed to be equal in size, so that the mass and heat transfer process can be described by a simple set of linear differential equations (Lakatos, 2008):

$$v\frac{dc_{i,k}}{dt} = \beta_k a\left[c_{i,k}(t) - c_{j,k}(t)\right], \quad c_{i,k}(0) = c_{i,k0}, \; k = 1,2,...K \tag{2.20}$$

$$v\frac{dc_{j,k}}{dt} = -\beta_k a\left[c_{i,k}(t) - c_{j,k}(t)\right], \quad c_{j,k}(0) = c_{j,k0}, \; k = 1,2,...K \tag{2.21}$$

The solutions of Eq.(2.20-21) at time θ is:

$$c_{i,k}(\theta) = c_{i,k0} + \frac{\omega_k}{2}\left(c_{j,k0} - c_{i,k0}\right) \tag{2.22}$$

$$c_{j,k}(\theta) = c_{j,k0} - \frac{\omega_k}{2}\left(c_{j,k0} - c_{i,k0}\right) \tag{2.23}$$

where

$$\omega_k := 1 - \exp\left[-2\frac{\beta_k a\theta}{v}\right], \; k = 1,2...K\,. \tag{2.24}$$

where β_k is the diffusive mass transfer coefficient for component k, a is the contact area, θ is the contact time and v is the volume of droplets.

If the two droplets have different volume or mass, then:

$$\omega_k := 1 - \exp\left[-\beta_k a\theta\left(\frac{m_i + m_j}{m_i m_j}\right)\right], \; k = 1,2...K \tag{2.25}$$

Using Eq.(2.25) the concentrations of droplets are:

$$c_{i,k}(\theta) = c_{i,k0} + \frac{m_i}{m_i + m_j}\omega_k\left(c_{j,k0} - c_{i,k0}\right) \tag{2.26}$$

$$c_{j,k}(\theta) = c_{j,k0} - \frac{m_j}{m_i + m_j}\omega_k\left(c_{j,k0} - c_{i,k0}\right) \tag{2.27}$$

Naturally, the contact area and contact time are the same for all species, but the diffusive mass transfer coefficients may differ from each other due to the possibly different diffusion rates of the chemical species. Furthermore, since the turbulent fluctuations are random variables of the contact area and contact time of the droplets and the parameters $\omega_k \in [0,1]$, k=1,2…K are also random, with distribution functions F_{ω_k} determined by the distributions of the individual parameters involved in expression Eq.(2.24).

Heat transfer expressions are similar to that of mass transfer. In no system exists with identical size droplets. Equations for heat transfer for different size droplets are shown below.

The temperature of droplets after heat exchange:

$$T_i(\theta) = T_{i0} + \frac{c_{p_j} \cdot m_j}{c_{p_i} \cdot m_i + c_{p_j} \cdot m_j} \cdot \omega \cdot \left(T_{j0} - T_{i0}\right) \tag{2.28}$$

$$T_j(\theta) = T_{j0} - \frac{c_{p_i} \cdot m_i}{c_{p_i} \cdot m_i + c_{p_j} \cdot m_j} \cdot \omega \cdot \left(T_{j0} - T_{i0}\right) \tag{2.29}$$

where

$$\omega = 1 - \exp\left[-ha\theta\left(\frac{m_i c_{pi} + m_j c_{pj}}{m_j c_{pj} m_i c_{pi}}\right)\right] \tag{2.30}$$

If the heat transfer between droplets is complete (ω=1), the temperature of the two droplets will be the same:

$$T_{new}(\theta) = \frac{c_{p_i} \cdot m_i \cdot T_{i0} + c_{p_j} \cdot m_j \cdot T_{j0}}{c_{p_i} \cdot m_i + c_{p_j} \cdot m_j} \tag{2.31}$$

The main phenomenological instrument of the population balance model of a coalescence/redispersion process is the collision frequency. It represents the probability per unit time of a pair of colliding droplets of specified states. Some of these collisions may end up with coalescence. The function S_{col}^{dd} is defined to provide the frequency of binary collisions without coalescence of droplets of volumes υ and υ', results in exchange of mass without aggregation.

$$\begin{aligned}
&\boldsymbol{M}_{\boldsymbol{c/r}}^{dd}\left[n(\upsilon,\boldsymbol{c},T,t)\right] = \\
&-\frac{1}{N(t)}\int_{T_{\min}}^{T_{\max}}\int_{T_{\min}}^{T_{\max}}\int_{\mathbf{0}}^{\boldsymbol{c_m}}\int_{\mathbf{0}}^{\boldsymbol{c_m}}\int_{0}^{\upsilon_m}\int_{0}^{1}\frac{S_{col}^{dd}(\upsilon,\upsilon')}{\boldsymbol{\omega} p_\upsilon}\delta_{T'}\left[\left(\frac{(T'-T)}{\omega_T\, p_\upsilon^T}+T\right)-T''\right] \\
&\delta_{\boldsymbol{c}'}\left[\left(\frac{(\boldsymbol{c}'-\boldsymbol{c})}{\boldsymbol{\omega}_c\, p_\upsilon^c}+\boldsymbol{c}\right)-\boldsymbol{c}''\right]F_{\boldsymbol{\omega}|\upsilon}(\boldsymbol{\omega})n(\upsilon,\boldsymbol{c}',T',t)n(\upsilon',\boldsymbol{c}'',T'',t)d\boldsymbol{\omega}\, d\upsilon'\, d\boldsymbol{c}'\, d\boldsymbol{c}''\, dT'\, dT'' \\
&+\frac{1}{N(t)}\int_{T_{\min}}^{T_{\max}}\int_{T_{\min}}^{T_{\max}}\int_{\mathbf{0}}^{\boldsymbol{c_m}}\int_{\mathbf{0}}^{\boldsymbol{c_m}}\int_{0}^{\upsilon_m}\int_{0}^{1}\frac{S_{col}^{dd}(\upsilon,\upsilon')}{\boldsymbol{\omega} p_\upsilon}\delta_{T}\left[\left(\frac{(T-T')}{\omega_T\, p_\upsilon^T}+T'\right)-T''\right] \\
&\delta_{\boldsymbol{c}}\left[\left(\frac{(\boldsymbol{c}-\boldsymbol{c}')}{\boldsymbol{\omega}_c\, p_\upsilon^c}+\boldsymbol{c}'\right)-\boldsymbol{c}''\right]F_{\boldsymbol{\omega}|\upsilon}(\boldsymbol{\omega})n(\upsilon,\boldsymbol{c}',T',t)n(\upsilon',\boldsymbol{c}'',T'',t)d\boldsymbol{\omega}\, d\upsilon''\, d\boldsymbol{c}'\, d\boldsymbol{c}''\, dT'\, dT''
\end{aligned} \tag{2.32}$$

where $\omega \in [0,1]$ is a random number characterizing the extent of homogenization of concentrations with distribution function $F_{\boldsymbol{\omega}|\upsilon}$, $p_\upsilon = p_\upsilon^T p_\upsilon^c$, $\boldsymbol{\omega} = \omega_T \boldsymbol{\omega}_c$ and N denotes the total number of droplets.

$$\omega_c := 1 - \exp\left[-\beta_{\upsilon\upsilon''} a_{\upsilon\upsilon''} \theta_{\upsilon\upsilon''} \left(\frac{m_\upsilon + m_{\upsilon''}}{m_\upsilon m_{\upsilon''}}\right)\right], \; p_\upsilon^c = \frac{m_{\upsilon''}}{m_\upsilon + m_{\upsilon''}} \tag{2.33}$$

$$\omega_T := 1 - \exp\left[-h_{\upsilon\upsilon''} a_{\upsilon\upsilon''} \theta_{\upsilon\upsilon''} \left(\frac{m_\upsilon C_\upsilon + m_{\upsilon''} C_{\upsilon''}}{m_\upsilon C_\upsilon m_{\upsilon''} C_{\upsilon''}}\right)\right], \; p_\upsilon^T = \frac{m_{\upsilon''} C_{\upsilon''}}{m_\upsilon C_\upsilon + m_{\upsilon''} C_{\upsilon''}} \tag{2.34}$$

The first and second terms on the right hand side of Eq.(2.32) describe the rates of decrease and increase in the number of droplets in state (υ,$\boldsymbol{c}$,T), respectively.

2.3. Meso-scale model of the droplet population

An aggregation event may also result in a sudden concentration change in which total homogenization of concentrations is assumed. Since both the pure mass exchange and aggregation events are collision induced processes, together they form a random, discrete event process which is superimposed on the continuous process of polymerizations reactions. As a consequence, the concentrations in a droplet are governed by the Eq.(2.35) stochastic differential equation:

$$d\boldsymbol{c}(t) = \boldsymbol{R}_r\left[\boldsymbol{c}(t), T(t)\right]dt + \int_V \varphi_i(\upsilon, \boldsymbol{c}) N(\upsilon, dt) dV \tag{2.35}$$

where N is a Poisson process giving the number of collision events in volume V of the suspension. The frequency of collisions depends on the volumes of droplets, while function φ_i describes the concentration jumps of the collision events. φ_i depends on the parameter ω and the volume of droplets. i as subscript can be *c/r* (if the collision event is coalescence/redispersion and results in mass exchange) or it can be *a* (if the collision event is aggregation).

The volume of droplets may changes continuously in time, because of the polymerization reactions and the significant difference between the densities of monomer and polymer. Droplet volumes may also change step-wise due to collision-induced aggregation. Additionally, droplets travelling in the viscous carrier phase may suffer break up due to the shear forces, which is a random,

discrete process, too. The concentrations in a break up event are assumed to be unchanged therefore the volume of a droplet is governed by the Eq. (2.36) stochastic differential equation:

$$d\upsilon(t) = f_\upsilon\left[\boldsymbol{R}_r\left(\boldsymbol{c}(t), T(t)\right)\right]dt + \int_V \varphi_i(\upsilon) N(\upsilon, dt) dV + \int_V \varphi_b(\upsilon) N_b(\theta, dt) dV \tag{3.36}$$

where the terms on the right hand side describe, in turn, the rates of change of a droplet volume due to polymerization reactions, aggregation, breakage and coalescence/redispersion. Functions φ_i and φ_b describe the volume and concentration jumps caused by a collision event (aggregation and coalescence/redispersion) respectively, as well as the volume jump caused by a break up event. N_b denotes a Poisson process counting the break up events in volume V of the suspension. N_b depends on the properties of the viscous turbulent carrier phase characterized by a parameter θ.

The temperature of droplets can change continuously in time due to polymerization reactions, and may also change step-wise due to collisions induced events. Both the pure heat exchange and aggregation events are collisions induced processes. Together they form a random, discrete process which is superimposed on the continuous process of polymerizations reactions. The temperatures in a break up event are assumed to be unchanged. As a consequence, the concentrations in a droplet are given by the Eq.(2.37) stochastic differential equation:

$$dT(t) = f_T\left[\boldsymbol{R}_r\left(\boldsymbol{c}(t), T(t)\right)\right]dt - ha\left[T(t) - T_f\right] + \int_V \varphi_i(T) N(\upsilon, dt) dV \tag{2.37}$$

where the terms on the right hand side describe, in turn, the rates of change of a droplet temperature due to polymerization reactions, the heat transport to the continuous phase, aggregation and coalescence/redispersion.

The set of differential equations (2.35)-(2.37) describes the behaviour of droplets entirely by tracking the time evolution of the state of each droplet individually. However, this mathematical model is too complex. Instead of following the evolution of each single droplet, it is reasonable to consider the collective description of those utilising their statistical similarities, and defining an appropriate mesoscopic length-scale between the micro- and macro-scales.

The system of stochastic differential equations (2.35)-(2.37) generates a Markov process. Following the procedure by Lakatos et al. (2006) and Lakatos (2011) a population balance equation can be derived, including also the collision

induced terms, governing the behaviour of population density function of droplet population. The population density function is given as a mapping $(\upsilon,\boldsymbol{c},t)\rightarrow n(\upsilon,\boldsymbol{c},t)$ where $n(\upsilon,\boldsymbol{c},t)d\upsilon d\boldsymbol{c}$ provides the number of droplets being in the volume interval $(\upsilon,\upsilon+d\upsilon)$ and concentration region $(\boldsymbol{c},\boldsymbol{c}+d\boldsymbol{c})$ at time t in a unit volume of the reactor. Then the population balance equation takes the form

$$\frac{\partial n(\upsilon,\boldsymbol{c},T,t)}{\partial t}+\frac{\partial}{\partial \upsilon}\left(\frac{d\upsilon}{dt}n(\upsilon,\boldsymbol{c},T,t)\right)+\frac{\partial}{\partial \boldsymbol{c}}\left(\frac{d\boldsymbol{c}}{dt}n(\upsilon,\boldsymbol{c},T,t)\right)= \boldsymbol{M}_{c/r}^{dd}\left[n(\upsilon,\boldsymbol{c},T,t)\right]+\boldsymbol{M}_{\boldsymbol{a}}\left[n(\upsilon,\boldsymbol{c},T,t)\right]+\boldsymbol{M}_{\boldsymbol{b}}\left[n(\upsilon,\boldsymbol{c},T,t)\right] \tag{2.38}$$

where on the left hand side are the rates of change of the population density function due to the deterministic continuous processes, while the terms on the right hand side represent the collision-induced processes.

In Eq.(2.38), the rates of the deterministic continuous changes are written as:

$$\frac{d\upsilon(t)}{dt}=f_{\upsilon}\left[\boldsymbol{R}_r\left(\boldsymbol{c}(t),T(t)\right)\right] \tag{2.39}$$

$$\frac{d\boldsymbol{c}(t)}{dt}=\boldsymbol{R}_r\left[\boldsymbol{c}(t),T(t)\right] \tag{2.40}$$

and

$$\frac{dT(t)}{dt}=f_T\left[\boldsymbol{R}_r\left(\boldsymbol{c}(t),T(t)\right)\right] \tag{2.41}$$

In order to describe the total heat balance for the stirred vessel, it is necessary to define the volume fraction of the continuous phase ε in the reactor, as:

$$1-\varepsilon(t)=\int_{T_{\min}}^{T_{\max}}\int_{\mathbf{0}}^{\mathbf{c_m}}\int_{\upsilon}^{\upsilon_m}\upsilon n(\upsilon,\boldsymbol{c},T,t)d\upsilon d\boldsymbol{c}dT \tag{2.42}$$

The heat balance for the continuous phase:

$$\rho_c C_c \varepsilon V\frac{dT_c}{dt}=V\int_{T_{\min}}^{T_{\max}}\int_{\mathbf{0}}^{\mathbf{c_m}}\int_{0}^{\upsilon_m}a_d h_{dc}\left(T-T_c\right)n(\upsilon,\boldsymbol{c},T,t)d\upsilon d\boldsymbol{c}dT-A_{cj}h_{cj}V\left(T_c-T_j\right) \tag{2.43}$$

where T_c, ρ_c, $\varepsilon$and C_c are, respectively, the temperature, density, volumetric ratio and heat capacity of the continuous phase. V is the reactor volume, a_d is the surface of a droplet, h_{dc} is the heat transfer coefficient between a droplet and the continuous phase, h_{cj} and A_{cj} denote the coefficient and the effective surface of heat transfer between the continuous phase and the cooling medium.

The heat balance for a droplet:

$$\rho_d C_d\frac{dT_d}{dt}=\left(-\boldsymbol{\Delta H}_r\right)\cdot\boldsymbol{R}_r\left(\boldsymbol{c}_d,T_d\right)-a_d h_{dc}\left(T_d-T_c\right) \tag{2.44}$$

where T_d, ρ_d and C_d are, respectively, the temperature, density and heat capacity of a droplet, $\boldsymbol{R}_r$ and $\boldsymbol{\Delta H}_r$ are the vectors of the reaction rates and reaction heats, and $\boldsymbol{c}_d$ is the vector of concentrations of species in a droplet.

The average monomer conversion over the reactor is expressed as

$$X(t) = 1 - \frac{\int_{T_{\min}}^{T_{\max}} \int_{\boldsymbol{c}_{\min}}^{\boldsymbol{c}_{\max}} \int_{0}^{\upsilon_{\max}} \varepsilon_m \rho_m \upsilon n(\upsilon, \boldsymbol{c}, t) d\upsilon d\boldsymbol{c} dT}{\int_{T_{\min}}^{T_{\max}} \int_{\boldsymbol{c}_{\min}}^{\boldsymbol{c}_{\max}} \int_{0}^{\upsilon_{\max}} \rho_m \upsilon n(\upsilon, \boldsymbol{c}, t) d\upsilon d\boldsymbol{c} dT} \tag{2.45}$$

where ε_m is the volume fraction of monomer in a droplet and ρ_m denotes the density of monomer.

The numerical solution of the multidimensional population balance equation is a difficult problem. Taking into account the randomness of collisions induced and break up processes; the model equations are solved by using the Monte Carlo method in this work.

3. Solution of the multi-variable population balance equation. A coupled continuous time – Monte Carlo method

In Section 2 a detailed multi-variable population balance equation was introduced for liquid-liquid dispersions. Solution of multi-variable population balance equations is a difficult problem. For single variable population balance equation a number of solution methods has been published. In contrast, for multi-variable equation only a few, as it was shown in Section 1.3. In the case of multi-variable population balance equations, pure numerical methods are useless. Numerical integration cannot handle the sudden changes in concentration, volume and temperature. The Monte Carlo method provides a solution for this problem. In this section a complex method is presented for solution the multi-variable population balance equation.

3.1. A coupled continuous time-Monte Carlo method

The Monte Carlo method developed in this work has been based on Irizzary's method (Irizzary, 2008a,b) with a number of modifications. Irizzary's method is based on the stochastic simulation algorithm (SSA). The exact SSA of a well-mixed chemical reaction system was developed by Gillespie (1977). The method is based on the answer to the following question: For a system in a given state, which E_f, reaction occurs next, and at what τ_{micro} time? The simulation generates random number pairs for E_f and τ_{micro} from conditional probabilities which are functions of the propensity function ($R(E_s)\mathrm{d}t$) for each reaction ($R(E_s)$). The propensity function is defined as

$R(E_s)\mathrm{d}t \equiv$ the probability that reaction E_s occurs in the time interval $(t,t+\mathrm{d}t)$.

In each iteration step of the SSA, two random numbers, r_1, r_2 are selected from the uniform distribution (0,1). The time for the next reaction is calculated as

$$\tau_{micro} = \frac{-\log(r_1)}{\sum_{j=1}^{T} R(E_j)} \tag{3.1}$$

The time is moved to $t+\tau_{micro}$. The reaction fired at ($t+\tau_{micro}$) is selected by solving the following equation (Irizzary, 2008a,b):

$$\sum_{s=1}^{f} R(E_s) < r_2 \sum_{s=1}^{T} R(E_s) \leq \sum_{s=1}^{f+1} R(E_s) \tag{3.2}$$

The selected event is E_f. These steps are repeated until a final time is reached. The method is based on the assumption that τ is small enough that the propensity functions will not change appreciably during τ. When this condition is satisfied, all reaction channels can be considered as independent events. Irizzary's method, the point ensemble Monte Carlo (PEMC) consists of the solution of the Jump Markov model, called the particle ensemble random product (PERP) model. This model is based on three ideas. First, the total population is discretized into subpopulations with respect to particle size in a specified interval. Each sub-population is viewed as a chemical species with the number of particles in the subpopulation representing the concentration of species. Second, the inter-particle interactions (i.e., coalescence, nucleation, breakage) are viewed as a set of special type of reactions, in which the reaction products are allocated stochastically to the existing species using probability functions that are mass conserving on average. Third, the original set of subpopulations is coupled with the system of chemical species. Irizzary (2008a,b) assumed that in the dispersed phase there are chemical reactions, but these reactions are much faster than the coalescence rate. Three events were taken into consideration in his work, namely coalescence, nucleation and binary breakage.

In contrast to the above, in this work systems with slow reactions in the dispersed phase are targeted, for example suspension polymerization. Therefore, the assumption of instantaneous chemical reactions like Irizzary (2008a,b), cannot be applied. Furthermore, polymerization reactions usually are highly exothermic, thus the heat effects should be taken into consideration, too. The discrete events considered are various, namely coalescence, coalescence/redispersion and breakage of dispersed elements.

The algorithm of the developed coupled continuous time-Monte Carlo method can be seen in Fig.3.1. Breakage and coalescence of dispersed elements are effected by the volume of elements, the local mechanical conditions in the

dispersion, turbulent energy dissipation and shear forces as well as by physical properties: viscosity and density of the phases, interfacial tension, and other interfacial phenomena, such as the surface charge of droplets.

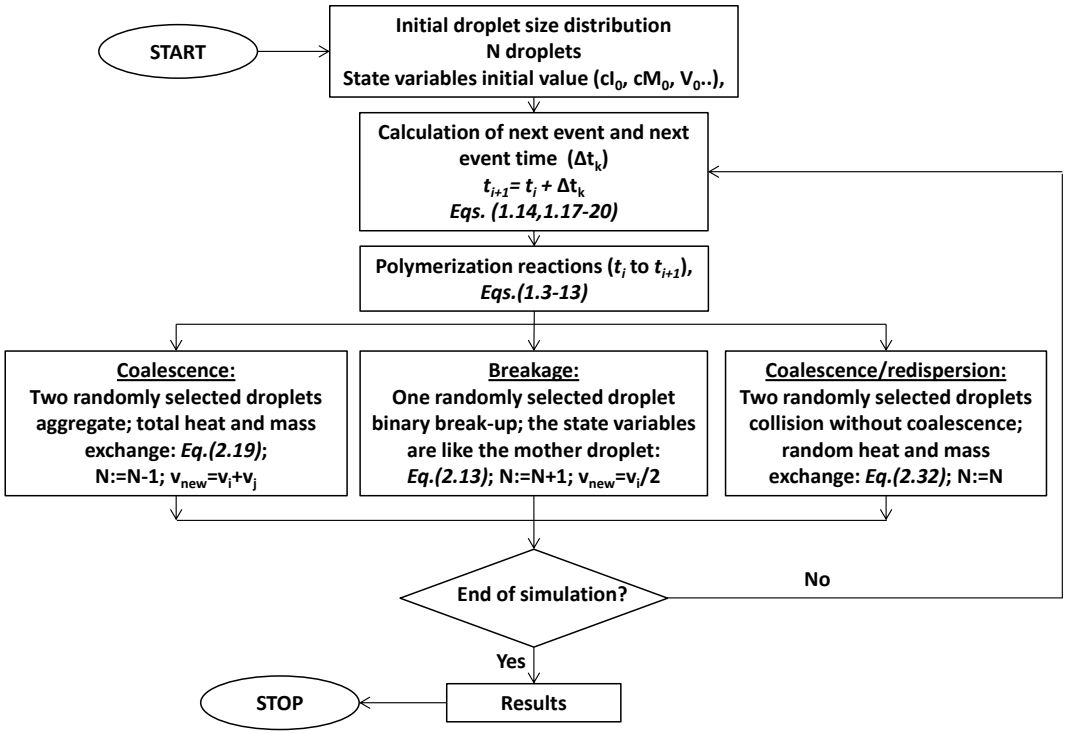

Figure 3.1. The algorithm of simulation

The simulated element diameter range is subdivided into equal parts, termed size classes. All elements are assigned into these classes, based on their actual diameters. The volumes of elements are changed continuously in time due to the reactions, since the densities of monomer and polymer differ significantly. In suspension polymerization, the volume of elements can be changed step-wise, too, because of collision-induced aggregation, coalescence/redispersion and breakage. In addition to the change of volume, the number of elements in classes can also vary. The collision and breakage processes are modelled as inhomogeneous Poisson processes independent from each other the intensities of which are computed individually for all classes. In the time intervals between subsequent events, computations are carried out using homogeneous approximations. The element or elements which take a share in events are selected randomly, using random numbers generated from the uniform probability distribution in the range of (0,1).

The steps of the solution method are as follows for suspension polymerization:

Initialization: Initial droplet size distribution is generated and all state variables are given an initial value. The number of droplets is *N*, time equals to zero. The simulated drop diameter interval is 1 μm to 250 μm, and this interval is sectioned to 25 equal parts. All state variables are given initial values (initiator concentration, temperature of polymerization, etc.).

Step 1: Selection of the next event and next event time from all possible events using the following equations.

The probability of one event to occur in process *k* is:

$$\text{Prob}(event\ \#=1) = \lambda_k\ \Delta t_k e^{-\lambda_k\ \Delta t_k} \tag{3.3}$$

The maximum with respect to Δt_k is the maximum probability that one event will occur. Fig.3.2 presents the place where the function has maximum, $x = \lambda_k \Delta t_k$. This function has maximum by x=1.

Therefore:

$$\Delta t_k = \frac{1}{\lambda_k} \tag{3.4}$$

The next event is selected by the following equation:

$$\min_{k \in \{\textbf{all events}\}} \left[\max_{\Delta t} \left\{ \text{Prob}\,(event\ \#=1) = \lambda_k\ \Delta t_{\ k} e^{-\lambda_k\ \Delta t_k} \right\} \right] \tag{3.5}$$

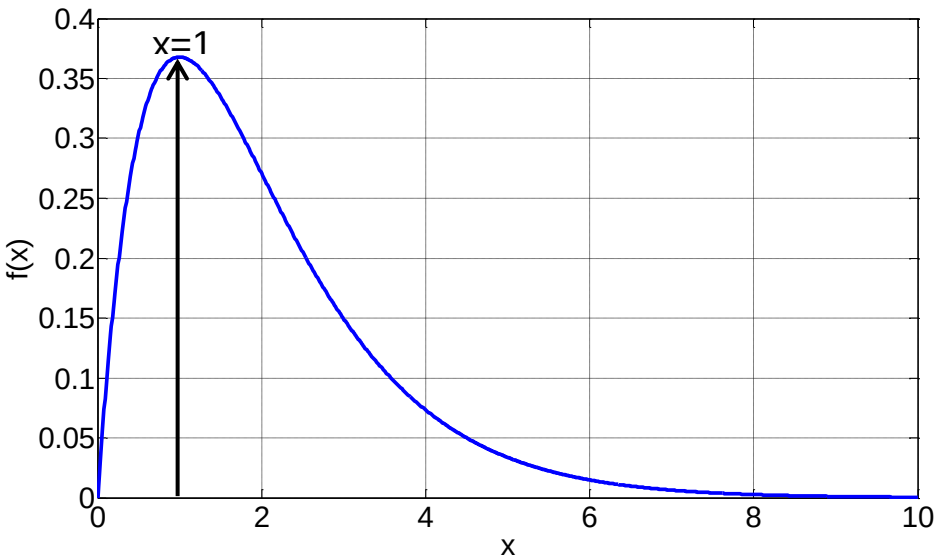

Figure 3.2. Definition of the maximum probability that one event occurs

where λ_k denotes the intensities (mean frequencies) of the collision and brake up events computed individually for all size classes. Collision and breakage frequencies and coalescence efficiency are calculated using equations (1.14; 1.18; 1.19) and the number of droplets in classes. For aggregation, breakage and coalescence/redispersion the λ_k is the following, respectively:

$$\lambda_a = S_a(d,d')N(d') \tag{3.6}$$

$$\lambda_b = S_b(d) \tag{3.7}$$

$$\lambda_c = S_{col}^{dd}(d,d')N(d') \tag{3.8}$$

After the selection of the next event the simulation time is set to: $t_{i+1} = t_i + \Delta t_k$.

Step 2: The polymerization reactions take place in the monomer droplets, so, for all droplets the set of intra-particle reactions are integrated from t_i to t_{i+1}. The concentration, temperature and volume of droplets are changed continuously in time because of the reactions.

Step 3: The formerly selected event occurs.

Case 1) The event is *collision of two droplets*:

Case 1.a) If this event is *coalescence/redispersion* then two droplets are selected randomly from the diameter classes *d* and *d'*. A random number $\omega_k \in [0,1]$ is generated to calculate the rate of species mass and heat exchange between the colliding droplets. The total number of droplets does not change and remains *N*.

Case 1.b) If the selected event is *coalescence* then two droplets are selected randomly from the diameter classes *d* and *d'*. These droplets are eliminated and a new droplet is formed from these droplets with size $\upsilon_{new} = \upsilon_i + \upsilon_j$. The properties i.e. concentrations of initiator and monomer, conversion, moments and temperature of the new droplets are calculated from the properties of coalesced droplets assuming homogeneous distributions of intensives. Then the number of elements is decreased (*N:=N-1*).

Case 2) The event is *break up of a droplet:*

A single droplet is selected randomly from the diameter class *d.* This droplet is eliminated and two new twin droplets are formed from that with

$\upsilon_{new} = \upsilon_i / 2$. All extensive quantities are derived from the volume change while the intensives remain the same. The number of element is increased (*N:=N+1*).

Step 4: If $t_{i+1} \geq t_{final}$ then stop, i.e. end the simulation, otherwise go to ***Step 1***.

3.2. Selection of the minimal population size for simulation

The first task before solving the multi variable population balance equation by MC method is to find the minimal population size. The time of simulation and the needed computer memory are depending on the number of simulated elements. Simulation experiments have been carried out to define the minimum number of simulated elements. For this purpose, a simple method (Fig.3.3) was worked out.

In these experiments, 10, 100, 1000 and 10000 elements were selected, choosing identical droplet volumes in all cases. A certain fraction of elements was chosen randomly marking those by neutral indicator. The distribution of indicator in the marked elements was uniform. Subsequently, a process of binary collisions of randomly chosen elements was computed assuming that in each collision event total equalization of indicator took place between the two colliding elements.

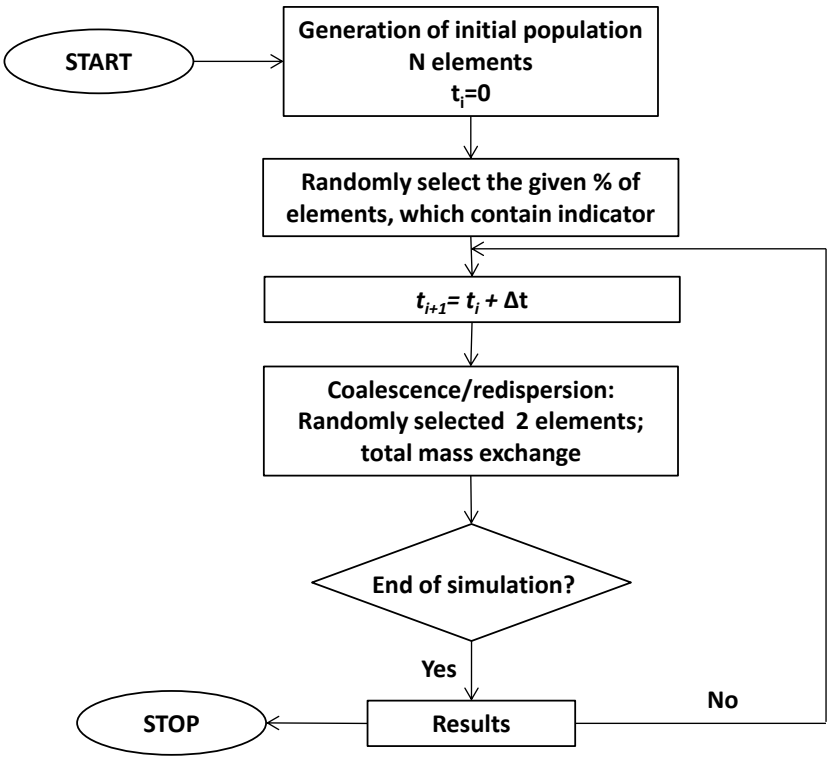

Figure 3.3. The algorithm of simulation

Neither aggregation nor breakage of elements occurred in the process. In this way, a pure micro-mixing process of indicator was simulated. All numerical experiments were repeated several times and the standard deviations of indicator distribution were evaluated.

The results of these numerical experiments are presented in Fig.3.4. Fig.3.4a illustrates the case when only ten elements were applied. It can be seen that significant fluctuations occurred during the course of the simulation process. Fig.3.4b shows the results for hundred elements indicating still significant fluctuations. Figs.3.4c and 3.4d present the results for thousand and ten thousands elements, respectively. The fluctuations here were negligible. From this analysis it can be seen that increasing the number of elements used in simulation decreases the fluctuations in results, and above thousand elements the simulation provides acceptable results. However, the time required for computations increased dramatically above five thousands elements (Fig.3.4e).

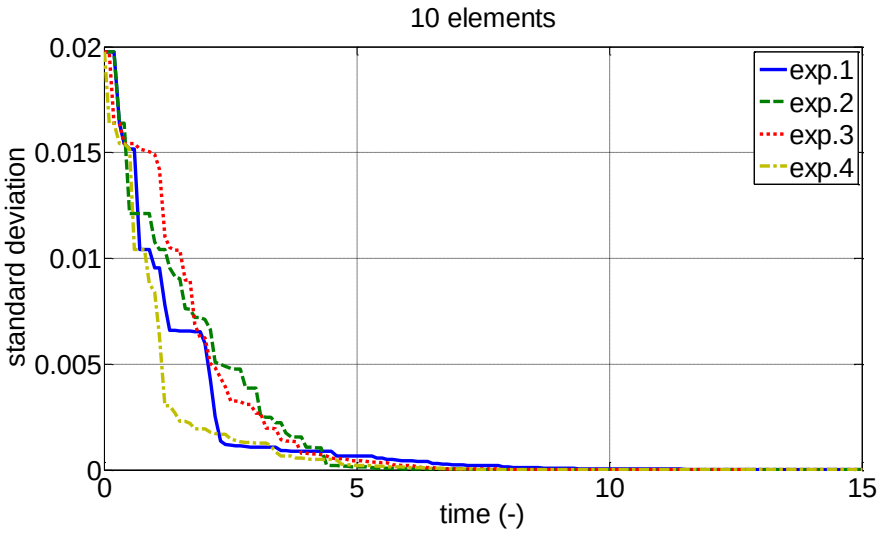

a,

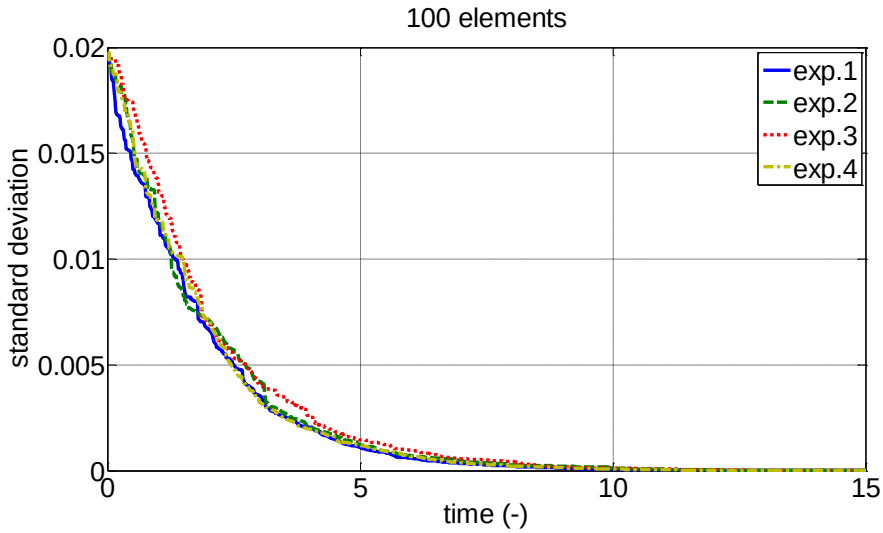
100 elements
standard deviation
time (-)
exp.1
exp.2
exp.3
exp.4
0.02
0.015
0.01
0.005
0
0
5
10
15

b,

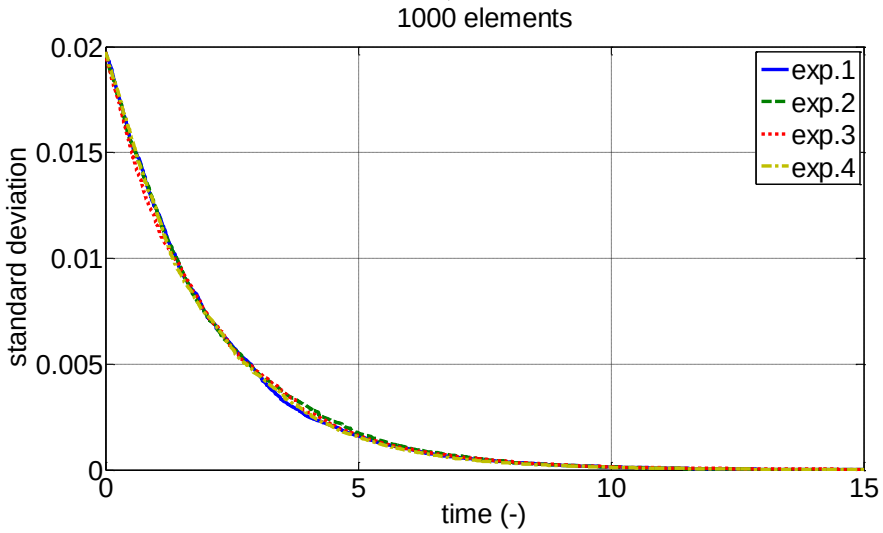
1000 elements
standard deviation
time (-)
exp.1
exp.2
exp.3
exp.4
0.02
0.015
0.01
0.005
0
0
5
10
15

c,

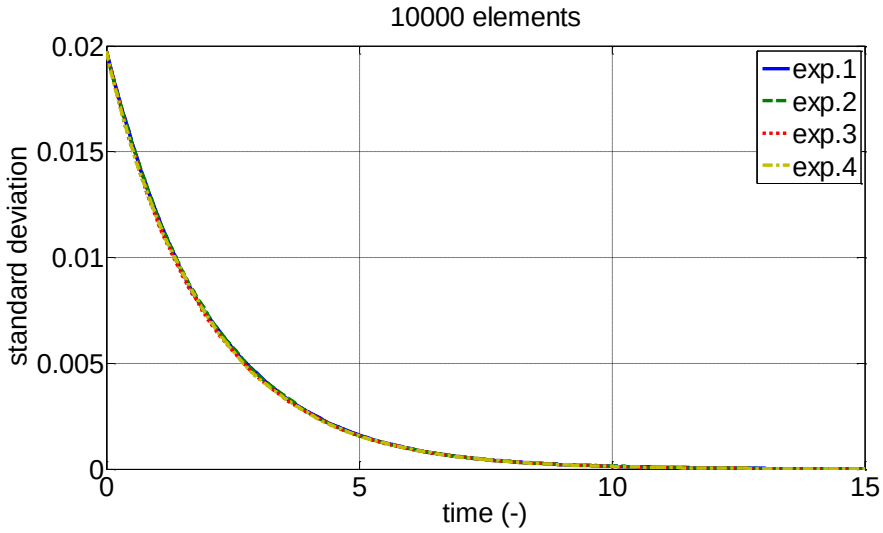
10000 elements
standard deviation
time (-)
exp.1
exp.2
exp.3
exp.4
0.02
0.015
0.01
0.005
0
0
5
10
15

d,

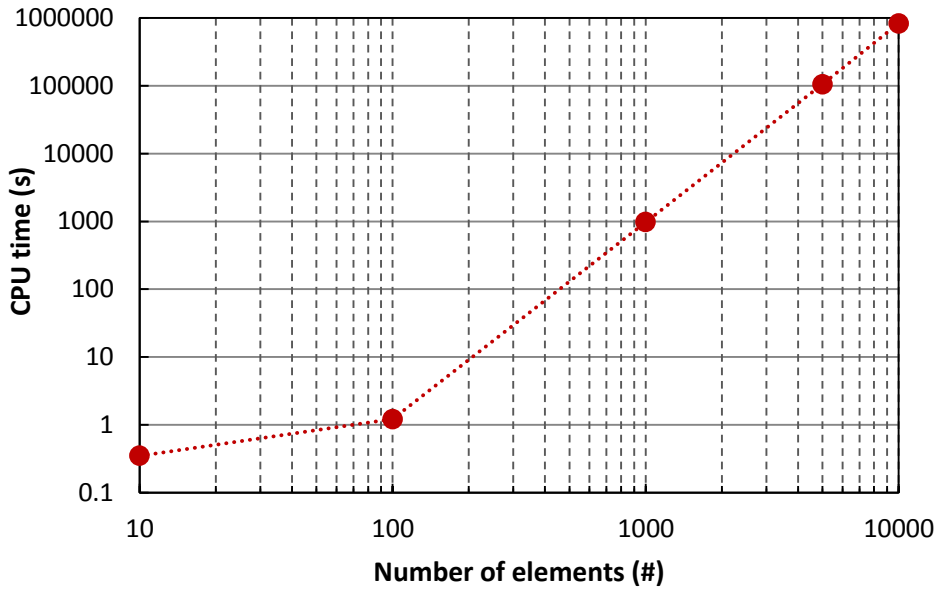

e,

Figure 3.4. Calculation of the population size

These results meet the literature descriptions. A typical sample population usually contains about 10^3 – 10^5 droplets/elements in order to ensure an accurate representation of the initial distribution and, at the same time, to minimize the computational requirements (Salikas et al., 2008). Therefore this work a 1000-5000 element population was used to examine the effects of coalescence-breakage processes on the average value of monomer conversion.

3.3. Application of the coupled continuous time – Monte Carlo method for the simulation of suspension polymerization of vinyl chloride

The dispersed phase, where the polymerization reactions take place, forms a continuous deterministic process. Parallel to this process, the coalescence, coalescence/redispersion and breakage of droplets form a stochastic discrete event process. The population balance equation described in Section 2 was used for modelling the phenomena in suspension polymerization. Since there are polymerization reactions in the droplets the balance equations are needed for all droplets.

In simulation, the two phase model description of polymerization of vinyl chloride has been used where the model equations are as follows:

Stage 1. $X < 0.1\%$

The droplets contain pure monomer only. Therefore, in this stage there is only one phase, the monomer phase.

Volume of droplets:

$$\upsilon = const. = \upsilon_1 \tag{3.9}$$

where υ_1 represents the volume of monomer rich phase.

Mass balance for initiator:

$$\frac{d(\upsilon c_I)}{dt} = -\upsilon_1 k_{d_1} c_{I_1} \tag{3.10}$$

Mass balance for monomer:

$$\frac{d(\upsilon c_M)}{dt} = -\upsilon_1 \left(2 f k_{d_1} c_{I_1} c_{M_1} + k_{p_1} c_{M_1} \nu_{0_1} + k_{tM_1} c_{M_1} \nu_{0_1}\right) \tag{3.11}$$

Moment balances for live polymer radicals:

$$\frac{d(\upsilon \nu_{0_1})}{dt} = \upsilon_1 \left(2 f k_{d_1} c_{I_1} - k_{t_1} \nu_{0_1}{}^2\right) \tag{3.12}$$

$$\frac{d(\upsilon \nu_{1_1})}{dt} = \upsilon_1 \left(2 f k_{d1} c_{I_1} - k_{t_1} \nu_{0_1} \nu_{1_1} + k_{tM_1} c_{M_1} (\nu_{0_1} - \nu_{1_1}) + k_{p_1} c_{M_1} \nu_{01}\right) \tag{3.13}$$

$$\begin{aligned} &\frac{d(\upsilon \nu_{2_1})}{dt} = \\ &= \upsilon_1 \left(2 f k_{d1} c_{I_1} - k_{t_1} \nu_{0_1} \nu_{2_1} + k_{tM_1} c_{M_1} (\nu_{0_1} - \nu_{2_1}) + k_{p_1} c_{M_1} (\nu_{01} + 2\nu_{1_1})\right) \end{aligned} \tag{3.14}$$

The quasi-steady-state approximation (QSSA) is a standard procedure in the study of chemical reactions kinetics in situations where certain species have a very short time of existence (free radicals, very unstable molecules, etc.) with respect to other species. It assumed that variation of the unstable species is zero thus the size of the set of equations modelling the reactions reduced by the number of unstable species. In polymerization kinetics, QSSA is often used for the growing polymer chains:

$$\nu_{01} = \sqrt{\frac{2 f k_{d_1} c_{I_1}}{k_{t_1}}} \tag{3.15}$$

$$\nu_{1_1} = \frac{2 f k_{d_1} c_{I_1} + \left(k_{p_1} + k_{tM_1}\right) c_{M_1} \nu_{0_1}}{k_{tM_1} c_{M_1} + k_{t_1} \nu_{0_1}} \tag{3.16}$$

$$\nu_{2_1} = \frac{2fk_{d_1}c_{I_1} + k_{p_1}c_{M_1}\left(\nu_{01} + 2\nu_{1_1}\right) + k_{tM_1}c_{M_1}\nu_{0_1}}{k_{tM_1}c_{M_1} + k_{t_1}\nu_{0_1}} \tag{3.17}$$

Moment balances for dead polymer chains are:

$$\frac{d(\upsilon\mu_0)}{dt} = \upsilon_1\left(k_{tM_1}c_{M_1} + k_{t_1}\nu_{0_1}\right)\nu_{0_1} \tag{3.18}$$

$$\frac{d(\upsilon\mu_1)}{dt} = \upsilon_1\left(k_{tM_1}c_{M_1} + k_{t_1}\nu_{0_1}\right)\nu_{1_1} \tag{3.19}$$

$$\frac{d(\upsilon\mu_2)}{dt} = \upsilon_1\left(k_{tM_1}c_{M_1} + k_{t_1}\nu_{0_1}\right)\nu_{2_1} \tag{3.20}$$

The monomer conversion can be calculated as:

$$X = 1 - \frac{\upsilon c_M}{n_{M_0}} \tag{3.21}$$

where n_{M_0} (mol) is the initial number of moles of monomer.

Stage 2. 0.1% < X < X_c

The second stage extends from the time of appearance of the separate polymer phase to the critical conversion, X_c, at which the separate monomer phase disappears. There are two phases in this stage: the monomer rich and polymer rich phases. The concentration of monomer in each phase remains constant:

$$c_{M_1} = \frac{\rho_m}{M_w} \tag{3.22}$$

$$c_{M_2} = \frac{A\rho_m}{M_w\left(A + \frac{\rho_m}{\rho_p}\right)} \tag{3.23}$$

where

$$A = \frac{1 - X_c}{X_c} \tag{3.24}$$

and

$$X_c = 0.85 - 0.0019 \cdot (T - 273.16) \tag{3.25}$$

Mass balance for initiator:

$$\frac{d(\upsilon c_I)}{dt} = -\upsilon_1 k_{d_1}c_{I_1} - \upsilon_2 k_{d_2}c_{I_2} \tag{3.26}$$

Mass balance for monomer:

$$\frac{d(\upsilon c_M)}{dt} = -\upsilon_1\left(2fk_{d_1}c_{I_1}c_{M_1} + k_{p_1}c_{M_1}\nu_{0_1} + k_{tM_1}c_{M_1}\nu_{0_1}\right) - \\ -\upsilon_2\left(2fk_{d_2}c_{I_2}c_{M_2} + k_{p_2}c_{M_2}\nu_{0_2} + k_{tM_2}c_{M_2}\nu_{0_2}\right) \tag{3.27}$$

Moment balances for live polymer radicals (applying the QSSA):

$$\nu_{0_i} = \sqrt{\frac{2fk_{d_i}c_{I_i}}{k_{t_i}}} \tag{3.28}$$

$$\nu_{1_i} = \frac{2fk_{d_i}c_{I_i} + \left(k_{p_i} + k_{tM_i}\right)c_{M_i}\nu_{0_i}}{k_{tM_i}c_{M_i} + k_{t_i}\nu_{0_i}} \tag{3.29}$$

$$\nu_{2_i} = \frac{2fk_{d_i}c_{I_i} + k_{p_i}c_{M_i}\left(\nu_{0i} + 2\nu_{1_i}\right) + k_{tM_i}c_{M_i}\nu_{0_i}}{k_{tM_i}c_{M_i} + k_{t_i}\nu_{0_i}} \tag{3.30}$$

i=1,2 represents the monomer and polymer rich phases, respectively.

Moment balances for dead polymer chains are:

$$\frac{d(\upsilon\mu_0)}{dt} = \sum_i\left(\upsilon_i k_{tM_i}c_{M_i}\nu_{0_i}\right) + \sum_i\left(\upsilon_i k_{t_i}\nu_{0_i}^2\right) \tag{3.31}$$

$$\frac{d(\upsilon\mu_1)}{dt} = \sum_i\left(\upsilon_i k_{tM_i}c_{M_i}\nu_{1_i}\right) + \sum_i\left(\upsilon_i k_{t_i}\nu_{0_i}\nu_{1_i}\right) \tag{3.32}$$

$$\frac{d(\upsilon\mu_2)}{dt} = \sum_i\left(\upsilon_i k_{tM_i}c_{M_i}\nu_{2_i}\right) + \sum_i\left(\upsilon_i k_{t_i}\nu_{0_i}\nu_{2_i}\right) \tag{3.33}$$

i=1,2 represents the monomer and polymer rich phases, respectively.

The monomer conversion can be calculated as:

$$X = 1 - \frac{\upsilon c_M}{n_{M_0}} \tag{3.34}$$

$$\upsilon_1 = \upsilon_0\left(1 - X - AX\right) \tag{3.35}$$

$$\upsilon_2 = \upsilon_0 X\left(A + \frac{\rho_m}{\rho_p}\right) \tag{3.36}$$

Stage 3. $X > X_c$

Above the critical conversion the monomer phase disappears and the polymerization reactions take place only in the polymer rich phase.

Mass balance for initiator:

$$\frac{d(\upsilon c_I)}{dt} = -\upsilon_2 k_{d_2} c_{I_2} \tag{3.37}$$

Mass balance for monomer:

$$\frac{d(\upsilon c_M)}{dt} = -\upsilon_2 \left(2 f k_{d_2} c_{I_2} c_{M_2} + k_{p_2} c_{M_2} \nu_{0_2} + k_{tM_2} c_{M_2} \nu_{0_2}\right) \tag{3.38}$$

Moment balances for live polymer radicals applying the QSSA:

$$\nu_{0_2} = \sqrt{\frac{2 f k_{d_2} c_{I_2}}{k_{t_2}}} \tag{3.39}$$

$$\nu_{1_2} = \frac{2 f k_{d_2} c_{I_2} + \left(k_{p_2} + k_{tM_2}\right) c_{M_2} \nu_{0_2}}{k_{tM_2} c_{M_2} + k_{t_2} \nu_{0_2}} \tag{3.40}$$

$$\nu_{2_2} = \frac{2 f k_{d_2} c_{I_2} + k_{p_2} c_{M_2} \left(\nu_{0_2} + 2\nu_{1_2}\right) + k_{tM_2} c_{M_2} \nu_{0_2}}{k_{tM_2} c_{M_2} + k_{t_2} \nu_{0_2}} \tag{3.41}$$

Moment balances for dead polymer chains are:

$$\frac{d(\upsilon \mu_0)}{dt} = \upsilon_2 \left(k_{tM_2} c_{M_2} + k_{t_2} \nu_{0_2}\right) \nu_{0_2} \tag{3.42}$$

$$\frac{d(\upsilon \mu_1)}{dt} = \upsilon_2 \left(k_{tM_2} c_{M_2} + k_{t_2} \nu_{0_2}\right) \nu_{1_2} \tag{3.43}$$

$$\frac{d(\upsilon \mu_2)}{dt} = \upsilon_2 \left(k_{tM_2} c_{M_2} + k_{t_2} \nu_{0_2}\right) \nu_{2_2} \tag{3.44}$$

The monomer conversion can be calculated by

$$X = 1 - \frac{\upsilon c_M}{n_{M_0}} \tag{3.45}$$

$$\upsilon_2 = \upsilon_0 \left(1 - X + X \frac{\rho_m}{\rho_p}\right) \tag{3.46}$$

The mass balance equations were solved by using the rate coefficients published by Sidiropoulou and Kiparissides (1990).

For polymer properties, the weight and number average molecular weights have been calculated from the moments of live and dead polymer chains, as:

$$MW = \frac{\mu_2 + \nu_2}{\mu_1 + \nu_1} \cdot M_w \tag{3.47}$$

$$MN = \frac{\mu_1 + \nu_1}{\mu_0 + \nu_0} \cdot M_w \tag{3.48}$$

The ratio of weight average molecular mass to the number average molecular mass is called polydispersity index, PDI. This gives an idea about the homogeneity of a polymer.

$$PDI = \frac{MW}{MN} \tag{3.49}$$

Prediction and control of molecular weight averages, number of short- and long chain branches and terminal double bonds per polymer molecule is of considerable importance to the PVC industry since the low thermal stability of PVC linked to the formation of some branched and unsaturated molecular structures mainly generated by chain transfer to monomer. In vinyl chloride polymerization, the molecular weight distribution (MWD) and molecular weight averages are actually controlled by transfer to monomer and are almost independent of the initiator concentration and monomer conversion up to a conversion of about 85%. In this conversion range the MWD of the polymer will be given by the most probable distribution, and the polydispersity index will be very close to 2. In the reality it is usually between 1.7-1.9 (Sidiropolou and Kiparissides, 1990). The molecular weight averages of PVC, produced in suspension polymerization, are classified based on the Fikentscher's K-value. It is used for correlating relative viscosity with the average degree of polymerization (Titow, 1984).

Since polymerization is highly exothermic, therefore the heat balance in droplets was calculated, too. The energy balance for a droplet is given with the following equations:

$$\frac{\rho_d c_{p_d} \upsilon \, dT_d}{dt} = \dot{Q}_{reaction} + \dot{Q}_{trans\_d} \tag{3.50}$$

where

$$\dot{Q}_{reaction} = -\Delta H_r n_{M_0} M_w \frac{dX}{dt} \tag{3.51}$$

and

$$\dot{Q}_{trans\_d} = -h_{dc} a_{dc} \left(T_d - T_c\right) \tag{3.52}$$

The convective heat transfer coefficient was found using empirical correlations. The non-dimensional heat transfer coefficient, or Nusselt number of the droplet, is defined as:

$$Nu_d = d_d h_{dc} / k_c \tag{3.53}$$

where h_{dc} is the convective heat transfer coefficient, and k_c is the thermal conductivity of the continuous phase. For sphere like droplets or particles, around which a fluid is flowing, the Nusselt number can be calculated by various correlations (Bird et al., 2002). For droplets, the most commonly used formula is the Ranz-Marshall correlation:

$$Nu_d = 2.0 + 0.6\,\mathrm{Re}_d^{1/2}\,\mathrm{Pr}_c^{1/3} \tag{3.54}$$

The Reynolds number is defined as:

$$\mathrm{Re}_d = \rho_c d_d \bar{u} / \mu_c \tag{3.55}$$

where $\bar{u}$ is the average droplet velocity, ρ_c is the continuous phase density, and μ_c is the continuous phase viscosity.

The Prandtl number is defined as:

$$\mathrm{Pr}_c = \frac{c_p \mu_c}{k_c} \tag{3.56}$$

where c_p is the specific heat and k_c is thermal conductivity.

Since the reactor is assumed to be perfectly mixed on macro-scale, the temperature of the continuous phase is homogenous in the reactor. The heat transfer from each droplet to the continuous phase was calculated; therefore, the heat balance for the continuous phase can be described, as:

$$\frac{\rho_c c_{p_c} V_c \, dT_c}{dt} = \sum_{i=1}^{N} \dot{Q}_{trans\_d} + \dot{Q}_{trans\_j} \tag{3.57}$$

where N is the number of droplets and

$$\dot{Q}_{trans\_j} = U \cdot A \cdot \left(T_c - T_j\right) \tag{3.58}$$

where U is the overall heat transfer coefficient, which is calculated according to Eqs.(1.24-26). For the calculation of the Nusselt number for the continuous phase in Eq.(1.25) the following constants have been used: C=0.74, a=0.67, b=0.33. The viscosity correction term was neglected. Since the chilled water is not viscous, the constants used on the jacket are: C=0.023, a=0.8, b=0.33. The

viscosity correction term was neglected, too. The calculations were carried out assuming a 5 mm thick stainless steel wall (Sinnott, 2005). The resulting overall heat transfer coefficient is 770 W/m^{2}K.

The heat balance for the cooling jacket is:

$$\frac{\rho_j c_{p_j} V_j \, dT_j}{dt} = \dot{Q}_{trans\_j} + q_j \rho_j c_{p_j} \left(T_{j,in} - T_j \right) \tag{3.59}$$

where q_j is the flow rate and $T_{j,in}$ is the inlet temperature of the cooling water.

From these we can see that modelling and simulation of suspension polymerization is a really complex problem. We have a 10 dimensional population balance equation and we have many droplets with minimum 10 differential equations, which are needed to solve in every simulation step. The explicit Euler method can be used to calculate the differential equations, if time step is small enough, and the system is not stiff. This is a fast method, but for stability a small step size may be needed. The higher order Runge-Kutta methods have greater stability for relatively longer time steps.

3.3.1. The simulation results

The computer program has been developed in MATLAB, and all simulation runs has been carried out in MATLAB environment. Some preliminary simulations were carried out for testing some numerical solver method (ode23 and ode15s) in MATLAB. The results were compared with the results of explicit Euler method. The simulation experiments showed that the explicit Euler method gave the same results and the CPU time was much lower. So the explicit Euler method was used to calculate the differential equations. The calculated time steps during the simulation were enough small due to the high frequency of the discrete events.

The first step of the algorithm is the generation of the initial droplet size distribution. In suspension polymerization of vinyl chloride, the monomer is added continuously to the continuous aqueous phase. During the filling process the droplet size distribution is changed dynamically. This changing was not simulated. An intermediary state was generated using a beta distribution with parameters: a=2, b=11. The initial droplet size distribution was generated from this state with the calculated breakage and collision frequencies. The details are given as follows:

The beta probability density function for a given value x and given pair of parameters a and b is:

$$y = f(x|a,b) = \frac{1}{B(a,b)} x^{a-1}(1-x)^{b-1} \boldsymbol{I}_{(0,1)}(x) \tag{3.60}$$

where $B(a,b)$ is the beta function. Indicator function $\boldsymbol{I}_{(0,1)}(x)$ ensures that only values of x in the range (0,1) have nonzero probability.

Fig.3.5 shows how the initial size distribution was used to generate of the initial monomer droplet size distribution. The blue curve shows the continuous Beta distribution and the red curve represents the discretized Beta distribution. The number of elements contained in a single class needs to be recounted in order to be able to calculate the breakage and collision frequencies.

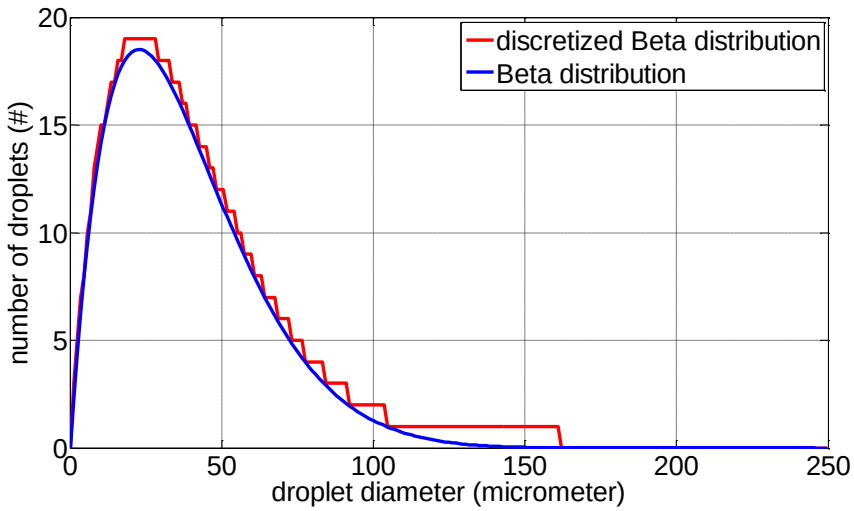

Figure 3.5. Droplet size distribution using beta distribution

Eqs.(1.14;1.18;1.19) used in the simulation to calculate the breakage and collision frequencies. The equations involve the energy dissipation rate ε, which is influenced by the impeller speed, impeller diameter, the power number of impeller and some physical properties of the liquid (Nere et al., 2003). The parameters C_I, C_{II}, C_{IV} and α in Eqs(1.14;1.18;1.19) were given by Alopaeus et al. (1999).

In this work, dissipation rates of 14 m^2/s^3 and 38 m^2/s^3 were used resulting from two different impeller speeds 250 rpm and 350 rpm, and assuming volume fractions of 0.3 and 0.1 for the dispersed phase (fi), respectively.

Fig.3.6 illustrates the breakage frequencies by different impeller speeds and volume fractions of dispersed phase. The differences are significant.

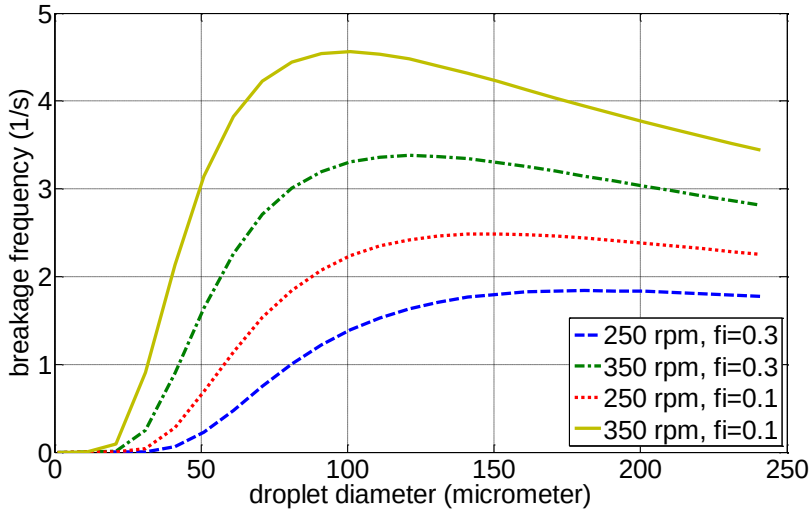

Figure 3.6. Effect of impeller speed and volume fraction of dispersed phase on breakage frequency

In Fig.3.7 can be seen the coalescence frequencies with different impeller speeds and dispersed phase fractions. On both of the x and y axis the droplet diameter is shown in micrometer. The simulations suggest that the effects of impeller speed and volume fraction of dispersed phase on the coalescence frequency are not so conspicuous in this range of droplet diameters; therefore the diameter of droplets is the dominant factor.

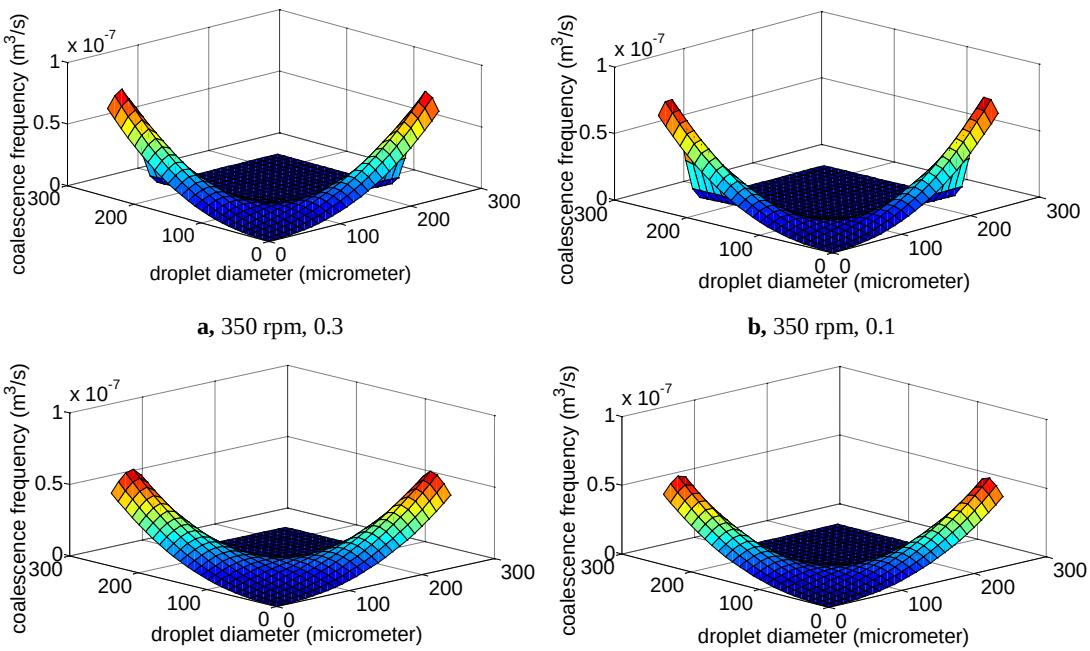

a, 350 rpm, 0.3 **b,** 350 rpm, 0.1

c, 250 rpm, 0.3 **d,** 250 rpm, 0.1

Figure 3.7. Effect of impeller speed and volume fraction of dispersed phase on coalescence frequency

In order to analyse the effects of the initial droplet size distribution and the distribution of initiator on monomer conversion during suspension polymerization of vinyl chloride the breakage and coalescence frequencies Eqs.(1.14;1.18;1.19) were applied to generate the initial droplet size distribution. In these cases, computations were carried out without reactions and the simulation results were compared to the monomer droplet size distributions from the literature published by Zerfa and Brooks (1996a,b) (Figure 3.8 (left side)).

As it is seen in Fig.3.8 the case when the impeller speed was 350 rpm and the volume fraction of dispersed phase was 0.3 the simulation data fit really well to experimental ones while for the volume fraction 0.1 of dispersed phase the similarity between the experimental and simulation size distribution is not so good. The parameters used in the simulation were measured out for 0.4 volume fraction. This is the reason for the simulation data with 0.3 volume fraction fit better than data with 0.1 volume fraction. It would have been necessary to apply other parameters for simulation the case of 0.1 volume fraction.

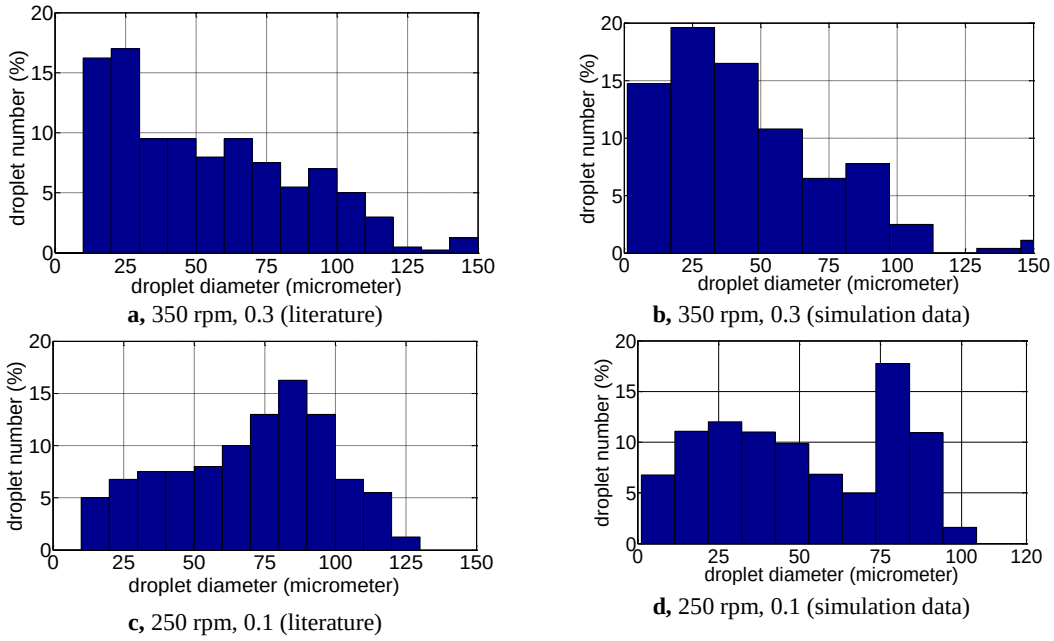

Figure 3.8. Comparison of experimental (Zerfa and Brooks, 1996a,b) and calculated data of the initial droplet size distributions.

Because the case when the impeller speed is 350 rpm, and the volume fraction of dispersed phase is 0.3 fit the literature data better, these parameters are used in all further simulation cases.

3.3.1.1 Algorithm verification

For simulation of suspension polymerization reactor of vinyl chloride the kinetic data were taken from the literature published by Sidiropoulou and Kiparissides (1990). In order to verify the simulation program, test simulation runs were performed with mono-dispersed initial size distribution of monomer droplets under isothermal conditions. The initial distribution of the same amount of initiator in the droplets was also uniform. This case provided an ideal reactor, mixed perfectly both on macro- and micro-scale, where all drops behave as identical perfectly mixed micro-reactors.

Fig.3.9 shows the change of monomer conversion with time. It can be seen that the simulation results and the experimental data (Sidiropoulou and Kiparissides, 1990) match remarkably well. So the computer program was verified by simulating the suspension polymerization of VC under isothermal conditions (50 °C).

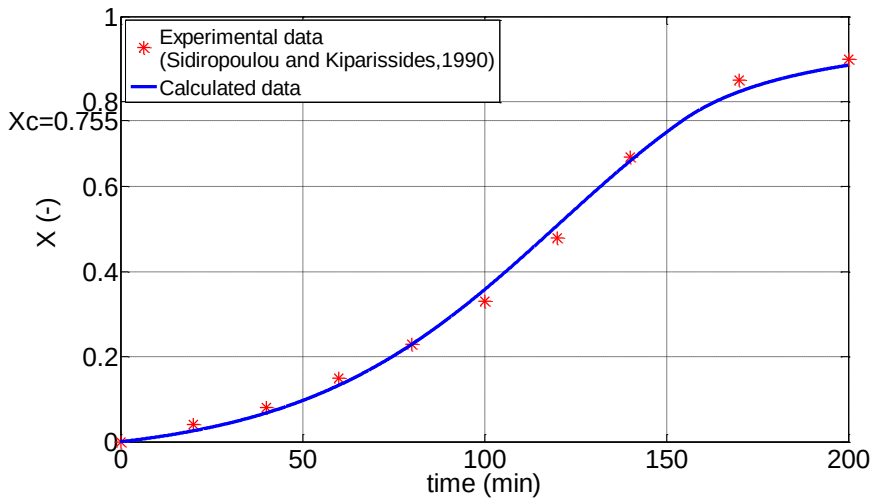

Figure 3.9. Experimental (*) and calculated (–) monomer conversion profile in an isothermal reactor. The droplet size distribution was uniform, all droplets contained the same amount of initiator, the amount of initiator was 0.0029 mole % based on monomer and the temperature was 50 °C.

3.3.1.2. Influence of initial initiator distribution and temperature

As a first task, the effect of initial initiator distribution on the monomer conversion and polymer properties was studied. Two cases of suspension polymerization of vinyl chloride can be distinguished by the method of add the initiator. In the first case, monomer and initiator are homogenized first, the mixture is filled into the reactor, than the reactor is heated to the reaction temperature. The advantage of this process is that the distribution of initiator is

perfect. The disadvantage is that the polymerization reactions take place not under isotherm conditions during the heating stage, therefore the properties of the polymer may be different and not homogeneous. In the second case, the monomer filled into the reactor and dispersed in the continuous aqueous phase by intensive stirring. The suspension heated to the polymerization temperature and after the initiator is added to the mixture. The advantage of this method is that the polymerization reactions take place under isothermal conditions; the properties of the polymer will be homogeneous. The disadvantage is that the initiator distribution may not be perfect. In this work, the second case was studied, i.e. the effect of the non-perfect initiator distribution.

The simulation runs were carried out in accordance with the procedure described in Section 3.1. First, the initial monomer droplet size distribution, as it is seen in Fig.3.8b, was generated and a fixed amount of initiator (0.29% on moles of monomer) was distributed randomly in the droplets. At the beginning of the process 25 %, 50 %, 75% or 100 % of droplets contain the initiator in parallel runs. All droplets can contain initiator up to the solubility limit. In all these cases, isothermal conditions were assumed. In the first case the temperature of polymerization was 50 °C and in the second case 55 °C. The droplet interactions considered are the coalescence, the binary breakage and the coalescence/ redispersion of droplets. When two droplets coalesce with each other, all components of the two droplets will mix. For this event, the concentration of monomer and initiator, the moments of the polymer chains, the volume and the conversion is recalculated. When a droplet breaks up, the state variables of the child droplets will be identical to the state variables of mother droplet. The volume of droplets will be equal. For the coalescence/redispersion event, elastic collision between the droplets assumed to occur during Stage 1 and Stage 2 of polymerization. Above the critical conversion, a solid shell grows up on the surface of droplets, which prevents the component transport between the two droplets. So if one of the colliding droplets is in Stage 3, an inelastic collision has been assumed.

The effects of inhomogeneities arising from the initial initiator distribution are shown in Fig.3.10 for two polymerization temperatures 50 °C (Fig.3.10a) and 55

°C (Fig.3.10b) under isothermal conditions. It can be seen that the more droplets contain initiator initially, the higher the monomer conversion is. The simulation results verify that a perfect initial initiator distribution is the most desirable to reach high conversion.

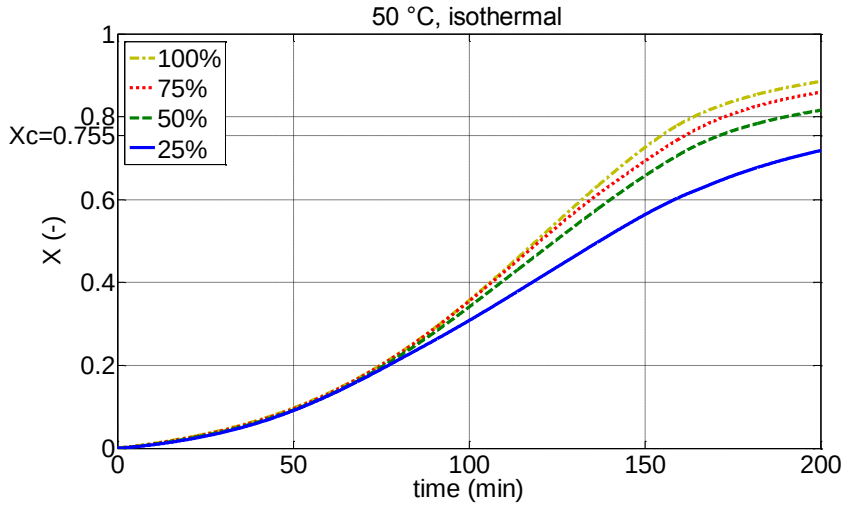

a,

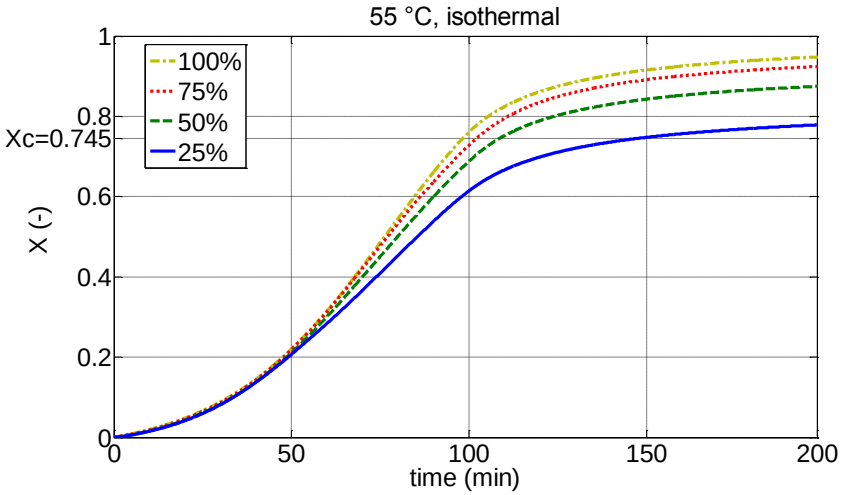

b,

Figure 3.10. The effect of initial initiator distribution on monomer conversion under isothermal conditions. The amount of initiator was 0.0029 mole % based on monomer and the continuous phase temperature was 50 °C (a) and 55 °C (b).

As it is seen in Fig.3.10, the higher the polymerization temperature is the higher the monomer conversion (at equal processing time and the same initial initiator distribution) is. In these cases, the influence of the initiator distribution proved to be significant. Although temperature speeds up the overall polymerization process, in Fig.3.11 and Fig.3.12 can be seen the complex results

of the temperature effects on the average polymer properties through the various competing chemical reactions.

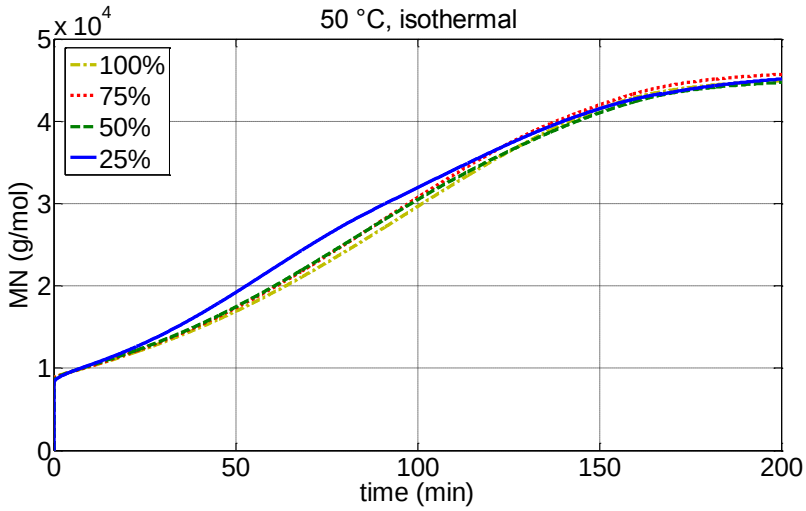

a,

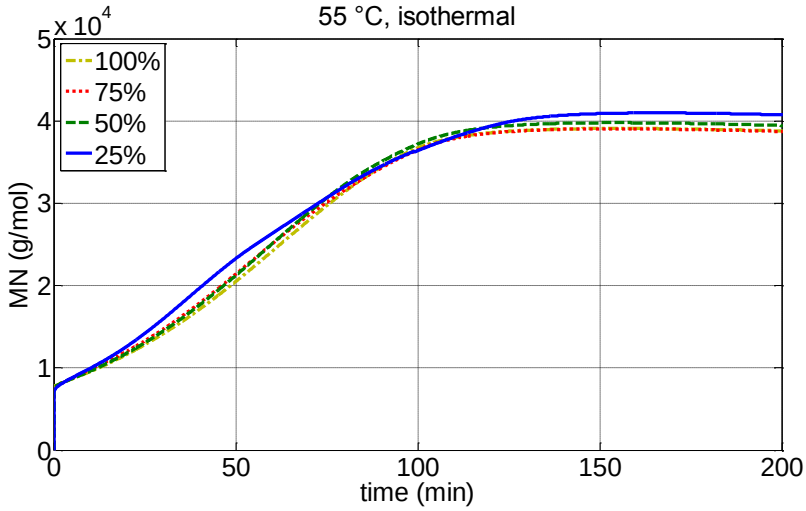

b,

Figure 3.11. The effect of initial initiator distribution on number average molecular weight under isothermal conditions. The amount of initiator was 0.0029 mole % based on monomer and the continuous phase temperature was 50 °C (a) and 55 °C (b).

Fig.3.11 and Fig.3.12 present the temporal evolutions of the number (MN) and weight average molecular weights (MW) of the polymer, respectively. Here, the effects of the initial initiator distribution appeared to be not so significant. Although in transient states some differences arise, the final values are practically very close to each other.

The results demonstrate well that the differences in the distribution of the initiator and the temperature of polymerization may affect the average monomer conversion and the polymer properties significantly. If initially 25% of droplets contain the initiator only, the monomer conversion is much lower than that for

100%. The temperature of polymerization has significant effect on polymer properties, too.

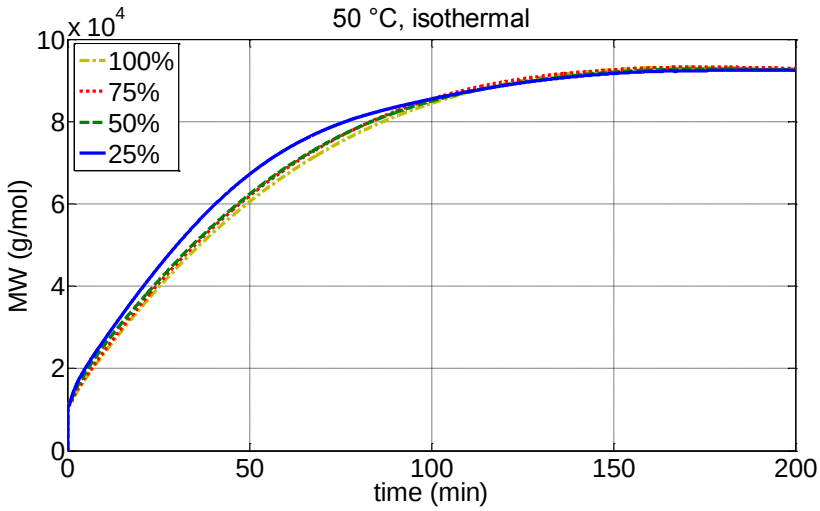

a,

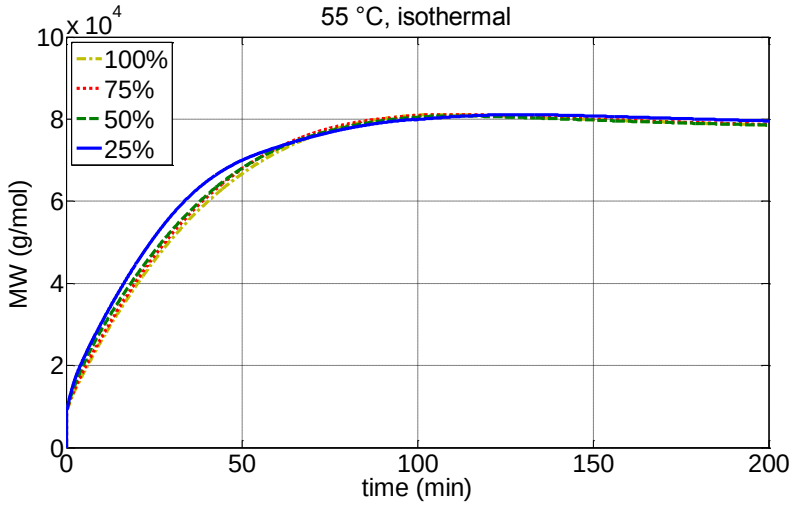

b,

Figure 3.12. The effect of initial initiator distribution on weight average molecular weight under isothermal conditions. The amount of initiator was 0.0029 mole % based on monomer and the continuous phase temperature was 50 °C (a) and 55 °C (b).

Based on the reported results and according to the actual performances of VC polymerization reactors, it is strongly advisable to operate in that macro- and micro-mixing regime where at least 50% of droplets contain the initiator.

In Fig.3.11, it can be seen that the number average molecular weight is lower on 55 °C than 50 °C. The individual reaction types were plotted with time to analyse the effect of temperature on the polymerization kinetics (Fig.3.13). The number of polymer chains was calculated (Fig.3.14):

$$\langle l \rangle_R = \frac{k_p \cdot [M] \cdot \nu_0}{k_t \cdot \nu_0^{\,2} + k_{tM} \cdot [M] \cdot \nu_0} \tag{3.61}$$

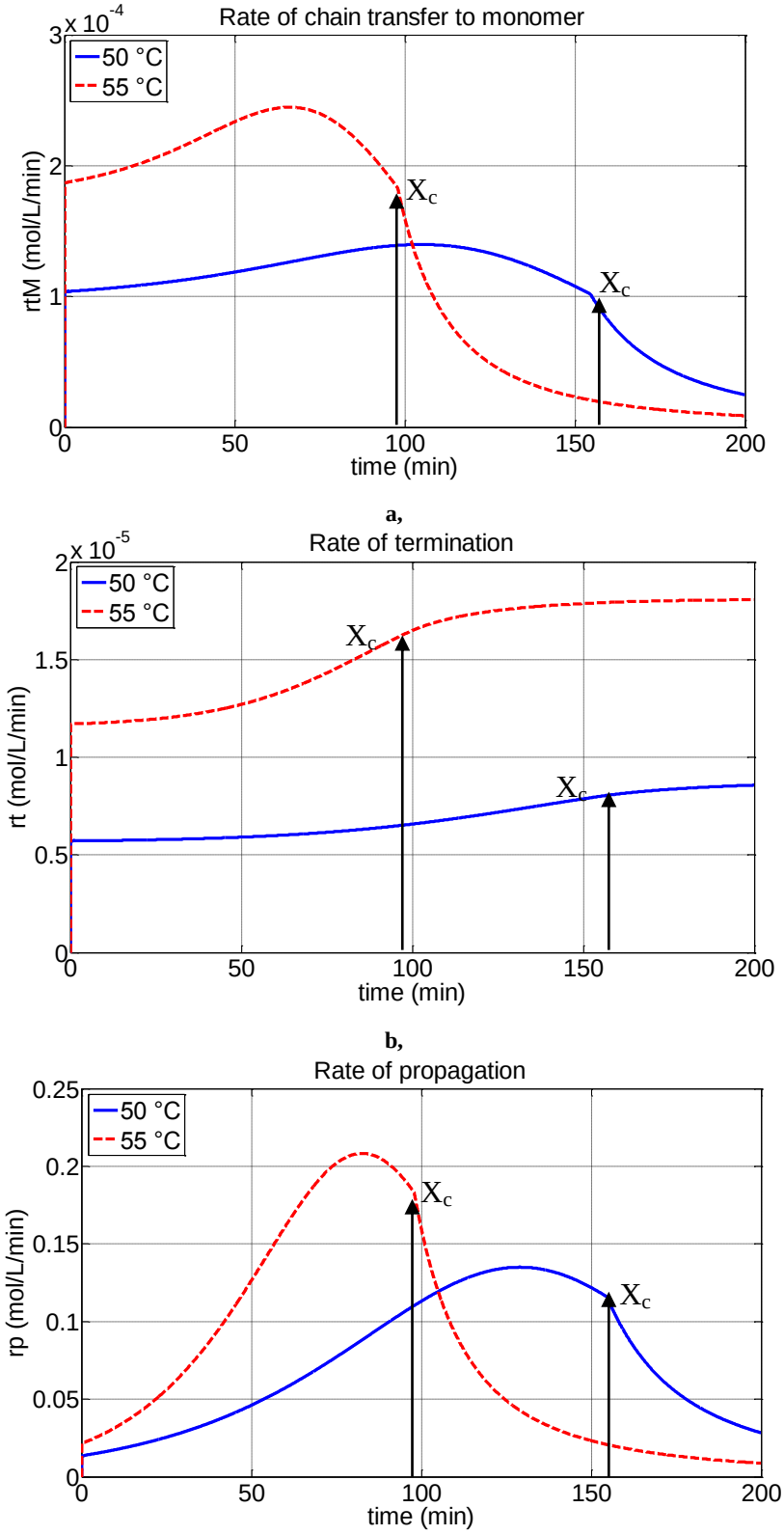

Figure 3.13. The effect of temperature on polymerization kinetics. Rate of chain transfer on monomer (a), rate of termination (b) and rate of propagation (c) with time at 50 °C (–) and 55 °C (--). X_c represent the time when the conversion reaches the critical conversion.

In Fig.3.14 can be seen the number of polymer chains with time at different temperature. From this figure can be seen that after the critical conversion the number of polymer chains decrease dramatically. At higher temperature, the decreasing is faster. Figs.3.13-14 give the interpretation of the phenomenon can be seen in Fig.3.11; at higher temperature the number average molecular weight is smaller.

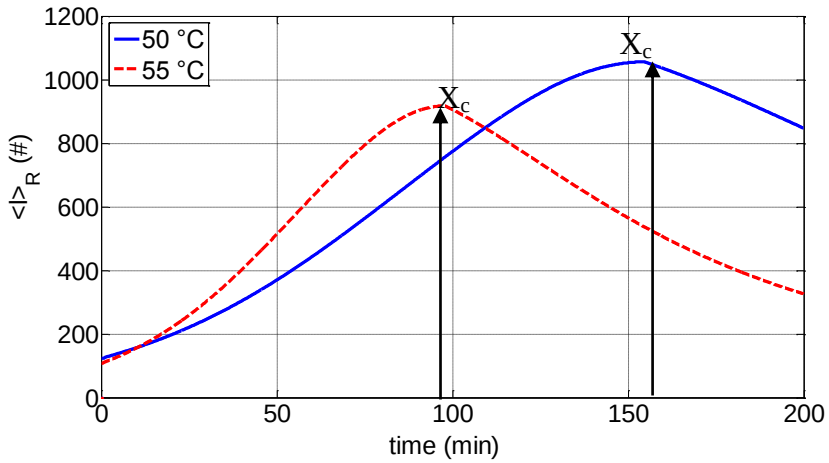

Figure 3.14. The number of polymer chains with time at 50 °C (–) and 55 °C (--). X_c represent the time when the conversion reaches the critical conversion.

Another interesting phenomenon is that the conversion increases with time, but MN and MW are constant (Fig.3.11-12). The sum of the zero order moment of live and dead polymer chains, and the sum of the first order moment of live and dead polymer chains were plotted to see the reason (Fig.3.15).

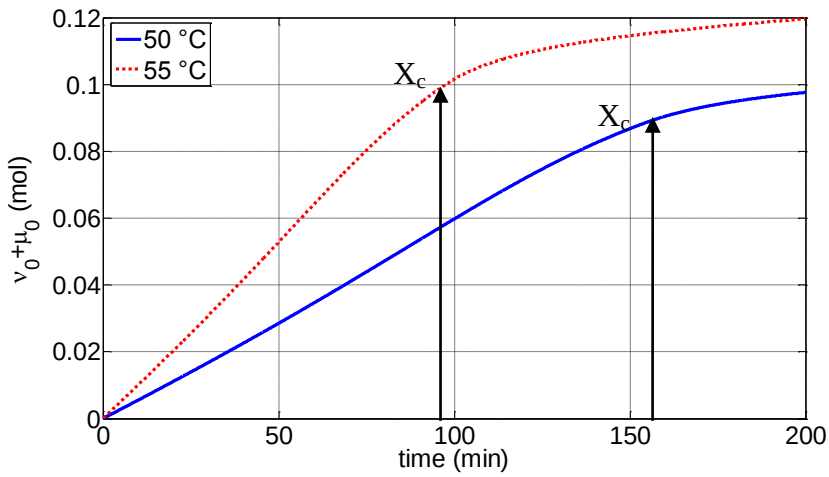

a,

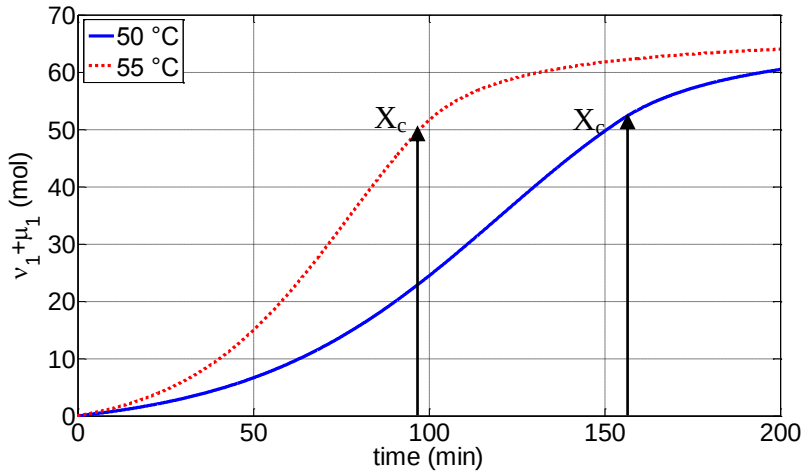

b,

Figure 3.15. The zero (a) and first (b) moment of live and dead polymer chains with time at 50 °C (–) and 55 °C (--). X_c represent the time when the conversion reaches the critical conversion.

As it is seen in Fig.3.15 above the critical conversion the curves will pall. This phenomenon is conspicuous at higher temperature. This is the reason why the MN and MW are constant at higher conversion.

3.3.1.3 Influence of initial droplet size distribution

The effects of the initial monomer droplet size distribution on the monomer conversion and polymer properties has been studied, too. The polymerization temperature was 50 °C. The case where initially all droplets have the same size has been compared to the case where the droplets have a non-uniform initial monomer droplet size distribution (Fig.3.8b). The uniform droplet diameter was 50 μm. In these simulations all meso-scale interactions, the coalescence, the binary breakage and the coalescence/redispersion of droplets were taken into consideration. Fig.3.16 shows the effect of initial monomer droplet size distribution together with different initial initiator distributions. Initially a random 25% (Fig.3.16a), 75% (Fig.3.16b) or 100% (Fig.3.16c) of droplets contain the initiator.

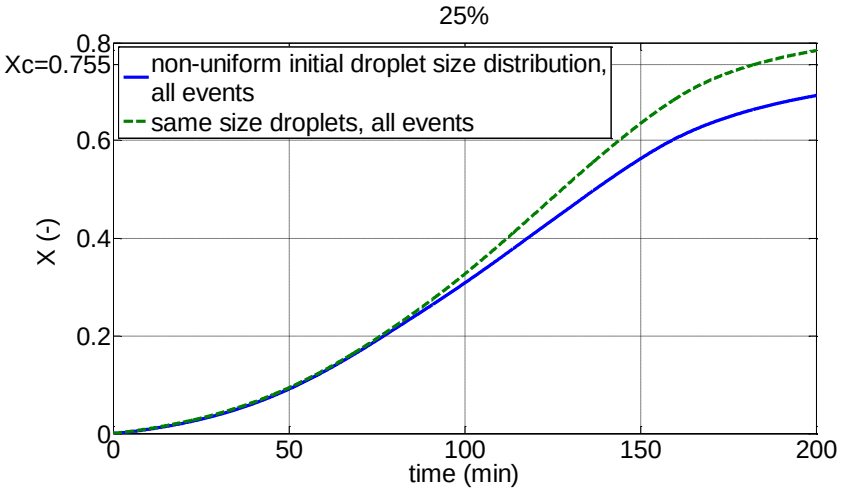

a, Initially 25% of droplets contain all the initiator

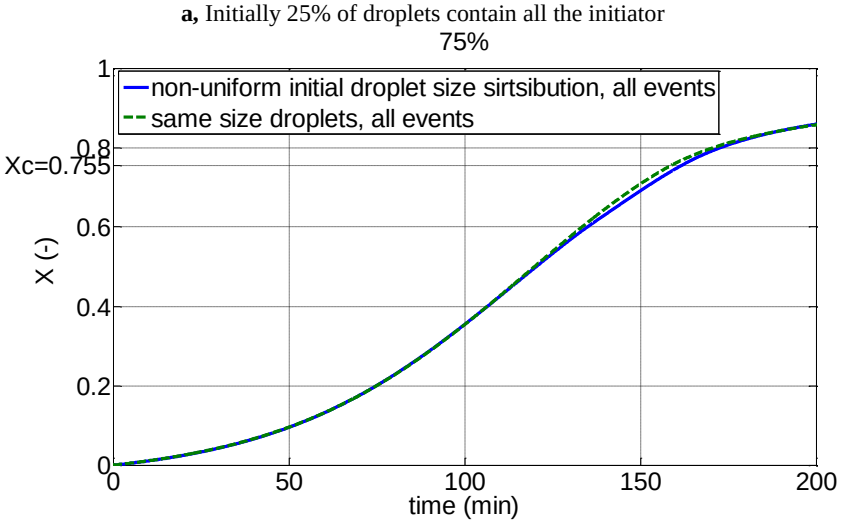

b, Initially 75% of droplets contain all the initiator

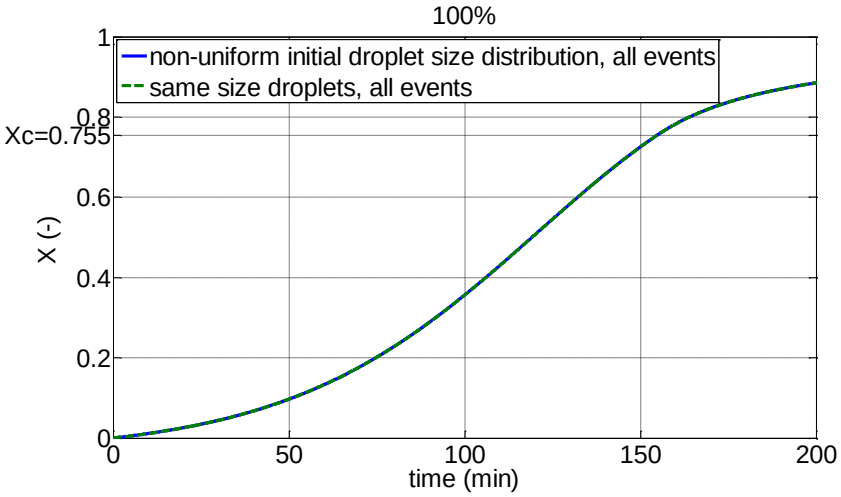

c, Initially 100% of droplets contain all the initiator

Figure 3.16. The effect of initial droplet size distribution on monomer conversion together with different initial initiator distributions. The amount of initiator was 0.0029 mole % based on monomer and the continuous phase temperature was 50 °C.

From Fig.3.16, it can be seen that the effect of initial monomer droplet size distribution is significant only if, initially a small number of droplets contain initiator. It can be seen in Fig.3.16a that the difference between the cases is significant. Fig.3.17 shows the number average molecular weights in the case of 25% initiated droplets. The time profiles for the two cases are quite close to each other, apart from a small deviation at intermediate conversions.

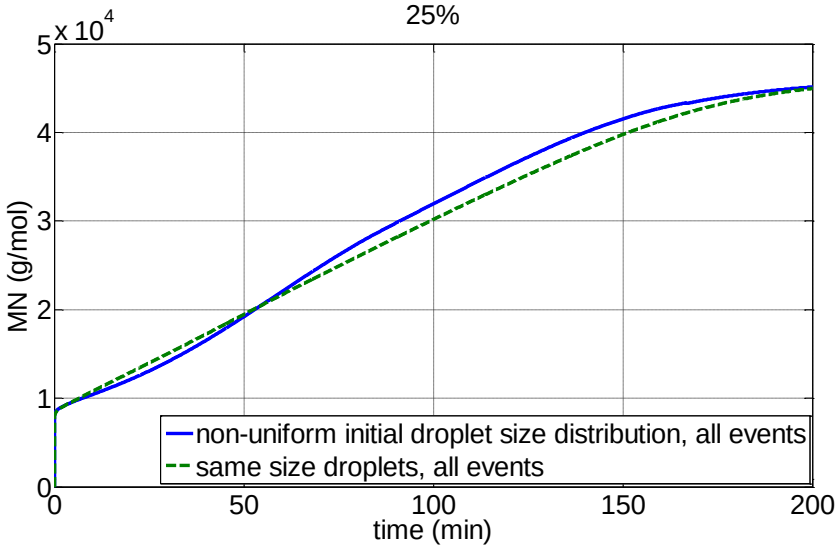

Figure 3.17. The effect of initial droplet size distribution on number average molecular weight, initially 25% of droplets contain initiator. The amount of initiator was 0.0029 mole % based on monomer and the continuous phase temperature was 50 °C.

The simulation results (Figs.3.16 and 3.17) demonstrated that a uniform initial droplet size distribution results in highest monomer conversion.

3.3.1.4 Influence of droplet interactions

The effects of droplet interactions on monomer conversion and polymer properties were studied. The temperature of the polymerization was 50 °C. In all simulations the monomer droplets had a non-uniform initial droplet size distribution (Fig.3.8b). Two cases were compared. In the first case, all meso-scale interactions were taken into consideration. In the second case it was assumed that the stabilization of droplets is perfect, therefore the coalescence and binary breakage of droplets are negligible and only coalescence/redispersion of droplets takes place in the reactor.

Fig.3.18 shows the effect of meso-scale interactions at different initial initiator distributions. Initially a random 25% (Fig.3.18a), 75% (Fig.3.18b) or 100% (Fig.3.18c) of droplets contain the initiator.

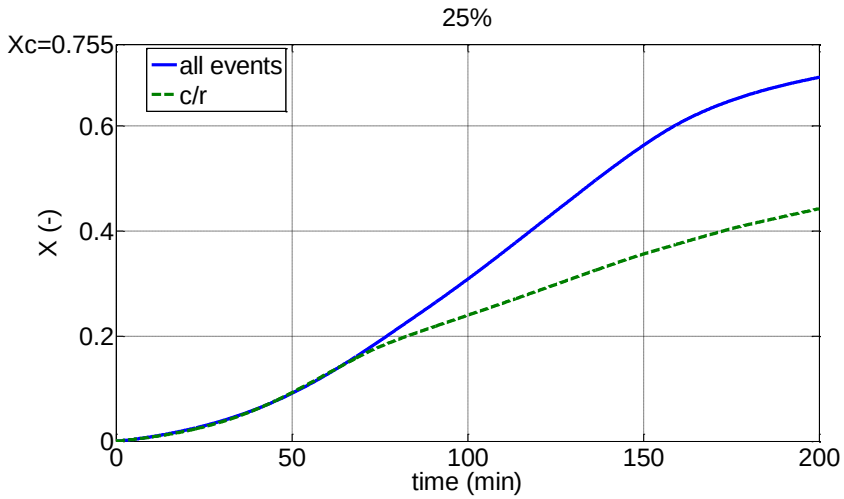

a, Initially 25% of droplets contain all the initiator

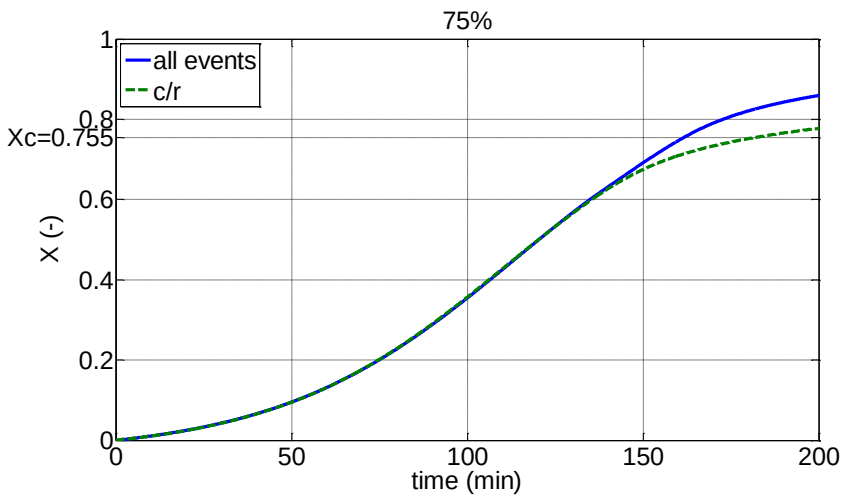

b, Initially 75% of droplets contain all the initiator

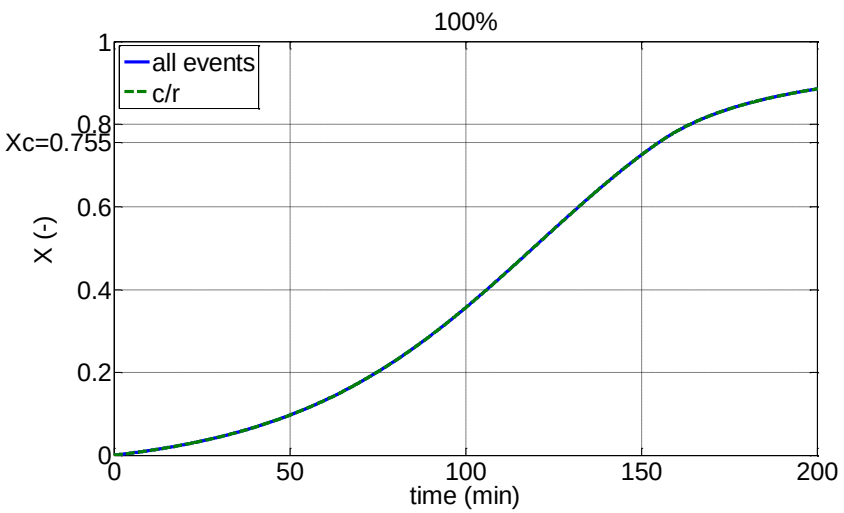

c, Initially 100% of droplets contain all the initiator

Figure 3.18. The effect of meso-scale interactions on monomer conversion together with non-uniform initial initiator distributions. The amount of initiator was 0.0029 mole % based on monomer and the continuous phase temperature was 50 °C

From Fig.3.18 can be seen that the effects of meso-scale interactions is significant if initially a relatively small number of droplets contain initiator, i.e. if the interactions significantly contribute to the redistribution of initiator and radicals. In Fig.3.18a and Fig.3.18b can be seen that the differences between the plotted cases are significant. Fig.3.19 shows the number average molecular weights in the cases of 25% (Fig.3.19a) and 75% (Fig.3.19b) initiated droplets.

It can be seen that the time profiles for the 75% initiated droplet case are quite similar, but at intermediate conversion, there is a small difference in the profiles. In the case of 25% initiated droplet case the difference between the two cases is remarkable, including the polymer properties, too.

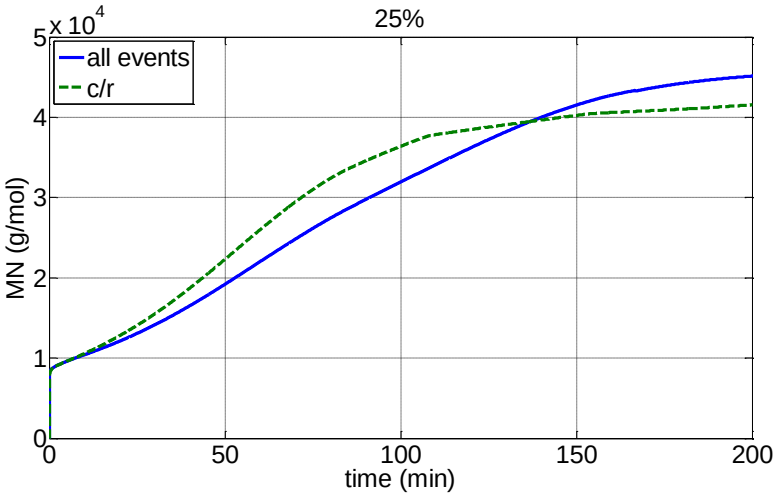

a, Initially 25% of droplets contain all the initiator

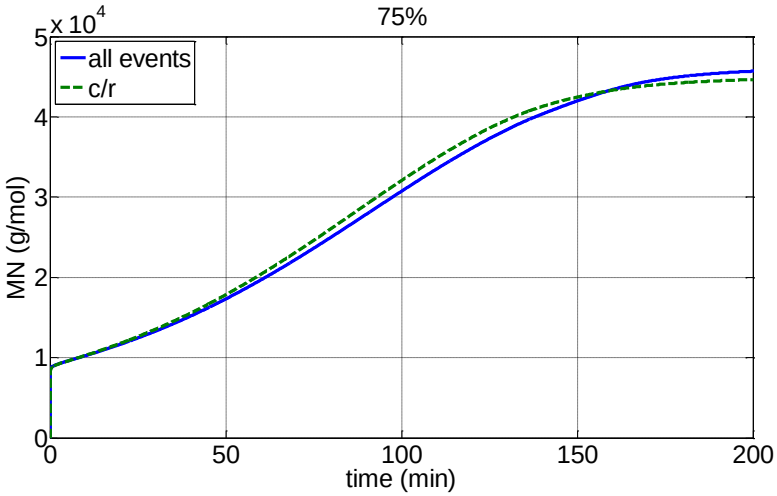

b, Initially 75% of droplets contain all the initiator

Figure 3.19. The effect of meso-scale interactions on number average molecular weight. Initially 25% (a) or 75% (b) of droplets contain initiator. The amount of initiator was 0.0029 mole % based on monomer and the continuous phase temperature was 50 °C

The simulation results (Figs.3.18 and 3.19) demonstrated that coalescence and breakage may help to redistribute the initiator and radicals between droplets significantly to reach a more uniform initiator distribution in the droplet population. Simulations for this section were carried out with a non-uniform initial droplet size distribution. It is reasonable to assume, however, that similar results would be obtained for the uniform case, too.

3.3.1.5 Influence of droplet temperature

The effect of temperature rise in the droplets was analysed in this section on monomer conversion and polymer properties. It is assumed commonly, that in suspension polymerization heat transfer between polymerizing droplets and the continuous phase is rapid and both phases have the same temperature (Meyer and Keurentjes, 2005). On the other hand, Nagy and Agachi (1997) demonstrated that variation of temperature could be maximum ± 0.5°C around the set point in order to ensure the proper quality of the product.

Since the reactions take place inside the monomer droplets and these reactions are highly exothermic, the temperature rise in the droplets during the process is of significant interest. In this section, the temperature rise in the droplets was computed under the conditions that the continuous phase was homogenised quickly and cooling of the reactor was perfect. Under these conditions, the temperature of the continuous phase was kept at 50 °C and 55 °C.

The initial droplet size distribution was non-uniform and the initial initiator distributions were the same as in the previous simulation runs. Behaviour of the system under isothermal and non-isothermal conditions was compared calculating the temperature rise in the droplets.

Fig.3.20 shows the time profile of average temperature of droplets for different continuous phase temperatures. The initial initiator distribution was uniform, so all droplets contain the same concentration of initiator and all meso-scale interactions were taken into consideration. In these simulations, the monomer droplets had initial droplet size distribution (Fig.3.8b). It can be seen that the higher the continuous phase temperature is the higher the rise of temperature in droplets is. When the temperature of continuous phase was kept at 50 °C the temperature rise in droplets was about 0.5 °C. If the temperature of continuous

phase was kept at 55 °C the temperature rise in droplets was about 1 °C. The convective heat transfer coefficient between the droplets and the continuous phase was calculated by empirical formulas, using Eqs.(3.53-56).

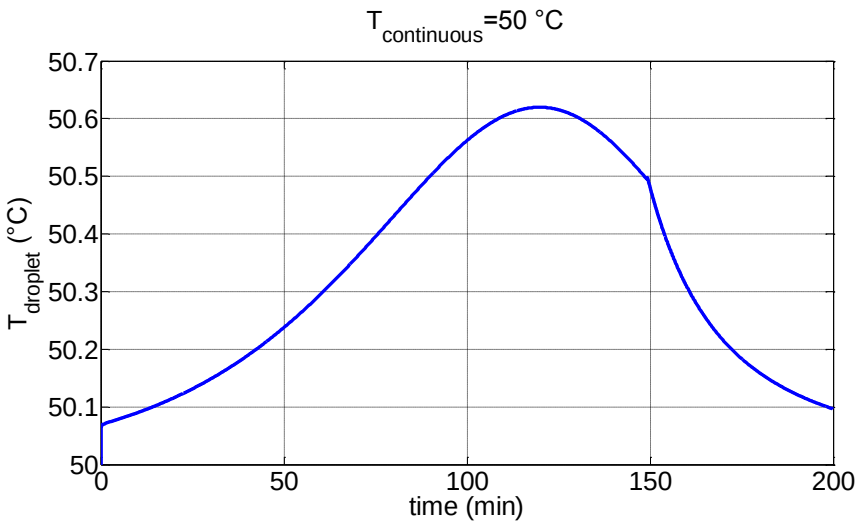

a, The temperature of continuous phase was 50 °C

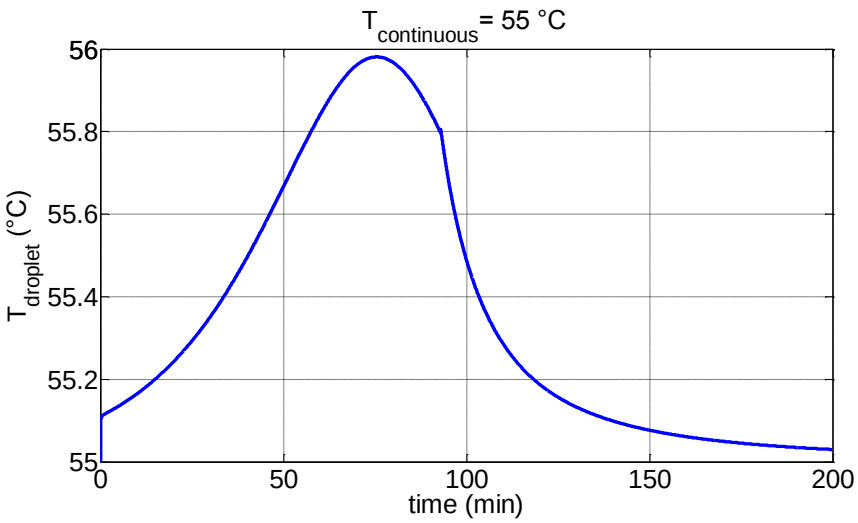

b, The temperature of continuous phase was 55 °C

Figure 3.20. The temperature rise in droplets during polymerization at different continuous phase temperature (a: 50 °C, b: 55 °C). The amount of initiator was 0.0029 mole % based on monomer, initially the initiator distribution was uniform.

From these results it can be seen that in both cases the temperature rise of droplets was in excess of 0.5°C. The effects of the temperature rise in droplets on the monomer conversion and the number average molecular weight of the polymer are presented in Fig.3.21-22. The case, where the temperature of droplets is assumed to be constant, was compared to the case where the temperature rise of droplets is calculated. Fig.3.21 presents the monomer conversions at 50 °C (3.21a)

and at 55 °C (3.21b). It can be seen that the effect of the above-mentioned 0.5 or 1 °C temperature rise in droplets causes differences between the isothermal and non-isothermal cases for intermediate conversions.

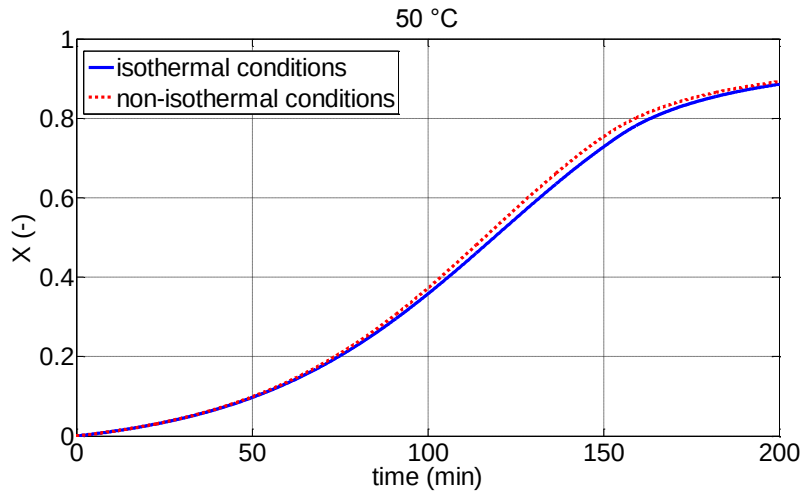

a,

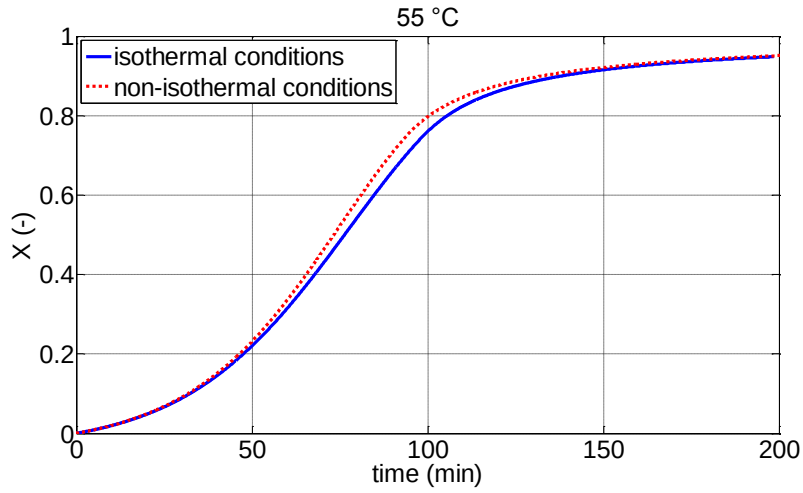

b,

Figure 3.21. The effect of the temperature rise in droplets on monomer conversion at different continuous phase temperature (a: 50 °C, b: 55 °C). The amount of initiator was 0.0029 mole % based on monomer, initially the initiator distribution was uniform.

Fig.3.22 shows the number average molecular weights under isothermal and non-isothermal cases at different temperatures. No significant differences can be seen in any of the cases. Note that the maximum temperature differences are only 0.5 and 1 °C. In the case of weight average molecular weight the differences were similarly small.

The results demonstrate that a 0.5°Cand 1°C change in temperature cause only small changes in the constitutive properties the particle size distribution. Note that

in these cases cooling of the reactor was perfect, namely the temperature of the continuous phase was kept constant.

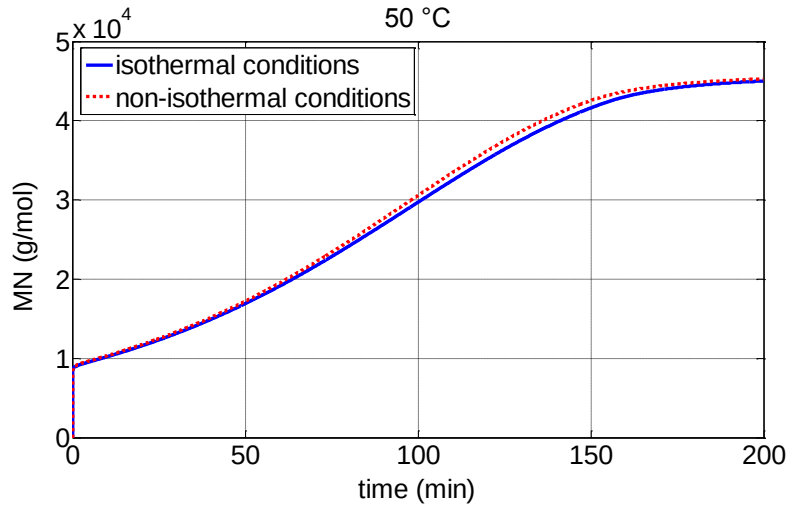

a,

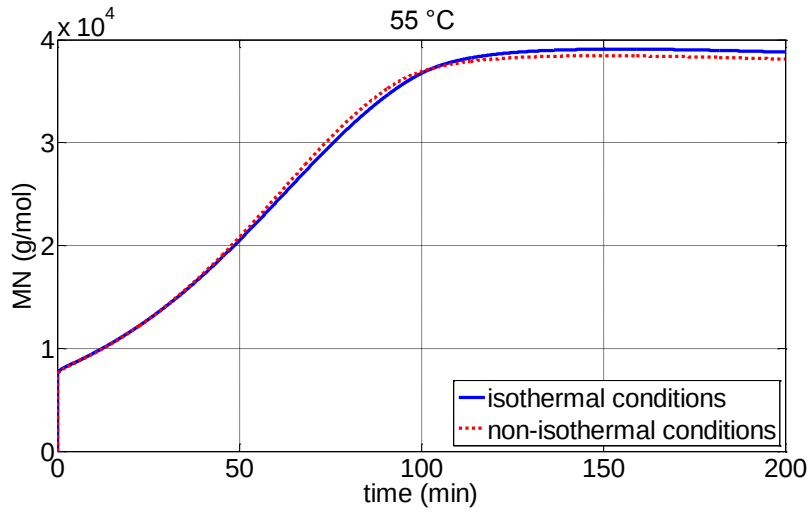

b,

Figure 3.22. The effect of the temperature rise in droplets on number average molecular weight at different continuous phase temperature (a: 50 °C, b: 55 °C). The amount of initiator was 0.0029 mole % based on monomer, initially the initiator distribution was uniform.

3.3.1.6 Influence of continuous phase temperature

The effect of temperature changes in the continuous phase on monomer conversion and polymer properties has been studied and is reported in this section. The total heat balance of the reactor has been calculated. The effects of initial initiator distribution was the same as in the previous cases. So in this only one case is shown in which the temperature of continuous phase and the temperature of cooling jacket were calculated.

As described in Section 3.2, simulations were carried out with a 2000 elements population. This is a representative population but in a normal industrial suspension polymerization reactor there are much more droplets. Thereto Eqs.(3.57-59) can be used to calculate the overall heat transfer coefficient between the reactor and cooling jacket. These parameters have been used for the simulation of a normal size stirred vessel. The number of droplets in a 1 m^3 reactor has been calculated and the transferred heat from droplets has been proportionally increased. After that the temperature of the continuous phase and cooling jacket were calculated by Eqs.(3.57-59). It was assumed that the temperature of continuous phase is homogeneous.

Although the aim of this work is not reactor temperature control, but if the temperature can hot be left without any control, to avoid instability and extremely high temperatures. Therefore, a simple control system was applied. During the calculation of reactions, the heat of polymerization reactions was calculated. In order to remove all the heat transferred to the dispersed phase, using the heat transfer coefficient referred above, the necessary flow rate of the cooling water was calculated in every simulation step. This is not a perfect control system but it was enough to keep the temperature in a stable range. The temperature of cooling water was 20 °C, and it can be seen in Fig.3.23 that the cooling jacket is not enough to keep the temperature around 50°C in ± 1°C range.

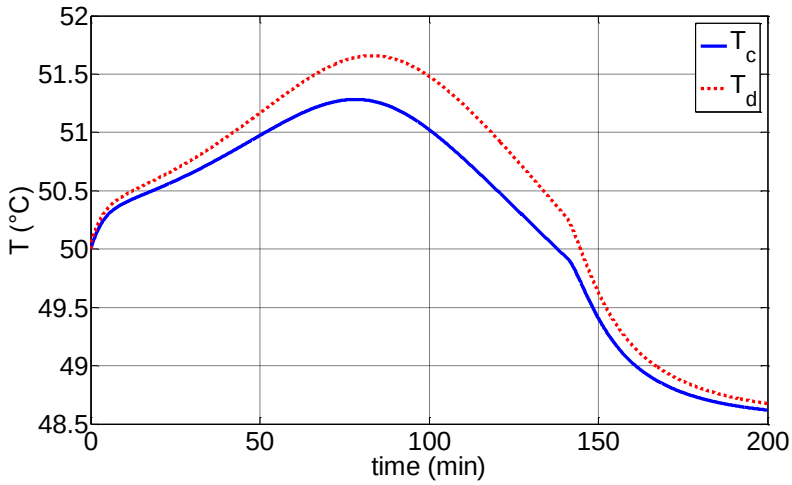

Figure 3.23. The temperature of the continuous phase (–) and the average temperature of the dispersed phase (··). The amount of initiator was 0.0029 mole % based on monomer, initially the initiator distribution was uniform and the temperature of polymerization was 50 °C.

When most of the heat transfer occurs via a cooling jacket, special strategies may be necessary to manage the heat transfer. For example a mixture of initiators could be used, with different half-lives and activation energies. Then it may become possible to match the heat generation rate with the cooling capacity of the reactor jacket. Another strategy is that the reactor cooling capacity is chosen to cope with heat generation rates in the later stages of batch operation, when auto-acceleration occurs, then the heat removal capacity of the reactor will not be fully utilized in the early stages of the polymerization. Another recommendation is that the reactor could be operated at a higher temperature in the early stages, to make full use of the cooling capacity (Meyer and Keurentjes, 2005). In industrial cases the use of reflux condensers can support the effect of the cooling jacket (Zerfa and Brooks, 1997).

In Fig.3.24, the calculated temperature change in the cooling jacket is shown. It is the result of control. It can be seen that it follows really well the temperature changing in the dispersed and continuous phase.

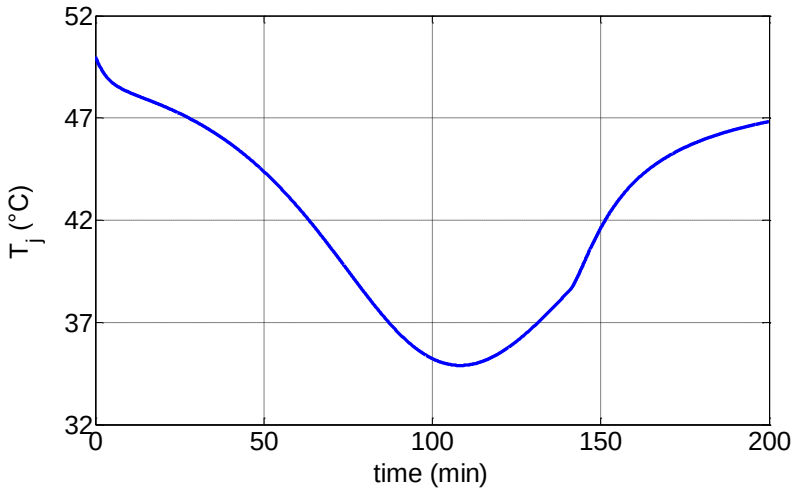

Figure 3.24. The temperature profile of the cooling jacket. The temperature of polymerization was 50 °C, the inlet temperature of cooling jacket was 20 °C.

Fig.3.25 shows the effect of the non-isothermal conditions on monomer conversion. It can be seen that there is some difference between the isothermal and non-isothermal cases for intermediate conversions.

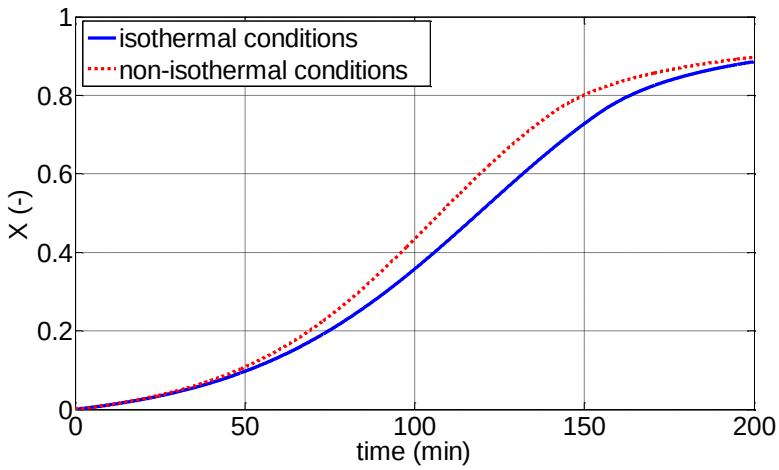

Figure 3.25. The monomer conversion profiles for isothermal (–) and non-isothermal (··) conditions. The amount of initiator was 0.0029 mole % based on monomer, initially the initiator distribution was uniform and the temperature of polymerization was 50 °C.

Fig.3.26 shows the effect of the non-isothermal conditions on number and weight average molecular weights. It can be seen that there are some differences between the cases even for the final product. So it can be seen that it is important to control the temperature in order to ensure the proper quality of the product.

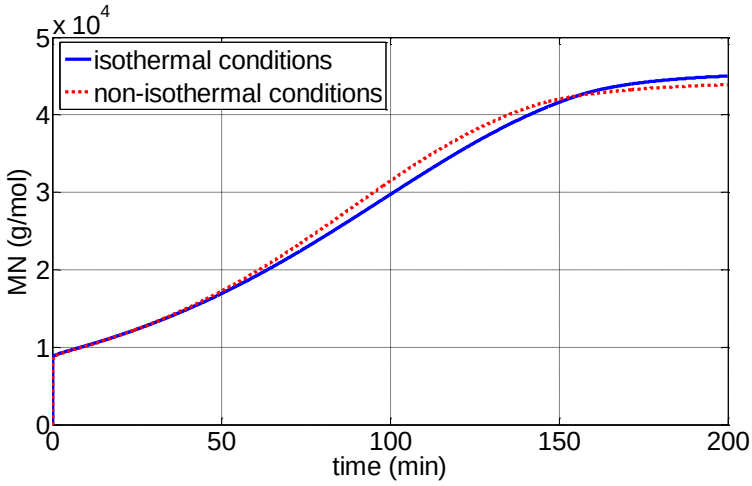

a, The number average molecular weight

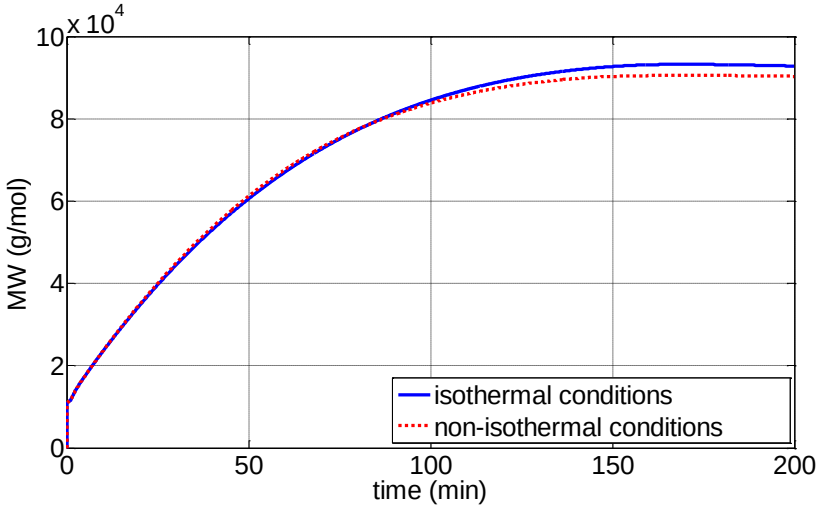

b, The weight average molecular weight

Figure 3.26. The weight (a) and number average (b) molecular weight for isothermal (–) and non-isothermal (··) conditions. The amount of initiator was 0.0029 mole % based on monomer, initially the initiator distribution was uniform and the temperature of polymerization was 50 °C.

4. Application of Monte Carlo method for the calculation of micromixing in turbulent, non-isothermal continuous stirred reactor

Continuous reactors are commonly used for producing synthetic polymers. In many cases, they offer certain advantages over batch reactors in terms of product quality and ease of handling reagents and product. Because reactions can reach a steady state in continuous reactors, this configuration can also be of fundamental value to study kinetics and mechanisms of reactions. In this section, it is demonstrated that the model and the worked out Monte Carlo method is suitable to analyse the behaviour of continuous reactors. In this section, a simple reaction is taking place in the reactor instead of polymerization.

In Section 1.3 the idea of micromixing in turbulent continuous stirred reactors has been summarized. A detailed study of a continuous stirred tank reactor (CSTR) combined with the generalized coalescence/redispersion model of micromixing was presented by Lakatos et al. (2011). Applying the population balance approach, fluid elements are identified as Kolmogorov microscale eddies under the given turbulence conditions, assumed to be generated in the eddy space by the energy cascade process. This model represents fluid as a population of a large number of fluid elements, which interact with each other by random pair-wise coalescence, instantaneous concentration homogenization and subsequent redispersion into identical pairs. For studying the properties and behaviour of a continuous stirred tank coalescence/redispersion reactor Lakatos et al. (2011) applied a multidimensional moment method, using the joint moments of concentrations.

The chemical reactions may be exothermic or endothermic, i.e. the temperature usually is changing throughout the reactions. The temperature influences the coefficients of reaction rates and in a non-isothermal reactor the reaction rate coefficients have to be calculated for every time step. For the temperature dependence of reaction rates the Arrhenius' equation used to be applied.

The general form of this equation is

$$k = Ae^{-E_a/(RT)} \tag{4.1}$$

where k is the rate coefficient, T is the temperature, A is the pre-exponential factor, E_a is the activation energy and R is the universal gas constant. Since this equation includes the temperature through an exponential function, computations with this equation by using the moment method is very complex, sometimes it is impossible. For that reason, the Monte Carlo method seems to be a good choice to simulate the system.

4.1 The analysed system and model equations

The continuous stirred tank reactor (CSTR) studied here, was assumed to be perfectly mixed on macro level. Since the model represents fluid as a population of a large number of fluid elements, which interact with each other by random pair-wise coalescence, therefore the mixing on micro level can be non-perfect. In this section only a coalescence/redispersion process is taken into consideration in simulations without the aggregation and breakage processes. Fig.4.1 shows the scheme of the modelled and simulated reactor.

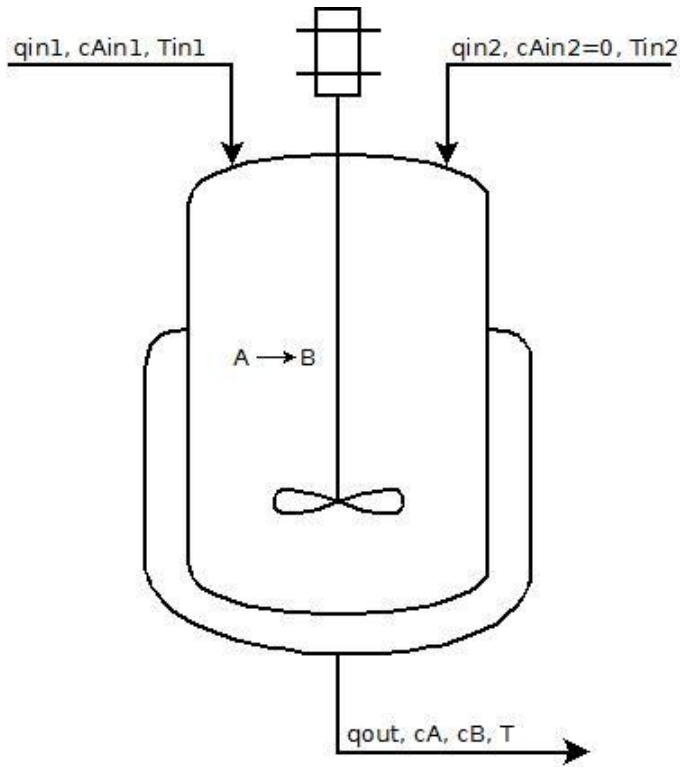

Figure 4.1. The scheme of the simulated continuous reactor

At the beginning of process, the reactor is full of fluid elements without component A, and temperature of the reactor was 30°C. The reactor has two inlet flows. One of them contains component A (temperature is 30 °C) the other inlet flow does not contain any A component but its temperature is 207 °C. It assumed that the volume of reaction mixture is constant during the process and all the fluid elements has the same volume. In the reactor, a second order reaction takes place:

$$A \xrightarrow{k} B \tag{4.2}$$

The balance equations of the CSTR, i.e. perfectly mixed on both macro- and micro-level are:

$$\frac{dVc_A}{dt} = q_{in,1}\, c_{A,in,1} + q_{in,2}\, c_{A,in,2} - q_{out}\, c_A - V\, k\, c_A^2 \tag{4.3}$$

$$\frac{dVc_B}{dt} = V\, k\, c_A^2 - q_{out}\, c_B \tag{4.4}$$

$$\frac{dV\rho\, c_p\, T}{dt} = \rho_1\, c_{p,1}\, q_{in,1}\, T_1 + \rho_2\, c_{p,2}\, q_{in,2}\, T_2 - \rho\, c_p\, q_{out}\, T + V(-\Delta H)\, k\, c_A^2 \tag{4.5}$$

where $q_{in,i}$ are the inlet flow rates, q_{out} is the outlet flow rate, $c_{A,in}$ the inlet concentration of component A.

The population balance model, formulated by Lakatos (2008), describing the behaviour of fluid elements in an ideally stirred reactor on macro level takes the following form:

$$\begin{aligned}\frac{\partial n(\boldsymbol{c},T,t)}{\partial t} + \sum_{k=1}^{K} \frac{\partial}{\partial c_k}\left[R_{ck}(\boldsymbol{c},T)\, n(\boldsymbol{c},T,t)\right] == \frac{1}{V} q_{in,1} n_{in,1}(c_{A,in,1},T_1,t) + \\ \frac{1}{V}\left[q_{in,2} n_{in,2}(c_{A,in,2},T_2,t) - q_{out}\, n(\boldsymbol{c}_{out},T,t)\right] + \boldsymbol{M}_i^{K}\left[n(\boldsymbol{c},T,t)\right]\end{aligned} \tag{4.6}$$

where k denotes components A and B, subject to the initial condition

$$n(\boldsymbol{c},T,t) = n_0(\boldsymbol{c},T) \tag{4.7}$$

In Eq.(4.6), operator $\boldsymbol{M}_i^{K}\left[n(\boldsymbol{c},T,t)\right]$ denotes the generalized coalescence/redispersion model of micromixing defined as

$$
\begin{aligned}
&\boldsymbol{M}_i^k\left[n(\upsilon,\boldsymbol{c},T,t)\right]= \\
&-\frac{2^K S_{col}}{N(t)}\int_{T_{\min}}^{T_{\max}}\int_{T_{\min}}^{T_{\max}}\int_{\mathbf{0}}^{\boldsymbol{c_m}}\int_{\mathbf{0}}^{\boldsymbol{c_m}}\int_{0}^{1}\frac{1}{\omega_T}\delta_{T'}\left[\left(\frac{(T'-T)}{\omega_T}+T\right)-T''\right]\prod_{k=1}^{K}\frac{1}{\omega_k}\delta_{c_k'}\left[\left(\frac{2(c_k'-c_k)}{\omega_k}+c_k\right)-c_k''\right]\times \\
&\times f_\omega(\boldsymbol{\omega})n(\upsilon,\boldsymbol{c}',T',t)n(\upsilon'',\boldsymbol{c}'',T'',t)d\boldsymbol{\omega}d\boldsymbol{c}'d\boldsymbol{c}''dT'dT'' \\
&+\frac{2^K S_{col}}{N(t)}\int_{T_{\min}}^{T_{\max}}\int_{T_{\min}}^{T_{\max}}\int_{\mathbf{0}}^{\boldsymbol{c_m}}\int_{\mathbf{0}}^{\boldsymbol{c_m}}\int_{0}^{1}\frac{1}{\omega_T}\delta_{T'}\left[\left(\frac{(T-T')}{\omega_T}+T'\right)-T''\right]\prod_{k=1}^{K}\frac{1}{\omega_k}\delta_{c_k'}\left[\left(\frac{2(c_k-c_k')}{\omega_k}+c_k'\right)+c_k''\right]\times \\
&\times f_\omega(\boldsymbol{\omega})n(\upsilon,\boldsymbol{c}',T',t)n(\upsilon'',\boldsymbol{c}'',T'',t)d\boldsymbol{\omega}d\boldsymbol{c}'d\boldsymbol{c}''dT'dT''
\end{aligned}
\tag{4.8}
$$

where the first term on the right hand side represents the rate of decrease in the number of fluid elements of concentration $\boldsymbol{c}$ because of colliding with fluid elements of concentration $\boldsymbol{c}''$, producing fluid elements of concentration $\boldsymbol{c}'$, and the second integral represents the rate of increase in the number of fluid elements with concentration c because of colliding two fluid elements of concentrations $\boldsymbol{c}'$ and $\boldsymbol{c}''$. In Eq.(4.8) K=2.

The boundary conditions for concentration variables specify closed system along the concentration coordinates:

$$
R_{ck}(\boldsymbol{c},T)n(\boldsymbol{c},T,t)\big|_{c_k=0}=0 \qquad \text{and} \qquad R_{ck}(\boldsymbol{c},T)n(\boldsymbol{c},T,t)\big|_{c_k=c_{k,m}}=0 \tag{4.9}
$$

In Eq.(4.8), S_{col} denotes the frequency of collisions of fluid elements, $\boldsymbol{\omega}=(\omega_1,\omega_2)$ denotes the vector of random variables with support [0,1] and probability density functions $f_\omega(\boldsymbol{\omega})=(f_{\omega 1}(\omega_1),\ f_{\omega 2}(\omega_2))$ which characterise the measure of concentration equalization of components A and B between two fluid elements induced by a coalescence/redispersion event. Further, δ_{c_k} stands for the Dirac-delta function with argument c_k, and ω_K is defined by Eq.(2.25).

4.2. The applied Monte Carlo method

The Monte Carlo method described in Section 3.1 was improved in order to model micromixing phenomena in continuous stirred vessels in which exothermic or endothermic chemical reactions take place. The reactor was perfectly mixed on macro-level, i.e. the average temperature and concentrations of species were constant over the reactor.

The elements, which are involved in coalescence/redispersion events, are selected randomly using random numbers generated from the uniform probability distribution in (0,1). In the intervals between subsequent events, computations are carried out using continuous time computations.

The steps of the solution method are presented in Fig.4.2 and is described as follows:

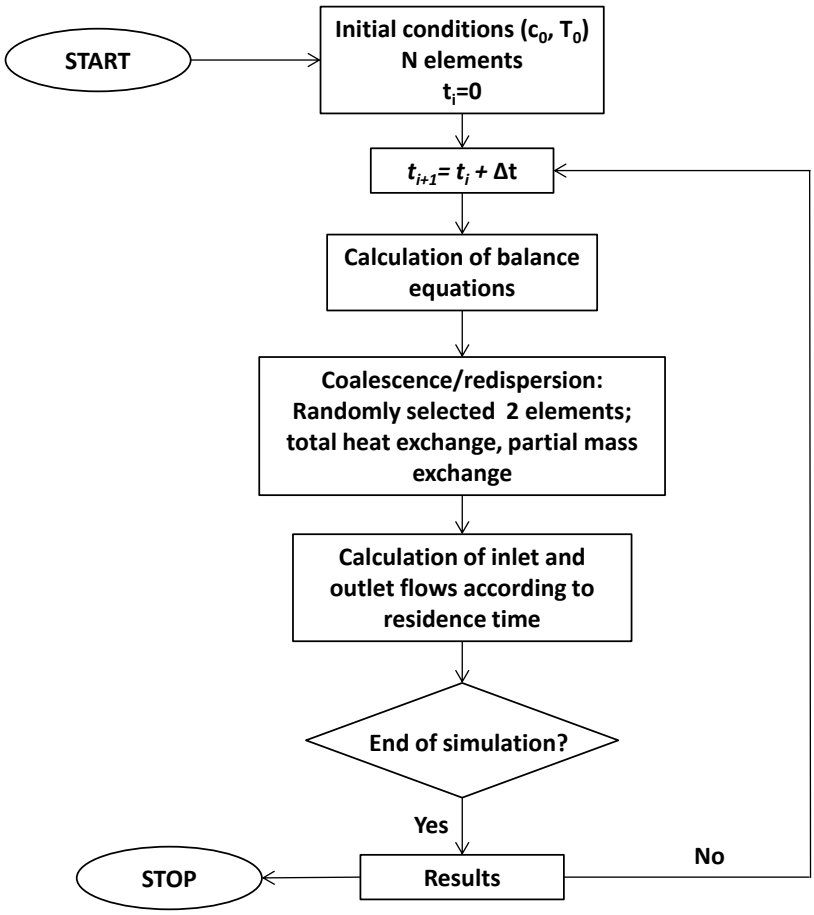

Figure 4.2. The algorithm of simulation of continuous, stirred reactor

Initialization: The initial number of fluid elements is defined. The number of fluid elements is *N*. Set the time equal to zero. All state variables are given initial values: concentrations of species inside the fluid elements and the temperature of fluid elements. Concentration and temperature classes are defined according to the limits of key component concentration and of the temperature limits of fluid elements.

Step 1: Set the simulation time to $t_{i+1} = t_i + \Delta t$, where Δt is the time step between two coalescence/redispersion processes. The time step Δt is a model parameter, it is necessary to calculate for each simulated system, i.e. reaction system. The time step Δt is needed to choose in relation to the mean residence time of the reactor, i.e. to make the simulation program suitable to describe the concentration and temperature profiles in a continuous stirred tank reactor mixed perfectly at both macro- and microscale.

Step 2: Reactions take place in the fluid elements, so, for all elements integrate the set of intra-particle reactions from t_i to t_{i+1}. The concentration and temperature of elements are changed continuously in time because of the reactions. The volume of elements is assumed to be constant during the process.

Step 3: The coalescence/redispersion events are calculated. The number of colliding elements is a variable parameter by means of which the degree of micromixing is modulated. The sufficient number of fluid element pairs is selected randomly. The members of the pairs collide with each other without coalescence, and total heat and partial mass exchange happens between them. The volume of elements does not change during the event, $V_i = \text{constant}$. The total number of elements does not change and remains N.

Step 4: The inlet and outlet flows are calculated according to the residence time. Since the reactor is perfectly mixed on macro-level therefore it is necessary to guarantee that the mean concentrations and temperature of the outlet flow are equal to the temperature and concentration inside the reactor:

$$\bar{c}_k = \sum_{i=1}^{m} \frac{n_i}{N} \bar{c}_{k\,i} \tag{4.10}$$

where $\bar{c}_k$ is the mean concentration of component k in the reactor, i denotes the serial number of a class, N is the total number of fluid elements in the reactor, n_i the number of fluid elements in the class i, $\bar{c}_{k\,i}$ is the mean concentration of component k in the class i.

A matrix is generated for determination of the fluid elements in the outlet flow. The columns of the matrix denote the concentration classes and the rows denote the temperature classes. In this matrix, it counts that how many elements are in the concentration and temperature classes. Using this matrix and the residence time, a suitable number of fluid elements from the classes are taken away and the same concentration and temperature can be guaranteed for the outlet flow and the inventory. The number of fluid elements in the inlet flow is the same as in the

outlet flow, since the volume of fluid elements are equal.

Step 5: If $t_{i+1} \geq t_{final}$ then stop, i.e. end the simulation otherwise go to ***Step 1***.

4.3. The simulation results

4.3.1 Algorithm verification

As a first step, the Monte Carlo algorithm developed was verified. In these cases, the fluid was described as a population of a large number of fluid elements, which interact with each other by random pair-wise coalescence. The initial conditions were the same as for the perfectly mixed case. A 10000 element population was used in simulation. In every step, a number of elements defined by the mean residence time was taken away and added also to the mixture. There were two input flows and the flow rates were equal. The elements in the first input flow contained component A, and their temperature was 30 °C. The elements in the second input flow did not contain component A, and their temperature was 207 °C. In the fluid elements, which contained component A, the chemical reaction took place and generated component B. In coalescence/redispersion events concentration (A and B) and heat transfer took place between the colliding fluid elements. The initially empty fluid elements got species A through these events.

In these simulations complete component and heat transport has been assumed (ω_T and ω_{ck} were 1) between the colliding droplets (Eq.4.8). The balance equations were calculated with the explicit Euler method, the time step was 0.01 s. In every time step (Δt=0.01s) all droplets take part in one collision (100%). With these parameters can be described the perfectly mixed CSTR, both in exothermic and endothermic cases.

Exothermic case:

Figs.4.3-4.5 present the cases when the chemical reaction taking place in the fluid elements was exothermic. The solid line represents the perfectly mixed CSTR (perfectly mixed both on macro- and micro-level), and the dotted line represents the CSTR calculated with Monte Carlo simulation. It is seen that there is a little differences in the steady state. This can be minimalized if the time step is smaller but then the calculation time will be much longer. The changes due to micromixing in concentration and temperature profiles were much higher than the

differences between steady states due to the time step, so the time step in simulations was 0.01 s.

Notation used in the following Figures: MC=simulation with Monte Carlo method, the first number is that how many percent of droplets take part in collision, the second number is ω_{ck} and the third number is ω_T.

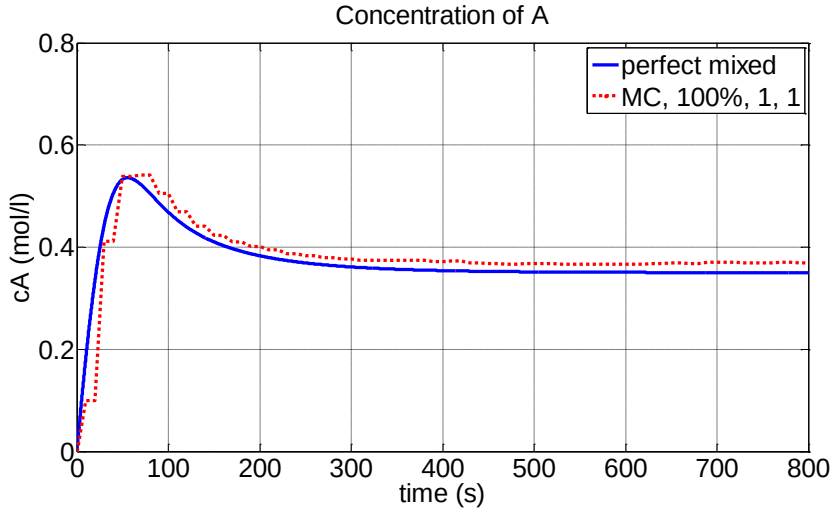

Figure 4.3. Evaluation of concentration of component A. $c_{A,in}$=4 mol/l, $T_{in,1}$=30 °C, $T_{in,2}$=207 °C, the reaction was exothermic

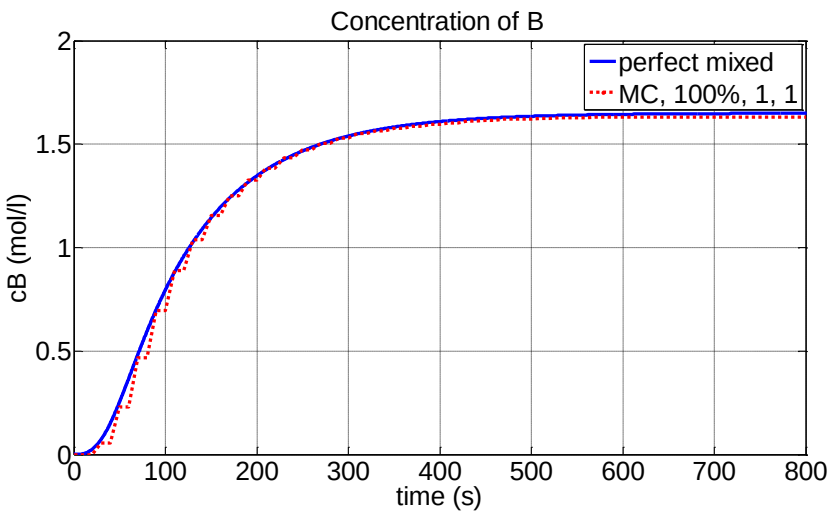

Figure 4.4. Evaluation of concentration of component B. $c_{A,in}$=4 mol/l, $T_{in,1}$=30 °C, $T_{in,2}$=207 °C, the reaction was exothermic

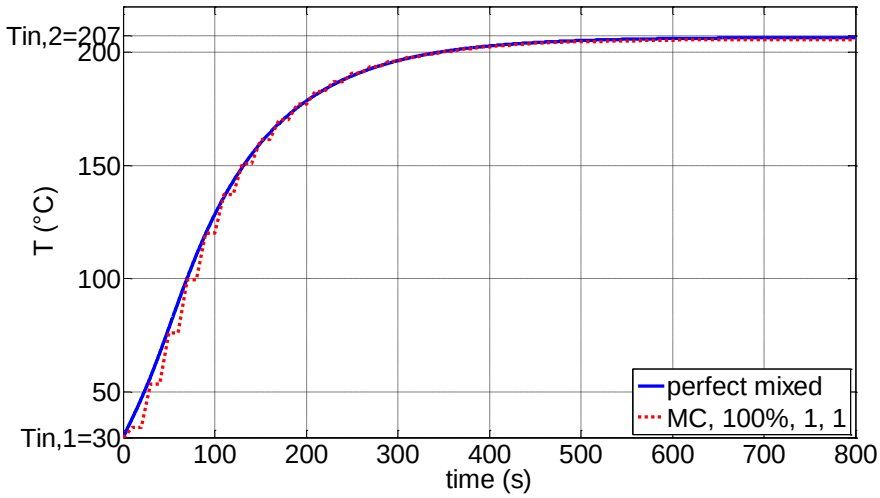

Figure 4.5. Evaluation of temperature of mixture. $c_{A,in}$=4 mol/l, $T_{in,1}$=30 °C, $T_{in,2}$=207 °C, the reaction was exothermic

Endothermic case:

Figs.4.6-4.8 shows the case when the chemical reaction was endothermic. The solid line represents the perfectly mixed CSTR, and the dotted line represents the CSTR with Monte Carlo simulation. The differences and the reasons for the differences are similar to that of the exothermic case.

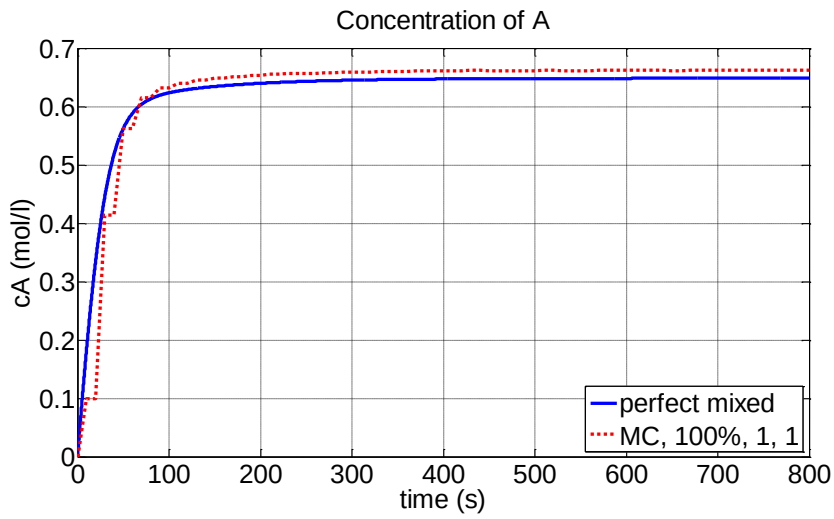

Figure 4.6. Evaluation of concentration of component A. $c_{A,in}$=4 mol/l, $T_{in,1}$=30 °C, $T_{in,2}$=207 °C, the reaction was endothermic

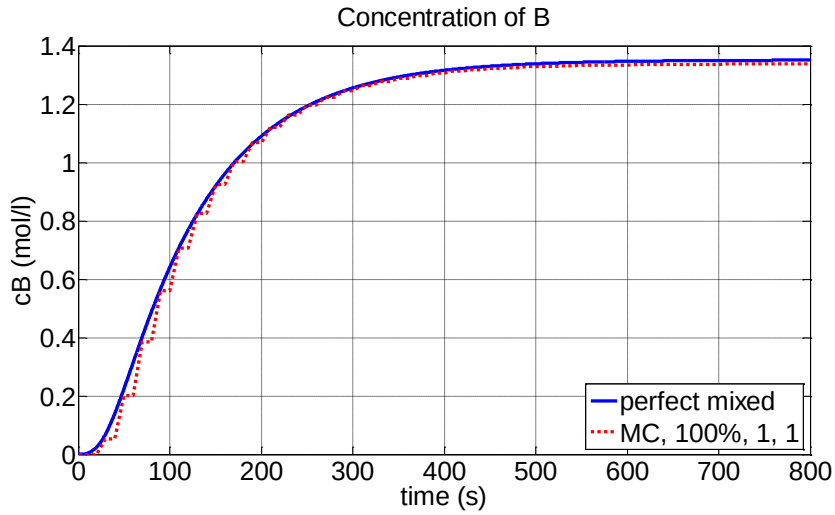

Figure 4.7. Evaluation of concentration of component B. $c_{A,in}$=4 mol/l, $T_{in,1}$=30 °C, $T_{in,2}$=207 °C, the reaction was endothermic

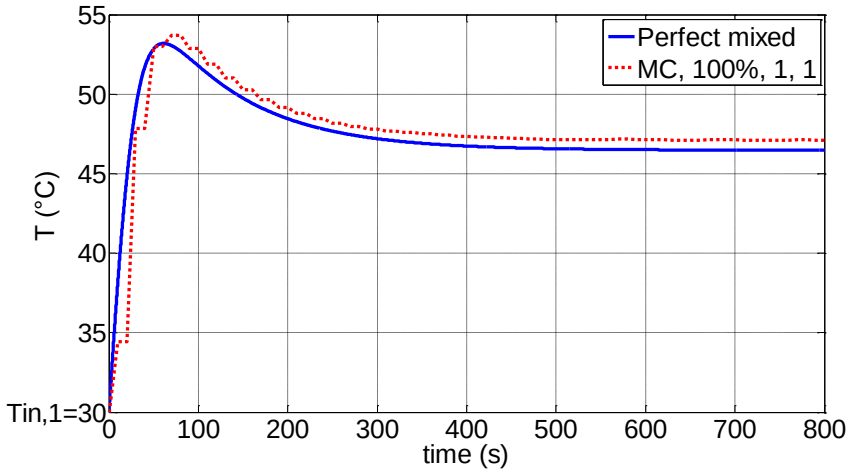

Figure 4.8. Evaluation of temperature of mixture. $c_{A,in}$=4 mol/l, $T_{in,1}$=30 °C, $T_{in,2}$=207 °C, the reaction was endothermic

4.3.2 Influence of micromixing

In this section, the effects of micromixing on the concentration of product are shown. During these simulations complete heat transfer has been assumed between the colliding fluid elements: ω_T=1 in Eq.(4.9). That means after colliding the temperature of the two colliding fluid elements becomes equal. In contrast the component transport ($0<\omega_{ck}<1$) is partial. The value of component transport during the simulation run was the same in all collision events for all components.

The value of ω_{ck} (Case I) and number of elements taking part in collision (Case II) during time interval Δt have been systematically varied (Table 4.1). Through

these parameters the effect of micromixing on the concentration of components and the temperature in the reactor can be analysed.

Table 4.1 The parameter combinations in simulation runs

Cases	Rate of component transport (ω_{ck})	Rate of heat transport (ω_T)	Number of elements taking part in collision
Case I	1	1	10000
	0.5		
	0.1		
	0.025		
	0		
Case II	1	1	10000
			8000
			1000

If ω_{ck} is 0, i.e. only total heat transfer was between the colliding fluid elements.

Exothermic case:

In Fig. 4.9-4.14 can be seen the effect of finite component transport by micromixing ω_{ck} and the effect of the number of elements used. Figs.4.9-4.14 represents the time profiles of concentrations of components A and B for various mixing conditions.

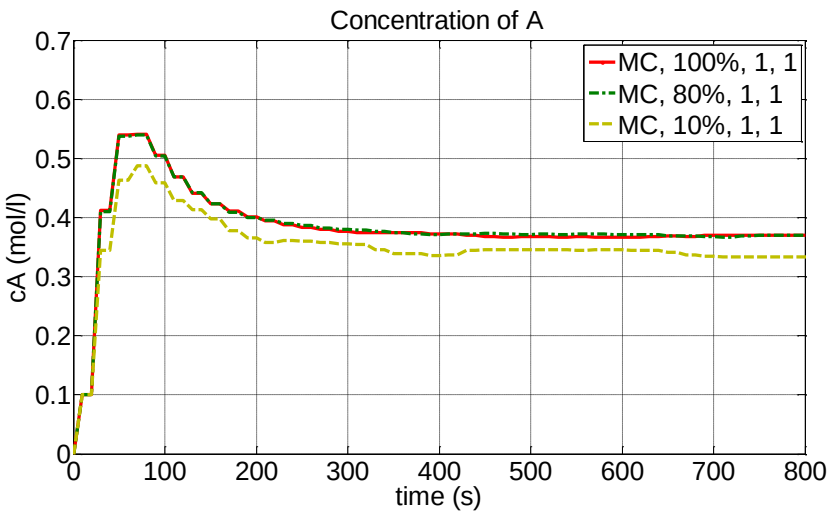

Figure 4.9. Effect of the number of colliding fluid elements on concentration of A. $c_{A,in}$=4 mol/l, $T_{in,1}$=30 °C, $T_{in,2}$=207 °C, the reaction was exothermic. Notation: MC: simulation with Monte Carlo method; percent of droplets take part in collision; ω_{ck} and ω_T.

It can be seen if ω_{ck}=1, the effect of the number of colliding fluid elements (100%, 80% or 10%) is not very significant (Figs.4.9, 4.11, 4.13). In contrast, the

effect of ω_{ck} is significant on the concentration of components A and B, and on the mixture temperature (Figs.4.10, 4.12, 4.14).

It is seen in Figs.4.10 and 4.12 that the lowest concentration of component A and the highest of B in steady state is reached when ω_{ck}=0, and ω_T=1. For the production of B the best is if complete heat transfer takes place between the fluid elements but the component transport is 0. It is not surprising if we see Fig.4.14 that the temperature of mixture is the highest in this case. Since the reaction is exothermic, higher temperature favours the production of component B.

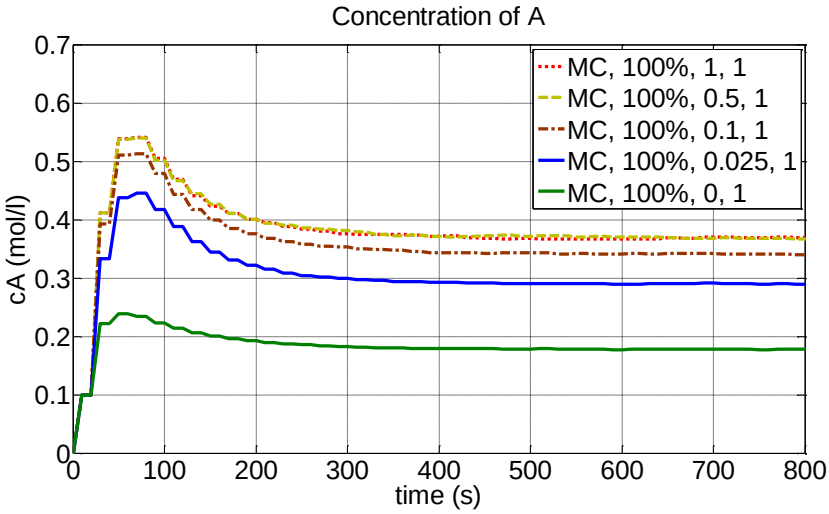

Figure 4.10. Effect of ω_{ck} on concentration of A. $c_{A,in}$=4 mol/l, $T_{in,1}$=30 °C, $T_{in,2}$=207 °C, the reaction was exothermic. Notation: MC: simulation with Monte Carlo method; percent of droplets take part in collision; ω_{ck} and ω_T.

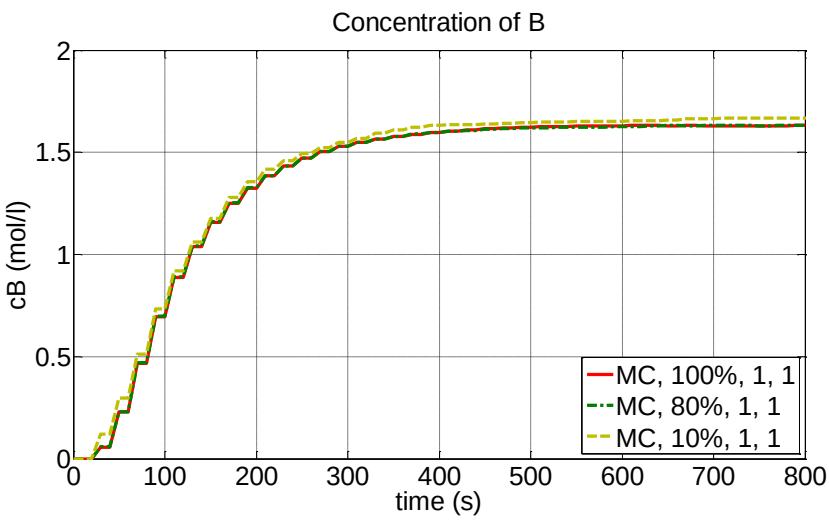

Figure 4.11. Effect of the number of colliding fluid elements on concentration of B. $c_{A,in}$=4 mol/l, $T_{in,1}$=30 °C, $T_{in,2}$=207 °C, the reaction was exothermic. Notation: MC: simulation with Monte Carlo method; percent of droplets take part in collision; ω_{ck} and ω_T.

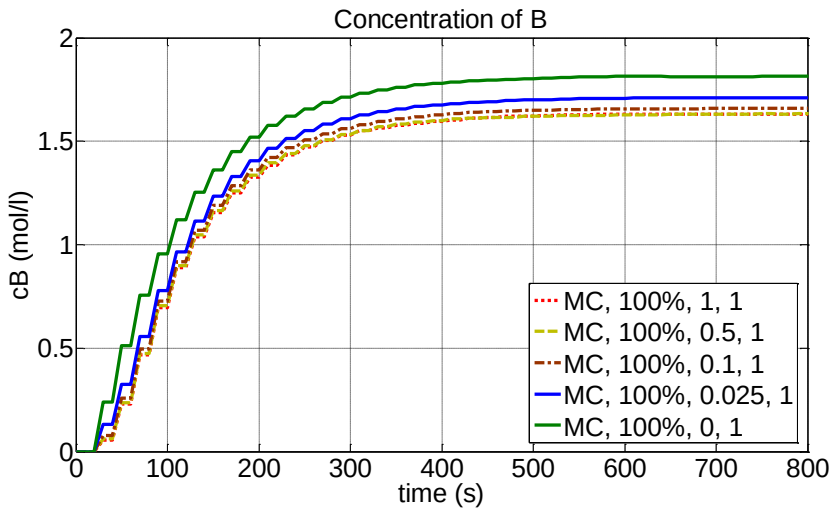

Figure 4.12. Effect of ω_{ck} on concentration of B. $c_{A,in}$=4 mol/l, $T_{in,1}$=30 °C, $T_{in,2}$=207 °C, the reaction was exothermic. Notation: MC: simulation with Monte Carlo method; percent of droplets take part in collision; ω_{ck} and ω_T.

In Figs.4.13 and 4.14, the temperature profiles of the mixture during the whole process are presented. Because the temperature rise more than 150 °C, in Figs.4.13 and 4.14 the steady states are shown enlarged on a separate scale. It is seen from the differences of the steady state values that the non-perfect mixing at micro-scale can cause a more significant overall temperature effect.

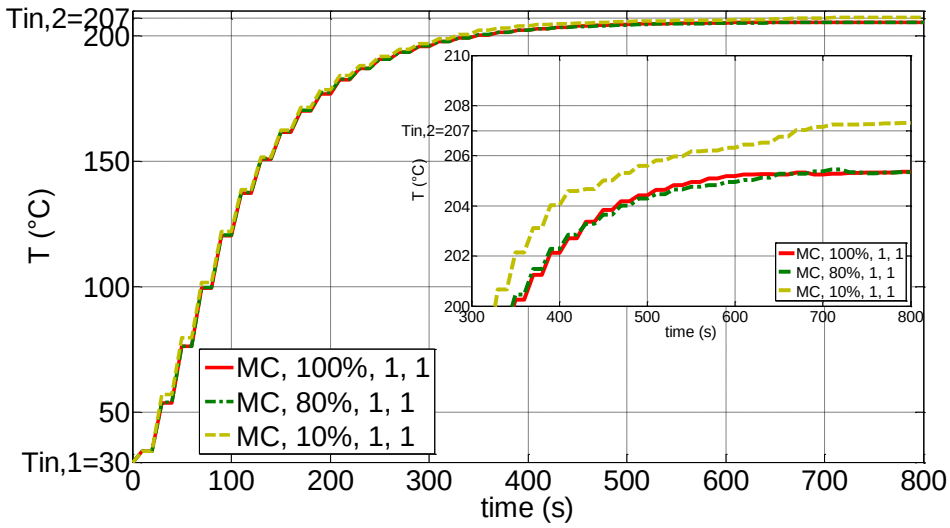

Figure 4.13. Effect of the number of colliding fluid elements on reaction mixture temperature. $c_{A,in}$=4 mol/l, $T_{in,1}$=30 °C, $T_{in,2}$=207 °C, the reaction was exothermic. Notation: MC: simulation with Monte Carlo method; percent of droplets take part in collision; ω_{ck} and ω_T.

As it is seen in Figs. 4.10, 4.12 and 4.14, if ω_{ck} is higher than 0.1 then the effect of this parameter is negligible. However if ω_{ck} is lower than 0.1, the changes are

significant. These changes are significant in the dynamic behaviour of the reactor, too. In reality, the temperature transport is about three orders of magnitude faster than component transport. Therefore, the case where ω_{ck} is lower than 0.1, describes a reality case.

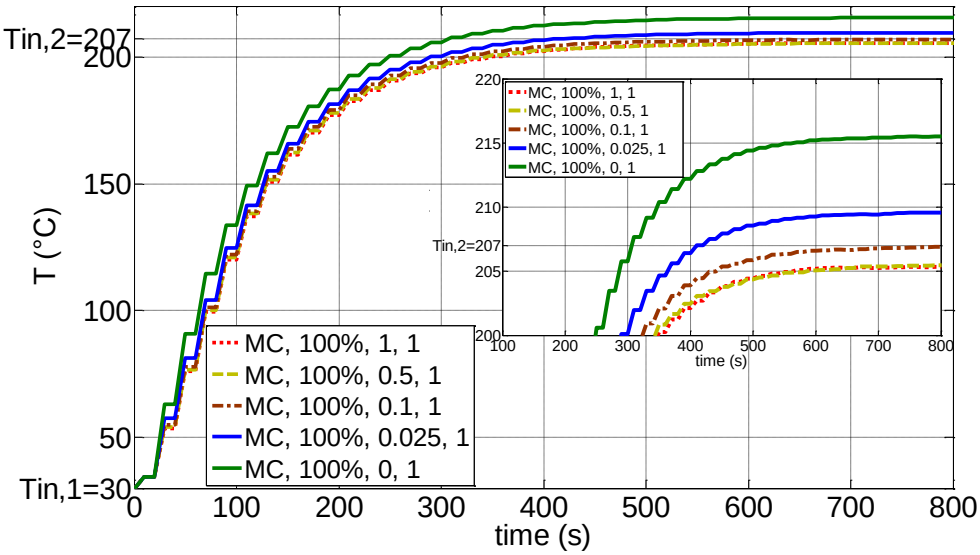

Figure 4.14. Effect of ω_{ck} reaction mixture temperature. $c_{A,in}$=4 mol/l, $T_{in,1}$=30 °C, $T_{in,2}$=207 °C, the reaction was exothermic. Notation: MC: simulation with Monte Carlo method; percent of droplets take part in collision; ω_{ck} and ω_T.

Endothermic case:

Figs 4.15-4.20 show the effect of ω_{ck} and of the number of elements taking part in collisions in endothermic reactions. In general, the results are similar to that of the exothermic case.

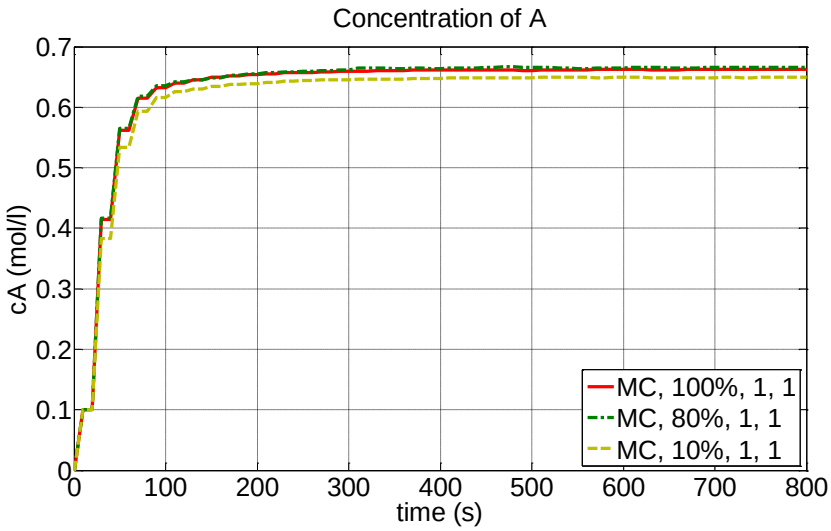

Figure 4.15. Effect of the number of colliding fluid elements on concentration of A. $c_{A,in}$=4 mol/l, $T_{in,1}$=30 °C, $T_{in,2}$=207 °C, the reaction was endothermic. Notation: MC: simulation with Monte Carlo method; percent of droplets take part in collision; ω_{ck} and ω_T.

It can be seen that the concentration of product is the highest when ω_{ck}=0, and ω_T=1. It is seen in Fig.4.20 that the temperature of the mixture is the lowest in this case. Since the reaction is endothermic, a lower temperature indicates a higher conversion of component B.

The effects of ω_{ck} are seen in Figs 4.16, 4.18 and 4.20. These effects are negligible if ω_{ck} is higher than 0.1. However if ω_{ck} is lower than 0.1 than the changes are significant. These changes are significant in the dynamic behaviour of the reactor, too.

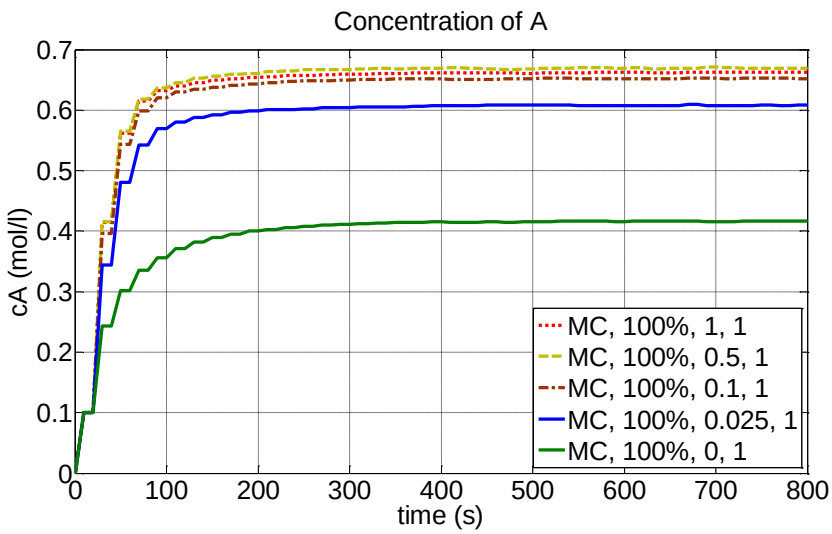

Figure 4.16. Effect of ω_{ck} on concentration of A. $c_{A,in}$=4 mol/l, $T_{in,1}$=30 °C, $T_{in,2}$=207 °C, the reaction was endothermic. Notation: MC: simulation with Monte Carlo method; percent of droplets take part in collision; ω_{ck} and ω_T.

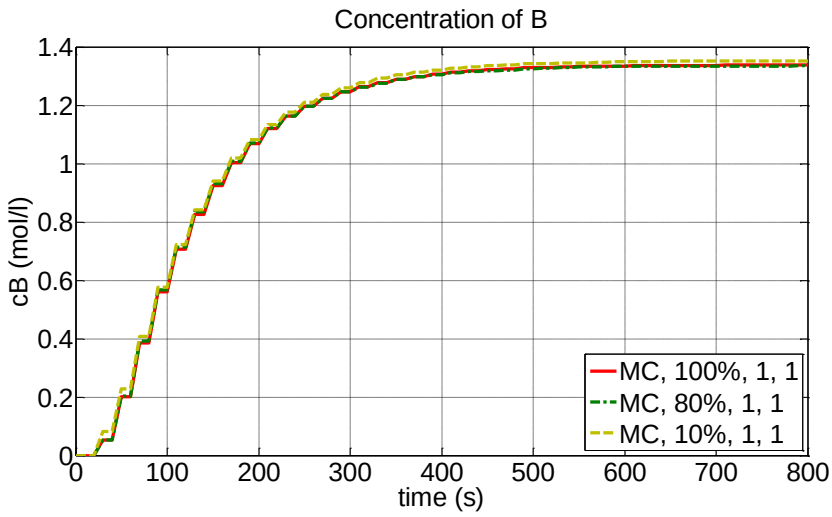

Figure 4.17. Effect of the number of colliding fluid elements on concentration of B. $c_{A,in}$=4 mol/l, $T_{in,1}$=30 °C, $T_{in,2}$=207 °C, the reaction was endothermic. Notation: MC: simulation with Monte Carlo method; percent of droplets take part in collision; ω_{ck} and ω_T.

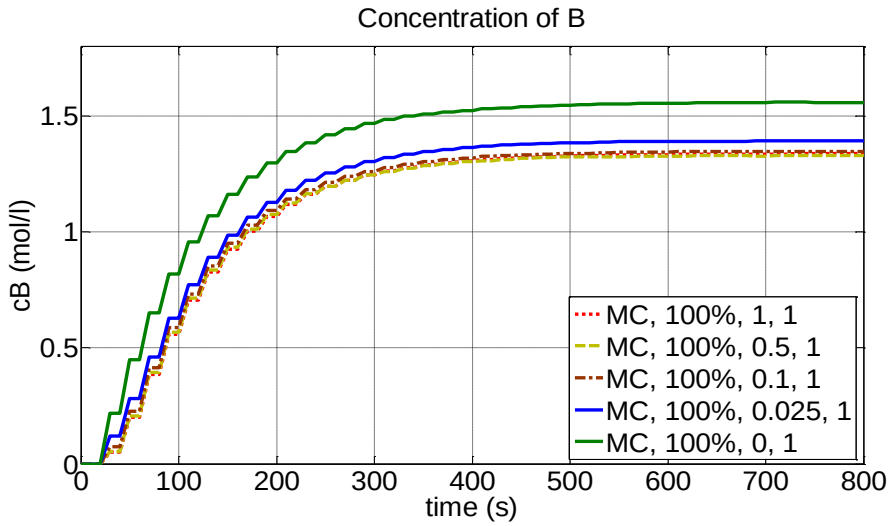

Figure 4.18. Effect of ω_{ck} on concentration of A. $c_{A,in}$=4 mol/l, $T_{in,1}$=30 °C, $T_{in,2}$=207 °C, the reaction was endothermic. Notation: MC: simulation with Monte Carlo method; percent of droplets take part in collision; ω_{ck} and ω_T.

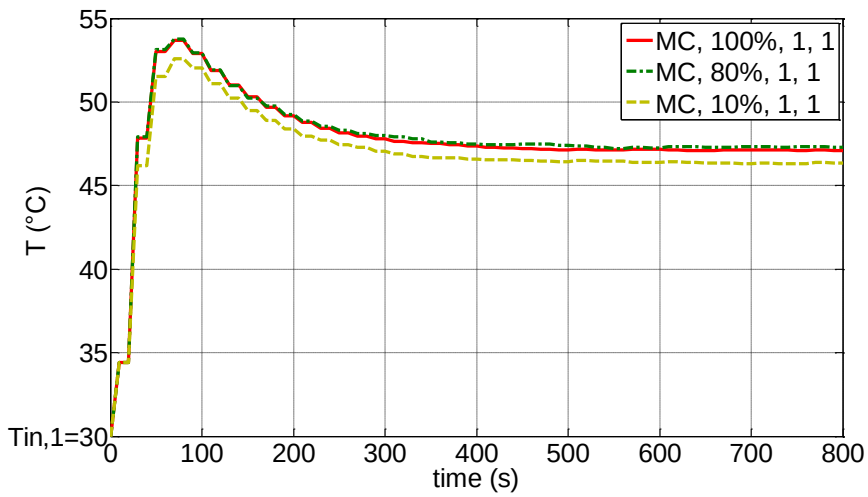

Figure 4.19. Effect of the number of colliding fluid elements on reaction mixture temperature. $c_{A,in}$=4 mol/l, $T_{in,1}$=30 °C, $T_{in,2}$=207 °C, the reaction was endothermic. Notation: MC: simulation with Monte Carlo method; percent of droplets take part in collision; ω_{ck} and ω_T.

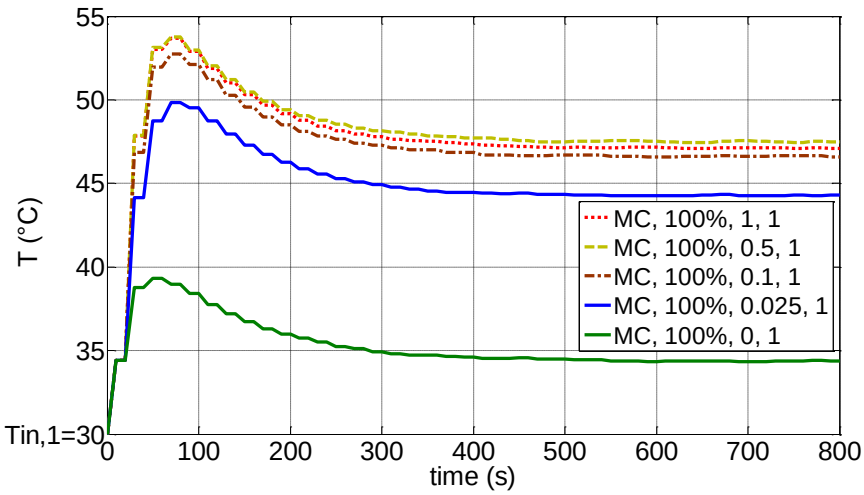

Figure 4.20. Effect of ω_{ck} reaction mixture temperature. $c_{A,in}$=4 mol/l, $T_{in,1}$=30 °C, $T_{in,2}$=207 °C, the reaction was endothermic. Notation: MC: simulation with Monte Carlo method; percent of droplets take part in collision; ω_{ck} and ω_T.

From these results we can see, that the evolved Monte Carlo method is suitable to analyse the effect of micromixing in continuous stirred reactors. It can be stated that the influence of micromixing is significant on these systems and it seems to be important to analyse these effects.

5. Summary and Theses

The dissertation dealt with mathematical modelling and analysis of phenomena of disperse systems. Systems, where chemical reactions take place in the dispersed phase are highly sensitive to micromixing phenomena, i.e. to collision induced coalescence, breakage and coalescence/redispersion of dispersed elements.

In Section 1, a detailed literature survey was presented about polymerization techniques focusing on suspension polymerization of vinyl chloride. The summary of modelling techniques was focused on the two-phase kinetic model of vinyl chloride polymerization and the population balance modelling. The solution techniques of population balance equations were reviewed, too.

In Section 2 a multi-dimensional population balance equation was presented which is suitable for describing the meso-scale interactions of dispersed elements and the continuous time changes in the dispersed elements due to chemical reactions. The primary aim of the work was modelling and analysis of suspension polymerization of vinyl chloride. In this system, the dispersed elements are monomer droplets in which exothermal polymerization reactions take place. Therefore, during the process the concentration of chemical species, the volume and the temperature of droplets are changing both continuously in time due to polymerization reactions, and stepwise due to the discrete events (coalescence, breakage and coalescence/redispersion). A multi-dimensional population balance equation was worked out for modelling disperse systems.

In Section 3 a coupled continuous time–Monte Carlo method was introduced for the solution of the multi-dimensional population balance equation which involves both continuous and discrete processes. A simulation program was worked out to analyse the suspension polymerization of vinyl chloride. Several simulation runs were carried out to study the effects of the:

- initial initiator distribution,
- initial monomer droplet size distribution,
- droplet interactions,
- temperature rise of droplets and
- temperature changes in the continuous phase.

The results showed that the improved multi-dimensional population balance equation and the developed coupled continuous time–Monte Carlo method is suitable to analyse suspension polymerization processes.

Since reactors are often work in continuous mode in industry, it is important that the developed solution technique is suitable for modelling continuously operated systems. In Section 4, it was demonstrated that reactors with more input flows are sensitive to micromixing phenomena. The coupled continuous time–Monte Carlo method and the simulation program was extended for modelling these cases. The results showed that the method and simulation programs developed are suitable for analysing the effects of micromixing on concentrations of components and the temperature of mixture in continuously operated reactors.

The introduced population balance equation, the coupled continuous time–Monte Carlo method and simulation programs are believed to be suitable for modelling and analysing other polymerization and reaction systems. It is planned to extend the model with the particle formation, and to analyse the investigated effects on particle size distribution.

5.1. Tézisek

1. **Kidolgoztam egy több-dimenziós populáció mérleg modellt szuszpenziós polimerizációs reaktorok modellezésére. A modell alkalmas a monomer cseppek között lezajló kölcsönhatások és a monomer cseppekben végbemenő kémiai reakciók egyidejű leírására.**

   a) A monomer cseppekben polimerizációs reakciók zajlanak, amelyek a koncentráció, térfogat és a hőmérséklet időben folytonos megváltozását eredményezik. A modell tartalmazza a kémiai reakciókból adódó, időben folytonos megváltozások leírását.

   b) A szuszpenziós polimerizációs reaktorokban az intenzív kevertetés hatására a monomer cseppek ütköznek egymással, a keverővel, a berendezés falával. A monomer cseppek egymással való ütközése révén, az ütközés energiájától függően koaleszcencia vagy koaleszcencia/ rediszperzió mehet végbe. Koaleszcencia esetén az ütközés energiája elég nagy ahhoz, hogy a cseppek közötti határ-réteget felszakítsa és a két ütköző csepp egyesülését eredményezze. Ekkor teljes koncentráció- és hőmérséklet kiegyenlítődés zajlik le. Koaleszcencia/rediszperzió

esetén csak komponens és hőátadás megy végbe a két monomer csepp között, aminek a mértéke függ a találkozási felület méretétől, az együtt-mozgás idejétől, valamint a komponens és a hőátadási együtthatók mértékétől. A monomer cseppek a folytonos fázisban kialakuló energiaörvényekkel is ütközhetnek, ami a cseppek széteséséhez vezethet. A szétesés során két darab azonos méretű és tulajdonságú csepp keletkezik. Az ismertetett események révén kialakuló időben diszkrét koncentráció, térfogat és hőmérséklet megváltozásokat tartalmazza a modell.

c) A monomer cseppekben az erősen exoterm polimerizációs reakciók révén hőmérsékletemelkedés következik be. Ez a hőmérsékletváltozás a monomer cseppek és a folytonos fázis közötti hőátadás révén hatással van a folytonos fázis hőmérsékletére is. Így a modell tartalmazza a reaktor teljes energiamérlegét.

Fontosabb kapcsolódó publikációk: 1, 2, 3, 10

2. **Kidolgoztam egy Monte Carlo módszert, amely alkalmas a diszperz rendszerek diszperz elemeiben végbemenő, időben folytonos és a diszperz elemek között lezajló, időben diszkrét események együttes számítására. Meghatároztam azt a minimális populáció méretet, amellyel már megfelelő pontossággal közelíthetők az ipari méretű reaktorokban kialakuló csepp-populációk tulajdonságai.**

a) Időben folytonos események: A meghatározott populációban minden egyes elemre a térfogat, koncentráció és hőmérsékletváltozás időben folytonos számítását teszi lehetővé a program.

b) Időben diszkrét események: Az ütközési és szétesési folyamatokat egymástól független, inhomogén Poisson folyamatként írtam le. A következő diszkrét esemény meghatározása a diszperz rendszerre jellemző ütközési és törési frekvenciák és valószínűségek alapján történik. Három egymástól független esemény számítását végeztem el: koaleszcencia, koaleszcencia/rediszperzió és a szétesés. Ezen események megváltoztathatják a diszperz elemek térfogatát, koncentrációját és hőmérsékletét. A program ennek számítását teszi lehetővé.

Fontosabb kapcsolódó publikációk: 1, 2, 3, 10

3. **A kidolgozott Monte Carlo módszert továbbfejlesztettem folyamatos, nem izotermikus reaktorokban a mikrokeveredés hatásának vizsgálatára. A kialakított módszer alkalmas olyan rendszerek vizsgálatára, amelyekben különböző hőmérsékletű és koncentrációjú betáplálások vannak, és a kémiai reakciók reakciósebességi együtthatói a hőmérsékletváltozásokból adódóan folyamatosan változnak.**

   a) A reaktorban lévő folytonos fázist nagyon sok, egymással kölcsönhatásban lévő fluidum elem-populációként írtam le. A fluidum elemekben kémiai reakciók mennek végbe, amennyiben a fluidum elemek minden olyan komponenst tartalmaznak, ami ehhez szükséges. A program a kémiai reakciók számítását időben folytonos eseményként teszi lehetővé. Így a fluidum elemekben a komponensek koncentrációjának, valamint a fluidum elemek hőmérsékletének számítása időben folytonos.

   b) A fluidum elemek között koaleszcencia/rediszperziós kölcsönhatásokat vettem figyelembe. E kölcsönhatások révén a fluidum elemek között komponens és hőátadás megy végbe. Ez a folyamat időben diszkréten változtatja a fluidum elemekben a komponensek koncentrációját, valamint a fluidum elemek hőmérsékletét. Mind a komponens, mind a hőátadásra külön lehet definiálni átadási tényezőt, de azok akár véletlenszerű értékeket is felvehetnek, ezzel még inkább közelítve a valóság sztochasztikus jellegét.

   Fontosabb kapcsolódó publikációk: 4, 9

5.2. Theses

1. **I developed a multi-dimensional population balance model for modelling suspension polymerization reactors. The model is suitable to describe random interactions between the monomer droplets by collisions and the polymerization reactions inside the monomer droplets, simultaneously.**

   a) Polymerization reactions take place in the monomer droplets. The volume, the concentration of components and the temperature of droplets vary continuously in time due to the reactions. The model contains descriptions of these time continuous changes due to the chemical reactions.

   b) The monomer droplets inside the suspension polymerization reactors collide with each other, with the agitator and the wall of the equipment

due to the intensive mixing. Coalescence or coalescence/redispersion of droplets takes place because of the collisions of monomer droplets, depending on the energy of collisions. In the case of coalescence the energy of collision is high enough to drain out the liquid film between the two colliding droplets, and it results in aggregation of the two droplets. In this event equalization of concentrations and the temperature is complete. In the event of coalescence/redispersion between two colliding monomer droplets partial component and heat exchange takes place. The degree of exchange depends on the surface of contact, on the time of moving together and on the coefficients of component and heat transfers. Monomer droplets can collide with the energy eddies inside the turbulent flow field, and due to this process a monomer droplet can break up. As a result of breakage of droplets, the properties of new droplets remain of the same value as of the origin was. The developed model contains the changes of concentrations of components, as well of the volume and temperature of droplets due to the discrete time events outlined above.

c) Temperature rise in droplets occurs due to the exothermic polymerization reactions. The temperature change of monomer droplets affects the temperature of continuous phase due to the heat exchange between the monomer droplets and the continuous phase. The model contains the energy balance of the reactor of the macro-scale.

Major related publications: 1, 2, 3, 10

2. I developed a Monte Carlo method which is suitable to compute the time continuous processes inside the dispersed elements and the stochastic collisions induced discrete event processes between the dispersed elements in disperse systems, simultaneously. I determined the minimal size of population of dispersed elements suitable for simulating the properties of droplets, formed in industrial reactors, with acceptable accuracy.

a) Events continuous in time: It is possible to compute the changes of the volume, the concentration of components and the temperature of all elements inside the population, continuously in time.

b) Random events discrete in time: The collision and breakage processes are modelled as inhomogeneous Poisson processes independent from

each other. Coalescence, breakage and coalescence/redispersion events, independent from each other, were calculated: These events can change the concentrations of components, and the volume, and temperature of dispersed elements. The next discrete event is calculated by the collision and breakage frequencies and probabilities characteristic for the given disperse system. The simulation program is suitable to calculate all these changes.

Major related publications: 1, 2, 3, 10

3. **I improved the Monte Carlo method for analysing the effects of non-isothermal micromixing in continuously operated adiabatic chemical reactors. The developed method is suitable to model and simulate chemical reactors working under realistic operation conditions in which non-isothermal micromixing of fluids plays important role.**

   a) The continuous phase inside the reactor is described as a population of large number of fluid elements which interact with each other. Chemical reactions take place in the fluid elements if the elements contain all of the necessary components. Chemical reactions are computed continuously in time so that calculation of concentrations of components and the temperature of fluid elements is continuous in time.

   b) Coalescence/redispersion processes between the fluid elements are taken into consideration. Component and heat transport takes place between the fluid elements due to the coalescence/redispersion. This process affects the concentration of components and the temperature of fluid elements discretely in time. Both the component and heat transfer coefficients can be defined, but those can be taken also of random nature. The stochastic character of the process revealed using the second case.

   Major related publications: 4, 9

5.3 Publications related to theses

Articles in international journals

1. Bárkányi, Á., S. Németh, B.G. Lakatos, 2013, Modelling and simulation of suspension polymerization of vinyl chloride via population balance model, **Computers & Chemical Engineering**, Vol. 59, pp. 211-218. /DOI: 10.1016/j.compchemeng.2013. 06.0008/
2. Bárkányi, Á, S. Németh, B.G. Lakatos, 2013, Modelling and Simulation of a Batch Poly(vinyl chloride) Reactor, **Chemical Engineering Transactions,** Vol. 32, pp. 769-774/ISBN: 978-88-95608-23-5; ISSN: 1974-9791, DOI: 10.3303/CET1332129/
3. Bárkányi, Á., B.G. Lakatos, S. Németh, 2011, Effects of mixing on the formation of polymer particles in suspension polymerization, **Chemical Engineering Transactions,** Vol. 24. pp. 613-618. /ISBN: 978-88-95608-15-0, ISSN: 1974-9791, DOI: 10.3303/CET1124103/
4. Lakatos, B.G., Á. Bárkányi,S. Németh, 2011, Continuous stirred tank coalescence/redispersion reactor. A simulation study. **Chemical Engineering Journal,** Vol. 169. pp. 247-257. /DOI: 10.1016/j.cej.2011.01.042/

Articles in Hungarian journals

5. Bárkányi, Á, B.G. Lakatos, S. Németh, 2012, Modelling of heat exchange between drops in suspension polymerization of vinyl chloride, **Periodica Polytechnica Chemical Engineering,** Vol. 56/2, pp. 55-64. /DOI: 10.3311/pp.ch.2012-2.02/
6. Bárkányi, Á., B.G. Lakatos, S. Németh, 2010, Modelling of polymer particle formation using population balance model, **Hungarian Journal of Industrial Chemistry,** Veszprém, Vol. 38(2). pp. 83-88. /HU ISSN: 0133-0276/
7. Bárkányi Á., Németh S., Lakatos G.B., 2011, A monomer kezdeti cseppméret-eloszlásának hatása a polimer termékek átlagos molekulatömegére, **Acta Agraria Kaposvariensis**, Kaposvár, Vol. 15., No. 3., pp. 155-170. /ISSN: 1418-1789/
8. Bárkányi Á., Németh S., Lakatos G.B., 2010, Vinil-klorid szuszpenziós polimerizációjának vizsgálata egyszerűsített populáció-mérleg modellel, **Acta Agraria Kaposvariensis,** Kaposvár, Vol. 14., No. 3. /ISSN: 1418-1789/

Articles in conference publication

9. Lakatos, B.G., Á. Bárkányi, S. Németh, Hybrid continuous time – Monte Carlo simulation of disperse systems, **27th European Simulation and Modelling Conference - ESM'2013**, Lancaster University, Lancaster, UK, 2013, pp. 13-20. /ISSN: 978-90-77381-79-3/

10. Bárkányi, Á, S. Németh, B.G. Lakatos, 2012, Modelling and simulation of suspension polymerization of vinyl chloride via population balance model, **Computer Aided Chemical Engineering**, Vol. 30, pp. 1108-1112. /ISBN:978-0-444-59520-1/

11. Bárkányi, Á, S. Németh, B.G. Lakatos, Modelling and Simulation of Suspension Polymerization of Vinyl Chloride, **5th International Interdisciplinary Technical Conference of Young Scientists**, Poznań, Lengyelország, 2012., pp. 27-31. /ISBN: 978-83-926896-4-5/

12. Bárkányi, Á, S. Németh, B.G. Lakatos, 2012, Modelling of heat exchange between drops in suspension polymerization of vinyl chloride, **Műszaki Kémiai Napok 2012**, Veszprém, 2012., pp. 60-67. /ISBN: 978-615-5044-54-0/

13. Bárkányi, Á., B.G. Lakatos, S. Németh, 2011, Modelling of suspension polymerization of vinyl chloride using the population balance approach, **Interfaces'11 elektronikus kiadvány** /ISBN: 978-963-9970-21-2/

14. Bárkányi Á., Németh S., Lakatos G.B., 2011, A mikrokeveredés hatása autokatalitikus reakciórendszer viselkedésére, **Műszaki Kémiai Napok 2011**, Veszprém, pp. 53-59. /ISBN: 978-615-5004-07-6/

15. Bárkányi Á., Németh S., Lakatos G.B., 2010, Vinil-klorid szuszpenziós polimerizációjának vizsgálata populáció-mérleg modellel, **Műszaki Kémiai Napok 2010**, Veszprém, pp. 178-181. /ISBN: 978-963-9696-93-8/

Lectures and posters

15. Bárkányi, Á, S. Németh, B.G. Lakatos, Modelling and Simulation of a Batch Poly(vinyl chloride) Reactor, **11th International Conference on Chemical & Process Engineering**, Milánó, 2013. 06. 02-05.

16. Bárkányi, Á, S. Németh, B.G. Lakatos, Effects of droplet interactions on polymer properties in suspension polymerization of vinyl chloride. A simulation study., **2nd Working Party on Polymer Reaction Engineering**, Hamburg, 2013. 05. 24-26.

17. Bárkányi, Á, S. Németh, B.G. Lakatos, Modelling and Simulation of Droplet Interaction in Suspension Polymerization of Vinyl Chloride Using Population Balance Model, **11th Workshop on Polymer Reaction Engineering**, Hamburg, 2013. 05. 21-24.

18. Bárkányi, Á, S. Németh, Stochastic simulation of droplets interactions in suspension polymerization of vinyl chloride, **Műszaki Kémiai Napok'13,** Veszprém, 2013. április

19. Bárkányi, Á, S. Németh, B.G. Lakatos, Modelling and simulation of suspension polymerization of vinyl chloride via population balance model, **European Symposium on Computer Aided Process Engineering,** London, Egyesült Királyság, 2012. 06. 17-20.

20. Bárkányi, Á, S. Németh, B.G. Lakatos, Modelling and Simulation of Suspension Polymerization of Vinyl Chloride, **5th International Interdisciplinary Technical Conference of Young Scientists,** Poznań, Lengyelország, 2012. 05. 16-18.

21. Bárkányi, Á, S. Németh, B.G. Lakatos, Modelling of heat exchange between drops in suspension polymerization of vinyl chloride, **Műszaki Kémiai Napok 2012**, Veszprém, 2012. 04. 24-26.

22. Bárkányi, Á, S. Németh, B.G. Lakatos, Modelling and simulation of vinyl chloride suspension polymerization, **CAPE Forum**, Veszprém, 2012. 03. 26-28. /ISBN: 978-615-5044-52-6/

23. Bárkányi, Á, S. Németh, B.G. Lakatos, Modelling of suspension polymerization of vinyl chloride using the population balance approach, **Interfaces'11**, Sopron, 2011. 09. 28-30. /ISBN: 978-963-9970-16-8/

24. Bárkányi, Á, S. Németh, B.G. Lakatos, Effects of mixing on the formation of polymer particles in suspension polymerization, **ICheaP-10 The 10th International Conference on Chemical & Process Engineering,** Firenze, Olaszország, 2011. 05. 08-11.

25. Bárkányi, Á, B.G. Lakatos, Effects of micromixing of solution on reaction crystallization, **International School of Crystallization,** Granada, Spanyolország, 2010. 05. 24-28.

26. Bárkányi, Á, S. Németh, B.G. Lakatos, Vinil-klorid szuszpenziós polimerizációjának vizsgálata Monte Carlo módszer alkalmazásával, **„Környezetbarát anyagok és technológiák" Konferencia és 56. Magyar Spektrokémiai Vándorgyűlés,** Veszprém, 2013. 07. 01-03.

27. Bárkányi, Á, S. Németh, B.G. Lakatos, Szuszpenziós polimerizációs poli(vinil-klorid) reaktor modellezése és szimulációja populáció mérleg modellel, **XVIII. Nemzetközi Vegyészkonferencia,** Nagyvárad, 2012. 11. 22-25.

28. Bárkányi, Á, S. Németh, B.G. Lakatos, A mikrokeveredés hatása autokatalitikus reakciórendszer viselkedésére, **Műszaki Kémiai Napok'11,** Veszprém, 2011. 04. 27-29.

29. Bárkányi, Á, S. Németh, B.G. Lakatos, A monomer kezdeti cseppméret-eloszlásának hatása a polimer termékek átlagos molekulatömegére, **IX. Alkalmazott Informatikai Konferencia,** Kaposvár, 2011. 02. 25.

30. Bárkányi, Á, S. Németh, B.G. Lakatos, Polimer szemcseképződés modellezése populáció mérleg-modellel, **Mobilitás és Környezet,** Veszprém, 2010. 08. 23-25.

31. Bárkányi, Á, S. Németh, B.G. Lakatos, Vinil-klorid szuszpenziós polimerizációjának vizsgálata populáció-mérleg modellel, **Műszaki Kémiai Napok'10,** Veszprém, 2010. 04. 27-29.

32. Bárkányi, Á, S. Németh, B.G. Lakatos, Vinil-klorid szuszpenziós polimerizációjának vizsgálata egyszerűsített populáció-mérleg modellel, **VIII. Alkalmazott Informatikai Konferencia,** Kaposvár, 2010. 01. 22.

List of Figures

References

Abdel-Alim, A.H., A.E. Hamielec, ***1972***, Journal of Applied Polymer Science, Vol. 16, pp. 783-799.

Ahmadzadeh, A., H. Arastoopour, F. Teymour, M. Strumendo, ***2008***, Chemical Engineering Research and Design, Vol. 86, pp. 329-343.

Alexopoulos, A.H. and C. Kiparissides, ***2005***, Chemical Engineering Science Vol. 60, pp. 4157–4169.

Alexopoulos, A.H., A.I. Roussos and C. Kiparissides, ***2004***, Chemical Engineering Science, Vol. 59, pp. 5751–5769.

Alexopoulos, A.H., C. Kiparissides, ***2007***, Chemical Engineering Science, Vol. 62, pp. 3970-3983.

Alopaeus, V., J. Koskinen, K.I. Keskinen, ***1999***, Chem. Eng. Sci., Vol. 54, pp. 5887-5899.

Alvarez, J., J. Alvarez, M. Hernandez, ***1994***, Chemical Engineering Science, Vol. 49(1), pp. 99-113.

Atanase, L.I., G. Riess, ***2010***, Colloids and Surfaces A: Physicocemichal and Engineering Aspects, Vol. 355, pp. 29-36.

Attarakih, M.M., H.-J. Bart, N.M. Faqir, ***2004***, Chemical Engineeging Science, Vol. 59, pp. 2567-2592.

Attarakih, M.M., H.-J. Bart, N.M. Faqir, ***2006***, Chemical Engineering Science, Vol. 61, pp. 113-123.

Azizi, F., A.M. Al Taweel, ***2011***, Chemical Engineering Science, Vol. 166, pp. 715-725.

Baccara, N., R. Kiffer, C. Charcosset, ***2009***, Chem. Eng. J., Vol. 148, pp. 517-524.

Baldyga, J., J.R. Bourne, ***1990***, Chem. Eng. Sci., Vol. 45, pp. 907-916.

Bannari, R., F. Kerdouss, B. Selma, A. Bannari, P. Proulx, ***2008***, Computers and Chemical Engineering, Vol. 32, pp. 3224-3237.

Bird, R.B., W.E. Stewart, E.N. Lightfoot, ***2002***, Transport Phenomena, John Wiley & Sons, New York

Bordás, R., V. John, E. Schmeyer, D. Thévenin, ***2012***, Computers & Fluids, Vol. 66, pp. 52-62.

Borwankar, R.P., D.T. Wasan, ***1986***, Chem. Eng. Sci., Vol. 41, pp. 199-201.

Brooks, B.W., ***2010***, Chemical Enginnering Technology, Vol. 33(11), pp. 1737-1744.

Buffo, A., M. Vanni, D.L. Marchisio, ***2012***, Chemical Engineering Science, Vol. 70, pp. 31-44.

Cheng, J., Feng X., Cheng D., Yang C., ***2012***, Chin. J. Chem. Eng., Vol. 20(1), pp. 178-190.

Coulaloglou, C.A. and L.L. Tavlarides, ***1977***, Chemical Engineering Science, Vol. 32, pp. 1289-1297.

Crosato-Arnaldi, A., P. Gasparini, G. Talamini, ***1968***, Makromol. Chem., Vol. 117, pp. 140.

Crundwell, F.K., ***1995***, Hydrometallurgy, Vol. 39, pp. 321-335.

Curl, R.L., ***1963***, AIChEJ., Vol. 9, pp. 175-181.

Das, P.K., ***1996***, Computers and Chemical Engineering, Vol. 20(3), pp. 307-313.

De Roo, T., J. Wieme, G.J. Heynderickx, G.B. Marin, ***2005***, Polymer, Vol. 46, pp. 8340-8354.

Debry, E., B. Sportisse, B. Jourdain, ***2003***, Journal of Computational Physics, Vol. 184, pp. 649-669.

Dhanasekharan, K.M., J. Sanyal, A. Jain, A. Haidari, ***2005***, Chemical Engineering Science, Vol. 60, pp. 213-218.

Díez, M.D., M. Fjeld, E. Andersen, B. Lie, ***2006***, Chemical Engineering Science, Vol. 61, pp. 229-245.

Dixon, D.G., ***1996***, Chemical Engineering Science, Vol. 51, pp. 4759-4767.

Dopazo, C., ***1979***, Phys. Fluids, Vol. 22, pp. 20-30.

Dowding, P.J., B. Vincent, ***2000***, Colloids and Surfaces, Vol. 161, pp. 259-269.

Efendiev, Y., M.R. Zachariah, ***2002***, Journal of Colloid and Interface Science, Vol. 249, pp. 30–43.

Evangelista, J.J., S. Katz, R. Shinnar, ***1969***, AIChE J., Vol. 15, pp. 843-853.

Fang, J.Z., Lee D.J., ***2001***, Chem. Eng. Sci., Vol56, pp. 3797-3802.

Fourcadea, E., H.C.J. Hoefsloota, G. van Vlietb, W. Bungeb, S.M.P. Multsersb, P.D. Iedemaa, ***2001***, Chem. Eng. Sci., Vol 56, pp. 6589-6603.

Fournier, M.C., L. Falk, J. Villermaux, ***1996***, Chem. Eng. Sci., Vol. 51, pp. 5053-5064.

Garcia, A.L., C. van den Broek, A. Aertsens, R. Serneels, ***1987***, Physica, Vol. 143A, pp. 535–546.

Gillespie, D.T., ***1977***, Journal of Physical Chemistry, Vol. 81, pp. 2340–2361.

Guichardon, P., L. Falk, ***2000***, Chem. Eng. Sci., Vol. 55, pp. 4233-4243.

Guichardon, P., L. Falk, J. Villermaux, ***2000***, Chem. Eng. Sci., Vol. 55, pp. 4245-4253.

Harada, M., K. Arima, W. Eguchi, S. Nagata, ***1962***, Mem. Fac. Eng. Kyoto Univ., Vol. 24, pp. 431-436.

Haseltine, E.L., D.B. Patience, J.B. Rawlings, ***2005***, Chemical Engineering Science, Vol. 60, pp. 2627-2641.

Hosseini, A., A.E. Bouaswaig, S. Engell, ***2012***, Chemical Engineering Science, Vol. 72, pp. 179-194.

Hsia, M.A., L.L. Tavlarides, ***1980***, The Chemical Engineering Journal, Vol. 20, pp. 225-236.

Hulburt, H., S. Katz,***1964***, Chemical Engineering Science, Vol. 19, pp. 555-574.

Immanuel, C.D., F.J. Doyle III, ***2005***, Powder Technology, Vol. 156, pp. 213-225.

Irizarry, R., ***2008a***, Chemical Engineering Science, Vol. 63, pp. 95-110.

Irizarry, R., ***2008b***, Chemical Engineering Science, Vol. 63, pp.111-121.

Jahanzad, F., S. Sajjadi, B.W. Brooks, ***2005***, Chemical Engineering Science, Vol. 60, pp. 5574-5589.

Janicka, J., W. Kolbe, W. Kollmann, ***1979***, J. Non-Equilib. Thermodyn., Vol. 4, pp. 47-66.

Judat, B., A. Racina, M. Kind, ***2004***, Chem. Eng. Technol., Vol. 27, pp. 287-292.

Kalfas, G., W.H. Ray, ***1993***, Industrial Engineering and Chemical Research, Vol. 32, pp. 1822-1830.

Kamp, J., S. Nachtigall, S. Maaß, M. Kraume, ***2012***, Czasopismo Techniczne Mechanika, Vol. 109(5), pp. 1-13.

Kelsall, D.G. and G.C. Maitland, ***1983***, Polymer Reaction Engineering. Influence of Reactor Engineering on Polymer Properties (K.H Reichert and W. Geisler, eds.), Hansen.

Kiparissides, C., ***1996***, Chemical Engineering Science, Vol. 51, No. 10, pp. 1637-1659.

Kiparissides, C., ***2006***, Journal of Process Control, Vol. 16, pp. 205-224.

Kiparissides, C., G. Daskalakis, D.S. Achilias and E. Sidiropoulou, ***1997***, Ind. Eng. Chem. Res., Vol. 36, pp. 1253-1267.

Kölbl, A., M. Kraut, K. Schubert, ***2008***, AICHE J., Vol. 54, pp. 639-645.

Kotoulas, C. and C. Kiparissides, ***2006***, Chemical Engineering Science, Vol. 61,pp. 332-346.

Kruis, F.E., A. Maisels, H. Fissian, ***2000***, AIChE J, Vol. 49(6), pp. 1735-1742.

Kuchanov, S.J. and D.N. Bort, ***1973***, Polym. Sci. USSR, Vol. 15, pp. 2712.

Kumar, S. and D. Ramkrishna, ***1996a***, Chemical Engineering Science, Vol. 51, pp. 1311–1332.

Kumar, S. and D. Ramkrishna, ***1996b*** Chemical Engineering Science, Vol. 51, pp. 1333–1342.

Kunowa, K., Schmidt-Lehr S., Pauer W., Moritz H.U., Schwede C., ***2007***, Macromol Symp., Vol. 259, pp. 32-41.

Lakatos, B.G., Zs. Ulbert, T. Bickle, ***1999***, in: Proc. 14th Int. Symp. Ind. Crystallization, Cambridge

Lakatos, B.G., Zs. Ulbert, ***2001***, in: Proc. 3rd ECCE, Dechema, Nuremberg, paper 374.

Lakatos, B.G., ***2008***, Chemical Engineering Science, Vol. 63, pp. 404-423.

Lakatos, B.G., ***2011***, Proceedings of Simultech 2011, pp. 186-191.

Lakatos, B.G., Á Bárkányi, S. Németh,***2011***, Chemical Engineering Journal, Vol. 169, pp. 247-257.

Lakatos, B.G., Cs. Mihálykó, T. Blickle, ***2006***, Chemical Engineering Science, Vol. 61, pp. 54-62.

Lehr, F., D. Mewes, ***2001***, Chemical Engineering Science, Vol. 56, pp. 1159–1166.

Liao, Y., D. Lucas, ***2009***, Chemical Engineering Science, Vol. 64, pp. 3389-3406.

Liao, Y., D. Lucas, ***2010***, Chemical Engineering Science, Vol. 65, pp. 2851-2864.

Liffman, K., ***1992***, Journal of Computational Physics, Vol. 100, pp. 116–127.

Lin, Y., K. Lee, T. Matsoukas, ***2002***, Chemical Engineering Science, Vol. 57, pp. 2241-2252.

Maisels, A., F.E. Kruis and H. Fissan, ***2004***, Chemical Engineering Science, Vol. 59, pp. 2231–2239.

Majumder, A., V. Kariwala, S. Ansumali, A. Rajendran, ***2012***, Chemical Engineering Science, Vol. 70, pp. 121-134.

Mantzaris, N.V., P. Daoutidis, ***2004***, Journal of Process Control, Vol. 14, pp. 775-784.

Mantzaris, N.V., P. Daoutidis, F. Sriec,***2001a***, Computers and Chemical Engineering, Vol. 25, pp. 1411-1440.

Mantzaris, N.V., P. Daoutidis, F. Sriec,***2001b***, Computers and Chemical Engineering, Vol. 25, pp. 1441-1462.

Mantzaris, N.V., P. Daoutidis, F. Sriec,***2001c***, Computers and Chemical Engineering, Vol. 25, pp. 1463-1481.

Marchisio, D.L. and R.O. Fox, ***2005***, Journal of Aerosol Science, Vol. 36, pp. 43–73.

Marchisio, D.L., J.T. Pikturna, R.O. Fox and R.D. Vigil, ***2003a***, A.l.Ch.E. Journal, Vol. 49 (5), pp. 1266–1276.

Marchisio, D.L., R.D. Vigil and R.O. Fox, ***2003b***, Journal of Colloid and Interface Science, Vol. 258, pp. 322–334.

Marshall, C.L., P. Rajniak, T. Matsoukas, ***2013***, Powder Technology, Vol. 236, pp. 211-220.

Martín, M., Montes F.J., Galán M.A., ***2008***, Chem. Eng. J., Vol. 145, pp. 232-241.

McGraw, R., ***1997***, Aerosol Science and Technology, Vol. 27, pp. 255–265.

McGraw, R., D.L. Wright, ***2003***, Aerosol Science, Vol. 34, pp. 189-209.

Meimaroglou, D., A.I. Roussos, C. Kiparissides, ***2006***, Chemical Engineering Science, Vol. 61, pp. 5620-5635.

Meimaroglou, D., C. Kiparissides, ***2007***, Chemical Engineering Science, Vol. 62, pp. 5295-5299.

Mesbah, A., H.J.M. Kramer, A.E.M. Huesman, P.M.J. Van den Hof, ***2009***, Chemical Engineering Science, Vol. 64, pp. 4262-4277.

Meyer, T., J. Keurentjes, ***2005***, Handbook of Polymer Reaction Engineering, WILEY-VCH Verlag GmbH & Co. KGaA, Weinheim

Mishra, B.K., ***2000***, Powder Technology, Vol. 110, pp. 246-252.

Modes, G., H.-J. Bart, D. Rodrigue-Perancho, D. Broder, ***1999***, Chem. Engng. Tech., Vol. 22, pp. 231-236.

Moguel, L.F., H. Muhr, A. Dietz, E. Plasari, ***2010***, Chemical Engineering Research and Design, Vol. 88, pp. 1206-1216.

Motz, S., A. Mitrovic, E.D. Gilles, ***2002***, Chemical Engineering Science, Vol. 57, pp. 4329-4344.

Nagy, Z., S. Agachi, ***1997***, Computers and Chemical Engineering, Vol. 21, No. 6, pp. 571-591.

Nandanwar, M.N., S. Kumar, ***2008***, Chemical Engineering Science, Vol. 63, pp. 3988-3997.

Narsimhan, G., J.P. Gupta, ***1979***, Chemical Engineering Science, Vol. 34, pp. 257–265.

Nere, N.K., A.W. Patwardhan, J.B. Joshi, 2003, Ind. Eng. Chem. Res., Vol. 42, pp. 2661-2698.

Nouri, L., Legrand J., Benmalek N., Imerzoukene F., Yeddou A., Halet F., ***2008***, Chem. Eng. J., Vol. 142, pp. 78-86.

Olaj, O.F., ***1977***, J. Macromol. Sci. Chem., Vol. A11, pp. 1307.

Orciuch, W., L. Makowski, A. Moskal, L. Gradon, ***2012***, Chemical Engineering Science, Vol. 68, pp. 227-235.

Oullion, M., G.K. Reynolds, M.J. Hounslow, ***2009***, Chemical Engineering Science, Vol. 64, pp. 673-685.

Pinto, M.A., C.D. Immanuel, F.J. Doyle III, ***2008***, Chemical Engineering Science, Vol. 63, pp. 1304-1314.

Platkowski, K., K.-H. Reichert, ***1999***, Polymer, Vol. 40, pp. 1057-1066.

Pope, S.B., ***1982***, Combustion Sci. Technol., Vol. 28, pp. 131-145.

Puel, F., G. Fevotte, J.P. Klein, ***2003***, Chemical Engineering Science, Vol. 58, pp. 3715-3727.

Ram, A., ***1997***, Fundamentals of Polymer Engineering, Plenum Press, New York.

Ramkrishna, D., ***2000***, Population Balances, Academic Press, London

Rong, F., D. Marchisio, R.O. Fox, ***2004***, Powder Technology, Vol. 139, pp. 7–20.

Rosen, M.J., ***2004***, Surfactant and Interfacial Phenomena, 3d ed., Wiley, New York.

Roussos, A.I., A.H. Alexopoulos and C. Kiparissides, ***2005***, Chemical Engineering Science, Vol. 60, pp. 6998–7010.

Roussos, A.I., A.H. Alexopoulos and C. Kiparissides, ***2006***, Chemical Engineering Science, Vol. 61, pp. 124–134.

Saeki, Y., T. Emura, ***2002***, Prog. Polym. Sci., Technical progress for PVC production, pp. 2055-2131

Salikas, V., C. Kotoulas, D. Meimaroglou, C. Kiparissides, ***2008***, The Canadian Journal of Chemical Engineering, Vol. 86, pp. 924-936.

Sheikh, F., R.D. Vigil, ***1998***, Chem. Eng. Sci., Vol. 53, pp. 2137-2142.

Sidiropoulou, E., C. Kiparissides, ***1990***, J. Macromol. Sci.-Chem., Vol. A27(3), pp. 257-288.

Sinnott, R.K., ***2005***, Coulson & Richardson's Chemical Engineering, Chemical Engineering Design, Vol. 6, 4th Edition, Elsevier, Oxford

Smallwood, P.V., ***1986***, Polymer, Vol. 27, pp. 1609-1618.

Smith, M., T. Matsoukas, ***1998***, Chemical Engineering Science, Vol. 53, pp. 1777–1786.

Spielman, L.A., O. Levenspiel, ***1965***, Chem. Eng. Sci., Vol. 20, pp. 247-254.

Su, J., Z. Gu, Y. Li, S. Feng and X. Y. Xu, ***2007***, Chem. Eng. Sci., Vol. 62, pp. 5897-5911.

Suresh, A.K., M. Chanda, ***1982***, Eur. Polym. J., Vol. 18, pp. 607.

Talamini, G., ***1966***, J. Polym. Sci., A-2, Vol. 4, pp. 535

Tan, H.S., M.J.V. Goldschmidt, R. Boerefijn, M.J. Hounslow, A.D. Salman, J.A.M. Kuipers, ***2005***, Chemical Engineering Research and Design, Vol. 83(A7), pp. 871-880.

Tandon, P., D.E. Rosner, ***1999***, Journal of Colloid and Interface Science, Vol. 213, pp. 273–286.

Tavare, N.S., ***1995***, Industrialcrystallization Process Simulation Analysis and Design, Plenum Press, New York.

Titow, W.V., ***1984***, PVC Technology, Elsevier Applied Science Publishers, New York.

Tobin, T., D. Ramkrishna, ***1999***, The Canadian Journal of Chemical Engineering, Vol. **77**(6), pp. 1090-1104.

Tsouris, C. and L.L. Tavlarides, ***1994***, A.I.Ch.E. Journal, Vol. 40, pp. 395-406.

Ugelstad, J., H. Flogstad, T. Hertzberc, E. Sund, ***1973***, Macromol. Chem., Vol. 164, pp. 171.

Ugelstad, J., H. Levrik, B. Gardinovacki, E. Sundo, ***1971***, Pure Appl. Chem., Vol. 26, pp. 121.

Ulbert, Zs., B.G. Lakatos, ***2005***, Chem. Eng. Sci., Vol. 60, pp. 3525-3536.

Ulbert Zs., B.G. Lakatos, ***2007***, AIChE Journal, Vol. 53(12), pp. 3089-3107.

Vale, H.M., T.F. McKenna, 2005, Progress in Polymer Science, Vol. 30, pp. 1019-1048.

Valentas, K.J., N.R. Amundson, ***1966***, Industrial and engineering chemistry, Vol. 5, pp. 533-542.

Vanni, M., ***2000***, Journal of Colloid and Interface Science, Vol. 221, pp. 143–160.

Wang, L., D.L. Marchisio, R.D. Vigil and R.O. Fox, ***2005b***, Journal of Colloid and Interface Science, Vol. 282, pp. 380–396.

Wang, L., R.D. Vigil and R.O. Fox, ***2005a***, Journal of Colloid and Interface Science, Vol. 285, pp. 167–178.

Weinstein, O., R. Semiat, D.R. Lewin, ***1998***, Chemical Engineering Science, Vol. 53, pp. 325-339.

Wright, D.L., R. McGraw, D.E. Rosnery, ***2001***, Journal of Colloid and Interface Science, Vol. 236, pp. 242–251.

Xie, T.Y., A.E. Hamielec, P.E. Wood, D.R. Woods, ***1991a***, Journal of Vinyl Technology, Vol. 13, No. 1, 2-25.

Xie, T.Y., A.E. Hamielec, P.E. Wood, D.R. Woods, ***1991b***, Polymer, Vol. 32, No. 3, pp. 537-557.

Yang, H.J., Chu G.W., Xiang Y., Chen J.F., ***2006***, Chem. Eng. J., Vol. 121, pp. 147-152.

Yoon, C., R. McGraw, ***2004a***, Journal of Aerosol Science, Vol. 35, pp. 561–576.

Yoon, C., R. McGraw, ***2004b***, Journal of Aerosol Science, Vol. 35, pp. 577–598.

Yuan, H.G., G. Kalfas, W.H. Ray, ***1991***, JMS-REV. Macromol. Chem. Phys., C31(283), pp. 215-299.

Zerfa, M., B. W. Brooks, ***1996a***, Chem. Eng. Sci., Vol. 51, No. 12, pp. 3223-3233.

Zerfa, M., B. W. Brooks, ***1996b***, Chem. Eng. Sci., Vol. 51, No. 14, pp. 3591-3611.

Zerfa, M., B.W. Brooks, 1997, Chem. Eng. Sci., Vol. 52, No. 14, pp. 2421-2427.

Zerfa, M., B. W. Brooks, ***1998***, Colloids and Surfaces, Vol. 132, pp. 267-273.

Zhang, S.X., W.H. Ray, ***1997***, Industrial Engineering Chemistry Research, Vol. 36, pp. 1310-1321.

Zhao, H., A. Maisels, T. Matsoukas, C. Zheng, ***2007***, Powder Technology, Vol. 173, pp. 38-50.

Zhao, H., C. Zheng, ***2009***, Powder Technology, Vol. 193, pp. 120-123.

Zhao, H., C. Zheng, ***2013***, Computers & Fluids, Vol. 71, pp. 196-207.

Zhao, H., F.E. Kruis, C. Zheng, ***2010***, Journal of Computational Physics, Vol. 229, pp. 6931-6945.

Zhu, G.-Y., A. Zamamiri, M. A. Henson, M. A. Hjortsø, ***2000***, Chemical Engineering Science, Vol. 55, pp. 6155-6167.

Köszönetnyilvánítás

Köszönettel tartozom témavezetőimnek, Dr. Lakatos Bélának és Dr. Németh Sándornak a folyamatos szakmai útmutatásukért és türelmükért, ami hozzájárult a dolgozat elkészültéhez.

Köszönöm az egész családomnak, különösen szüleimnek, hogy mind az egyetemi, mind a doktorandusz éveim alatt bármikor számíthattam szerető tanácsaikra és támogatásukra, ezzel biztosítva azt, hogy nekem csak az éppen előttem álló megpróbáltatásokra kelljen koncentrálnom.

Köszönöm a Pannon Egyetem Folyamatmérnöki Intézeti Tanszék valamennyi munkatársának, hogy bíztak bennem, és ha elakadtam, akkor segítettek.

Valamint utoljára, de nem utolsó sorban köszönöm férjemnek, hogy elviselte azokat az időszakokat, amikor nem volt könnyű mellettem, mert mindig a feladataimon járt az eszem. Köszönöm, hogy kitartott mellettem és támogatott mindenben.